An Experimental Study of OH Uptake by Surfaces of Tropospheric Importance under Dry and Wet Conditions

by

Jong-Ho Park
M.S. Chemistry, Korea University, 2001

Submitted to the Department of Chemistry
In partial fulfillment of the requirements for the degree of

DOCTOR of PHILOSOPHY in CHEMISTRY
at the
MASSACHUSETTS INSTITUTE OF TECHNOLOGY

[June 2008]
January 2008

Author.....
Department of Chemistry
January 14, 2008

Certified by.....
Mario J. Molina
Institute Professor
Thesis Supervisor

Accepted by .....
Robert W. Field
Chairman, Department Committee on Graduate Students

This doctoral thesis has been examined by a Committee of the Department of Chemistry as follows:

Professor Jeffrey I. Steinfeld.....
Thesis Chairman

Professor Mario J. Molina.....
Research Advisor

Professor William H. Green.....
Department of Chemical Engineering

An Experimental Study of OH Uptake by Surfaces of Tropospheric Importance under Dry and Wet Conditions

by

Jong-Ho Park

Submitted to the Department of Chemistry
on January 14, 2008 in Partial Fulfillment of the
Requirements for the Degree of
DOCTOR of PHILOSOPHY in CHEMISTRY

ABSTRACT

The effect of relative humidity (RH) on OH uptake by surfaces of tropospheric importance was investigated. Due to diffusion limitation conditions, experiments were performed with parallel reactors packed with beads and using a surface dilution technique. A virtual cylindrical reactor approximation was developed to further quantify and confirm the reaction probability of OH for the surfaces of interest. While OH exposure of hydrophobic organic surfaces (paraffin wax, pyrene, and methane soot) did not result in measurable change in their relative hydrophilic properties, the presence of water vapor enhanced the OH reactivity on a hydrophilic organic surface (glutaric acid). The RH effect on OH uptake by sea salt and its components was dependent on the nature of the cations. Redistribution of surface ions under humid environments caused changes in pH on the inorganic surfaces, thereby influencing the rate-determining step in the reaction mechanism of heterogeneous OH uptake. This segregation effect explains why the RH effect on OH uptake by sea salt is determined by $MgCl_2$ rather than NaCl. Experimental evidence suggests that adsorbed water on the surfaces of SiO_2 and Al_2O_3 is responsible for enhancement in OH reactivity with mineral dust surfaces under high humidity conditions.

Mass spectra of the gas-phase species produced from the heterogeneous reaction of OH with NaCl were obtained in order to characterize the reaction products and the kinetic mechanism. Evidence for gas-phase HCl, supplemented with kinetics modeling and experiments on heterogeneous O_3 reactivity strongly suggest that Cl_2, sole product of the heterogeneous reaction, transforms to HCl in the presence of H radicals. The Cl_2 yields per OH collision were determined to be 0.020 and 0.022 at 0% and 6% of RH, respectively. Enhancement in Cl_2 production was observed under wet conditions, consistent with a measured chlorine deficit on the NaCl surface. Two alternate reaction mechanisms are proposed to describe the heterogeneous OH uptake by NaCl.

Thesis Supervisor : Mario J. Molina
Title : Institute Professor

To Eunsook, June, and Sean

Acknowledgements

I would not say that the last five years were easy for me. However, I could keep moving forward thanks to many people, and finally did a wonderful job.

First, I want to thank my advisor, professor Mario Molina, for his invaluable advice, guidance, and encouragement. It was a great experience to work in his group. Even though he is one of the busiest scientists in the world, he has never been reluctant to share his time with me whenever I need him. I also admire his humble attitude. I remember that he delivered us mails in person going up and down the stairs in the Green Building. He is the only delivery man who won the Nobel prize. I appreciate the advices and helps from my former advisor, professor Jong-Ho Choi in Korea University. He is the person who initiated my enthusiasm for the physical chemistry.

Working at the Molina group let me have many best friends. Thanks to my best Russian friend, Andrey Ivanov. He always welcomed and gave invaluable advices to solve the problems that I had. He also told me many Russian proverbs to encourage me when I was depressed. Kirsten Johnson, my best American friend, shared a lot of things including her experience about science and even her cookies. Thank you so much for your kindness, Kirsten. Ingrid Kohl is my best Austrian friend that I have to emphasize her helps. She was willing to do the experiment with me when I just joined the group. Even though it was not so long before she left for Austria, she made me familiar with the experiment by sharing her precious experience. Thanks to the other best friends: Rainer Volkamer, Jun Noda, Miguel Zavala, Elizabeth Fitzgerald, Edward Dunlea, Gregory Poskrebyshev, Philip Sheehy, and Van Tran. I also express my thanks

to Luisa Molina.

Thanks to my Korean friends: Hohjai Lee and his wife, Li Zhang, Keehyun Choi, Changsik Song, Jeongkwon Kim, Jae-Gook Lee, Byungkwon Min, Chankyu Joo and Mi Hee Lim. I could not have survived from the tough five years without you all.

My best thanks to my parents and my brother. I can not imagine how much I owe from them in my life. My dad and mom always trust me to give the best supports. I have been learning from them almost everything that I must know to live as a good citizen, a good son, and a good parent. They also provided me Jong-Sung. He is not only my brother, but also my friend and supporter. It is wonderful to be your son and brother. I also give my appreciation to Jeong-Eun Hong, my sister-in-law.

Finally, no words can be enough for my wife, Eunsook, and my two sons, June and Sean. This is for you.

Contents

List of Figures

List of Tables

Chapter 1

Introduction

1.1. OH Radicals in the Troposphere

As a key oxidant, the hydroxyl radical (OH) is involved in numerous reactions with tropospheric constituents. One of the most important examples of its involvement is the OH-initiated oxidation of volatile organic compounds (VOCs), such as aldehydes, alkanes, and alkenes, which eventually leads to their removal from the troposphere. Ozone (O_3) abundance in the troposphere has been also established to be mostly determined by its catalytic cycle reactions with HO_x (= OH + HO_2) with indirect involvement of NO_x (= NO_2 + NO) as is schematically described in Figure 1.1.

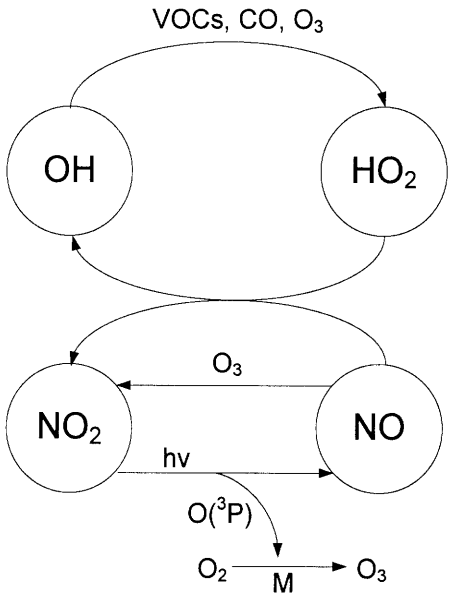

Figure 1.1 Radical cycling reactions of OH in the troposphere

The production of OH is initiated by the photodissociation of ozone molecules under the effect of ultraviolet (UV) radiation to generate electronically excited oxygen atoms followed by reaction with water vapor.

$$O_3 + h\nu\ (\lambda < 320\text{nm}) \rightarrow O(^1D) + O_2 \qquad (1.1)$$

$$O(^1D) + H_2O \rightarrow 2\ OH\ (v = 1, 2, 3) \qquad (1.2)$$

The newly formed OH is rotationally and vibrationally excited [Saunder *et al.*, 1992, Park *et al.*, 2002, 2003], which is efficiently deactivated by collision with nitrogen and oxygen molecules [D'Ottone, 2004].

Another source of OH is the fast reaction between HO_2 and NO with a rate constant of 8.8×10^{-12} cm^3 $molecule^{-1}$ s^{-1} [Atkinson *et al.*, 2004].

$$NO + HO_2 \rightarrow NO_2 + OH \qquad (1.3)$$

Photolysis of gaseous nitrous acid (HONO) is the other major source producing directly OH.

$$HONO + h\nu\ (\lambda \sim 350nm) \rightarrow OH + NO \qquad (1.4)$$

Although the contribution of each possible source of OH, and hence, the OH concentration, depend on the actinic flux, concentrations of ozone, water vapor, nitrogen monoxide (NO), nitrogen dioxide (NO_2), and HONO, a global average [OH] in the troposphere ranges from several 10^5 molecule cm^{-3} at nighttime to 5×10^6 molecule cm^{-3} at daytime [Seinfeld *et al.*, 1998]. OH is found to be a short-lived radical with a lifetime of approximately one second even under clean atmospheric conditions [Heard *et al.*, 2003]. The main sinks of OH in the gas phase are its reactions with carbon monoxide (CO) and methane (CH_4) [Seinfeld *et al.*, 1998].

$$OH + CO + O_2 \rightarrow HO_2 + CO_2 \qquad (1.5)$$

and,

$$OH + CH_4 \rightarrow CH_3 + H_2O \qquad (1.6)$$

$$CH_3 + O_2 + M \rightarrow CH_3O_2 + M \qquad (1.7)$$

1.2. Discrepancy between Models and Field Measurements of OH Concentrations in the Troposphere

Although establishing models to account for the measurements is necessary, consistent overestimations of the atmospheric models in OH concentrations have been reported by field measurements. These overestimates range from 20% [Poppe *et al.* 1994] to a factor of 4 [Eisele *et al.*, 1994], as summarized in Table 1.1. Such discrepancies indicate that there are missing sinks of OH, which are unaccounted in the models. It has been suggested that gas phase reactions of OH with unmeasured biogenic hydrocarbons, such as isoprene [Eisele *et al.*, 1994] and β-pinene type species [Mckeen *et al.*, 1997], could be considered as one of possible missing sinks.

Table 1.1 Summary of model overestimations of [OH]

Campaign	Model Overestimation of [OH]	Reference
Deuselbach (1983) and Schauinsland (1984)	20%	[Poppe *et al.* 1994]
Fritz Peak, Colorado (1991)	Factor of 4	[Eisele *et al.*, 1994]
Mauna Loa Observatory (1992)	Factor of 2	[Eisele *et al.*, 1996]
Fritz Peak / Idaho Hill (1993)	51%	[Crosley, 1997] [Mckeen *et al.*, 1997]
Mace Head (1996)	40%	[Carslaw *et al.*, 1999]
MCMA-2003 (2003)	30%	[Shirley *et al.*, 2006]

1.3. Heterogeneous Losses of OH as Additional Missing Sinks

In addition to the gas phase reactions with unmeasured biogenic hydrocarbons, OH heterogeneous loss on aerosol particles, is not included currently in the models, and has also been suggested to explain the discrepancies. Historically, OH heterogeneous reactions have been largely overlooked due to the short lifetime of OH in the troposphere. However, the heterogeneous sink of OH can be important under certain conditions in polluted air and liquid cloud droplets. For example, Saylor *et al.* [1997] estimated that the fraction of heterogeneous loss under urban conditions ($[NO_x]$ = 10 ppbv, and [VOC] = 10^8 molecule cm^{-3}) would be 30% of the gas phase loss at 10^5 particle/cm^3 of aerosol density and 0.1 of an reaction probability for HO_2 (γ_{HO2} defined in the section 1.4), and even 190% at the same density and γ_{HO2} = 1, while it would be negligible at low aerosol density (<10^3 particle/cm^3). In this case, knowledge of OH heterogeneous chemistry, including reaction mechanisms and their rates, is required to improve modeling accuracy.

Heterogeneous radical reactions become important even under extremely clean conditions. This is because of slower radical sinks through gas-phase reactions with organics or NO_x, and therefore, the contribution of heterogeneous reactions to total radical loss becomes more significant. The remote marine boundary layer is an example where the concentrations of VOC's and NO_x are low and that of aerosols is moderate; under these conditions the contribution of the OH heterogeneous chemistry can be greatest.

As a first demonstration, Isaksen and Crutzen [1977] included a heterogeneous loss channel for OH and HO_2 (hydroperoxyl) radicals into a high sensitivity to HO_x (= OH + HO_2) photochemical model using high reaction probability values for OH and

HO_2 radicals ($\gamma_{OH} = \gamma_{HO2} = 1$). However, subsequent experimental determinations of the reaction probabilities showed that these values are usually much smaller than unity, especially in the case of inorganic aerosols.

Despite the short lifetime of OH in the troposphere, heterogeneous reactions involving OH are now recognized to be important due to their ability to initiate the oxidation of organic particulates, to react with inorganic aerosols, to modifying their physical and chemical properties, to release photochemically active halogen products to the gas phase, and to determine cloud chemistry to a significant extent. At an average OH concentration ~0.02 ppt in the troposphere (~10^6 molecule cm^{-3}), radical uptake becomes often a rate-determining step in an entire process of further physicochemical transformation of aerosol particles. However, atmospheric modeling of aerosol chemistry is to a large extent constrained by the very limited experimental kinetic data on radical uptake.

1.4. Reaction Probabilities of OH on Aerosol Surfaces

Hanson *et al.* [1992] measured the reaction probabilities, γ, also known as *the uptake coefficient*, defined as the ratio of *the number of gas molecules reacting with the surface* to *the number of gas molecules colliding with the surface* [Brown, 1978; Kolb *et al.*, 1995; Molina *et al.*, 1996],

$$\gamma = \frac{number \cdot of \cdot gas \cdot molecules \cdot reacting \cdot with \cdot the \cdot surface}{number \cdot of \cdot gas \cdot molecules \cdot colliding \cdot with \cdot the \cdot surface} \qquad (1.8)$$

using a wetted wall flow tube and the laser induced fluorescence (LIF) detection technique. The reported γ_{OH} on pure liquid water and 28% w/w sulfuric acid (H_2SO_4)

are 0.0035 at 275K and 0.08 (the lower limit) at 249K, respectively. The value at room temperature was reported at 4.2 [± 2.8] $\times 10^{-3}$ by Takami et al. [1998]. At the same time, water ice showed essentially higher reactivity to OH uptake. Cooper *et al.* [1996] determined γ_{OH} on water ice using their low-temperature flow tube coupled to a resonance fluorescence detector. The measured reaction probability on fresh ice was 0.1 while it became smaller with time, approaching a steady state value of 0.03.

Table 1.2. The measured OH reaction probabilities for various aerosol surfaces

Surface	γ_{OH}	Reference
Liquid H_2O	0.0035	Hanson *et al.*, 1992
	0.0042	Takami *et al.*, 1998
H_2SO_4	0.08 (lower limit)	Hanson *et al.*, 1992
Water Ice	0.1 (initial) 0.03 (steady state)	Cooper *et al.*, 1996
$(NH_4)_2SO_4$	0.03	Cooper *et al.*, 1996
NaCl	0.0032	Ivanov *et al.*, 1996
NH_4NO_3	0.00347	Ivanov *et al.*, 1996
Halocarbon wax	6×10^{-4}	Bertram *et al.*, 2001
Paraffin wax	0.34	Bertram *et al.*, 2001
Stearic-palmitic acid	0.32	Bertram *et al.*, 2001
Pyrene	0.32	Bertram *et al.*, 2001
Soot	0.88	Bertram *et al.*, 2001
Al_2O_3	0.20	Bertram *et al.*, 2001

The flow tube-electron paramagnetic resonance experiments carried out by Ivanov *et al.* [1996] measured γ_{OH} for dry NaCl and ammonium nitrate (NH_4NO_3) at 3.2×10^{-3} at 300 K and 3.47×10^{-3} at 297 K, respectively, showing a negative temperature dependence. Recently, our laboratory used a flow tube coupled with a chemical ionization mass spectrometer (CIMS) to investigate the reaction probabilities of OH on organic surfaces

(halocarbon wax, paraffin wax, methyl-terminated monolayer, stearic-palmitic acid, vinyl-terminated monolayer, pyrene, soot). The results indicate that the organic materials react efficiently with OH via heterogeneous H-abstraction reactions. In our laboratory $\gamma_{OH} = 0.2$ for aluminum oxide (Al_2O_3) was also determined [Bertram et al., 2001]. The OH reaction probabilities for the aerosol surfaces measured in the early studies are summarized in Table 1.2.

1.5. Tropospheric Aerosols

Aerosols in the troposphere are solid or liquid particles with particle sizes ranging from a few nanometers to tens of micrometers. They originate from natural and anthropogenic sources. Ocean wave actions and wind-blown mineral dust are the most important examples of natural sources, while combustion is an example of an anthropogenic source. Aerosol composition and concentrations are highly dependent on location. For example, urban areas normally contain more organic aerosols due to high anthropogenic activities compared to remote regions. Ocean-originated particles, such as sea salt aerosol, are rich in a coastal area, while mineral dust aerosols are typically abundant in a desert region. Water droplets forming fog or clouds are also important aerosol particles in the troposphere [Seinfeld and Pandis, 1998; Pandis *et al.*, 1990; Wieprecht *et al.*, 2005]. A study of OH heterogeneous reactions on tropospheric aerosol surfaces provides not only invaluable kinetics information to improve atmospheric models, but is also fundamental for our understanding of the heterogeneous chemistry of radicals.

1.5.1. Organic Aerosols

Carbonaceous aerosol particles consisting of both elemental carbon (EC) and organic carbon (OC) account for a major fraction of tropospheric aerosols, especially in urban areas. Field measurements have shown that 10-50% of particulate matter in the troposphere is carbonaceous [Larry *et al.*, 1999] with a global anthropogenic emission of 12-24 Tg yr^{-1} [Cooke *et al.*, 1996; Penner *et al.*, 1998]. In particular, organics may comprise 15 – 60% of particulate matter < 10 μm in diameter (PM_{10}) in urban areas, for example [Rau, 1989; Bertram *et al.*, 2001]. Primary OC is emitted directly into the atmosphere while secondary OC, also known as secondary organic aerosol (SOA), is formed by condensation of hydrocarbons through gas-phase reactions onto an existing aerosol surface [Pandis *et al.*, 1992; Seinfeld and Pandis, 1998]. Oxidation of hydrocarbons in the gas phase by OH, O_3, or NO_2 followed by condensation on an aerosol surface is one of the examples of secondary OC formation as described in Figure 1.2. An amount of secondary OC also depends on the actinic flux and concentrations of pollutants. In most cases, primary OC dominates in the OC budget in the troposphere although the contribution of secondary OC increases during peak photochemical air pollution.

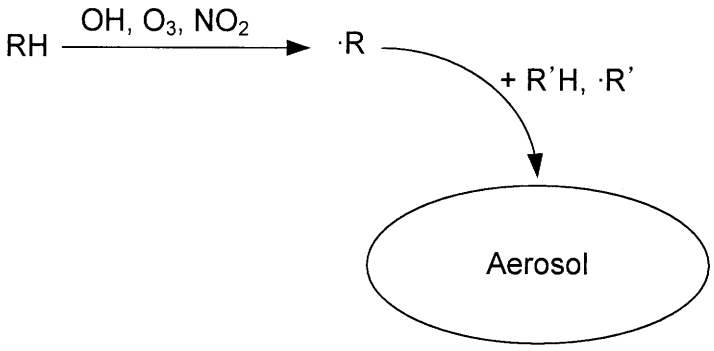

Figure 1.2 Formation of secondary OC by oxidation of hydrocarbons

Soot is the most important atmospheric carbonaceous particle formed as a by-product of the incomplete combustion of organic fuels. Soot exhibits complex climate effects and participates in a variety of tropospheric chemical reactions. Consisting of both EC and OC, soot also contains hydrogen (up to 10%). The efficiency of soot formation significantly depends on the carbon/oxygen ratio in a fuel-air mixture. In the following example [Seinfeld and Pandis, 1998];

$$C_mH_n + a\ O_2 \rightarrow 2a\ CO + 0.5n\ H_2 + (m-2a)\ C_s \qquad (1.9)$$

C_s is the soot formed. When m = 2a, which is the sufficient oxygen condition, no soot is formed, while the amount of soot, that is (m - 2a), increases under oxygen-poor conditions.

The elemental structure of soot is similar to that of graphite, which is stack of 2-Dimensional network planes. Then, these elements cluster with each other to form approximately 20-30 nm spherules which aggregate together into particles up to several microns in diameter. The structure and composition of soot particles are extremely complex and still not entirely understood.

1.5.2. Sea Salt

Sea salt particles are released to the troposphere by ocean wave actions followed by water evaporation. OH heterogeneous reactions on sea salt particles can play an important role in production of halogens, such as chlorine and bromine, responsible for further reactions in the troposphere and the stratosphere, including ozone destruction.

Sea salt is a complex mixture of different compounds. Although the composition of sea salt aerosols depends on the location of their origin, the major

components are sodium chloride (NaCl), magnesium chloride ($MgCl_2$), and sodium sulfate (Na_2SO_4). The typical composition of a sea salt mixture is listed in Table 1.2 [Lin *et al.*, 1991].

Table 1.3. Composition of sea salt [Lin *et al.*, 1991]

Composition	Percent by Weight (%)	Density (g/L)
NaCl	58.490	24.530
$MgCl_2 \cdot 6H_2O$	26.460	5.200
Na_2SO_4	9.750	4.090
$CaCl_2$	2.765	1.160
KCl	1.645	0.695
$NaHCO_3$	0.477	0.201
KBr	0.238	0.101
H_3BO_3	0.071	0.027
$SrCl_2 \cdot 6H_2O$	0.095	0.025
NaF	0.007	0.003

Although the composition of sea salt is initially the same as that of sea water when it is emitted form the ocean, field observations report a chloride deficit in the sea salt particles showing low Cl/Na ratio as they are aged [Junge, 1956; Cicerone, 1981; Keene *et al.*, 1990; Mouri *et al.*, 1993; McInnes *et al.*, 1994]. It is suggested that heterogeneous reactions between gas phase pollutants and sea salt particles are responsible for the depletion of chlorine, as follows [Hemminger, 1999].

$$NaCl(s) + HNO_3(g) \rightarrow NaNO_3(s) + HCl(g) \quad (1.10)$$

$$2\ NaCl(s) + H_2SO_4(g) \rightarrow Na_2SO_4(s) + 2\ HCl(g) \quad (1.11)$$

$$NaCl(s) + N_2O_5(g) \rightarrow NaNO_3(s) + ClNO_2(g) \quad (1.12)$$

$$NaCl(s) + 2\ NO_2(g) \rightarrow NaNO_3(s) + NOCl(g) \quad (1.13)$$

$$NaCl(s) + ClONO_2(g) \rightarrow NaNO_3(s) + Cl_2(g) \quad (1.14)$$

Besides gas phase pollutant, the O_3 and OH heterogeneous reactions on sea salt

particles have been studied and suggested as an additional chlorine deficit source [Oum *et al.*, 1998; Finlayson-Pitts, 2003]. However, the kinetics mechanisms for these reactions are still unknown.

1.5.3. Mineral Dust Particles

Mineral dust particles originate from very specific parts of the Earth's surface, mostly from desert regions, by wind actions [Prospero *et al.*, 2002]. Mineral dust particles are typically a mixture of various mineral compounds, such as silicon dioxide (silica, SiO_2), aluminum oxide (alumina, Al_2O_3), and calcium carbonate (calcite, $CaCO_3$). Due to their long lifetime, mineral dust particles can be transported at long distances and spread globally, affecting climate and the tropospheric chemistry as well as playing an important role in cloud physics and chemistry by acting as cloud condensation nuclei (CCN). In addition, mineral dust aerosols can affect the radiation balance in the atmosphere by reflecting, scattering, and absorbing the incident solar light [Prospero *et al.*, 2002; Laskin *et al.*, 2005; Vlasenko *et al.*, 2006]. Another important role of mineral dust particles is to provide reaction sites for uptake of atmospheric gaseous species that can be eventually involved the following redox reactions of catalytic destruction [Ross *et al.*, 1991; Matthijsen *et al.*, 1995; Dentener *et al.*, 1996]

$$HO_2 + Fe(III) \rightarrow Fe(II) + O_2 + H^+ \qquad (1.15)$$

$$HO_2 + Fe(II) + H^+ \rightarrow Fe(III) + H_2O_2 \qquad (1.16)$$

Mineral dust particles are initially practically insoluble even though they are hydrophilic. However, as they are exposed to the gas phase environment in the troposphere, the aerosol particles become soluble by reacting with labile species, such

as, for example, nitric acid (HNO_3). The following example shows conversion of initially insoluble calcium carbonate ($CaCO_3$) particles to soluble calcium nitrate ($Ca(NO_3)_2$) upon HNO_3 uptake on the aerosol particles in the troposphere [Krueger *et al.*, 2003].

$$CaCO_3(s) + 2\,HNO_3(g) \rightarrow Ca(NO_3)_2(aq) + H_2CO_3(aq) \qquad (1.17)$$

$$Ca(NO_3)_2(aq) + H_2CO_3(aq) \rightarrow Ca(NO_3)_2(aq) + H_2O + CO_2(g) \qquad (1.18)$$

1.6. Heterogeneous Reactions under High Humidity Conditions

Little is known of OH heterogeneous chemistry under real tropospheric conditions where water vapor is one of the major components of the troposphere, reaching up to 4% by volume. Relative humidity (RH) is defined as the ratio of the partial pressure of water (P_{H2O}) to its saturated vapor pressure (P^0_{H2O}) at a given temperature.

$$RH(\%) = 100 \cdot \frac{P_{H_2O}}{P^0_{H_2O}} \qquad (1.19)$$

Due to its relatively large dipole moment (1.83×10^{-18} esu·cm) and the ability to form strong hydrogen bonds, water vapor can be easily adsorbed on the aerosol surfaces, such as salts and dust particles, with high surface tension [Hemminger, 1999]. For example, several studies showed that a water monolayer starts to appear on the NaCl (100) surface even at 35% of RH, which is significantly below the deliquescence point of RH = 75% [Peters *et al.*, 1997]. A similar value was reported by Hemminger [1999] who showed that the first monolayer of water was completed at 20% of RH, whereas multilayer water was efficiently formed above 31 % RH. Hemminger also showed that the adsorbed water enhanced the ionic mobility on a surface at extremely low RH = 2%.

This result implies that OH heterogeneous reactions on aerosol surfaces can be influenced by RH of a much wider range. Therefore, for the tropospheric chemistry it is important to know how the OH heterogeneous reactions change under wet conditions.

1.6.1. Molecular water bonding to surfaces

Thiel *et al.* [1987] stated the following general features which describe the interaction of water with most surfaces. Since they are important and well described, four features were considered.

(1) Water bonds through the oxygen atom to the surface. Hydrogen bonds with the surface (O-H···S bonds, where S = surface) are rare. Similarly, water forms bonds to metal atoms in complexes and clusters via the oxygen atom [Nakamoto, 1970; Ferraro, 1971].

(2) Bonding is accompanied by net charge transfer to the surface. Therefore water acts as a Lewis base. Charge transfer to the surface manifests itself in a negative work function change upon adsorption.

(3) The internal bond angle, bond lengths, and vibrational frequencies of the molecules are only slightly perturbed from the gas phase values by the interaction with the surfaces.

(4) Formation of hydrogen-bonded clusters is common, even at very low coverages, because hydrogen bonding between two or more H_2O molecules is often energetically competitive with the molecule-substrate bond.

1.6.2. Technical problems in experiments with water vapor

Technical problems arise in experiments conducted at high water vapor pressure

conditions. Achieving a relative humidity of up to 50% requires a considerable flow of carrier gas that builds up relatively high pressure of 100-200 Torr inside a flow tube reactor. Such high pressure conditions significantly slow down the fast radical uptake rate which becomes already determined by diffusion of radicals to reactor walls [Rudich *et al.*, 1996; Zasypkin *et al.*, 1997; Pöschl *et al.*, 1998]. Increasing the surface area available for reaction by using a set of sub-size tube array or a glass bead packing inside a flow tube enables simultaneously to maximize the rate of a heterogeneous reaction and minimize diffusion limitations.

The sensitivity of chemical ionization mass spectroscopy (CIMS) detection is also affected by high water vapor pressure. Water vapor reduces significantly the CIMS sensitivity to OH due to efficient formation of water complexes with the SF_6^- reagent ion, such as $SOF_4^-(H_2O)_m$, $F^-(HF)_2(H_2O)_n$, and $F^-(HF)_n$ where m and n are complex numbers [Wickramanayake, 1986; Arnold *et al.*, 2001]. Besides complex formation with SF_6^-, OH also efficiently forms water clusters that reduce considerably its detection limit [Salcedo *et al.*, 2004]. Although dilution with an additional flow of He helps partially to minimize the efficiency of water-complex formation [Arnold *et al.*, 2001], calibration of sensitivities at different RH, or compensation of this effect by monitoring the reference are still necessary under high RH conditions, which the latter is simpler than former to be performed.

1.7. Chemical Ionization Mass Spectrometry (CIMS)

Compared to conventional electron impact (EI) ionization or laser induced ionization, CIMS provides much less destructive ionization of detected species [Hanson *et al.*, 1991, Villalta *et al.*, 1995; Seeley *et al.*, 1996; Lipson *et al.*, 1999]. For CIMS

detection, a parent ion (or regent ion), such as SF_6^-, F^-, O_2^-, and NO_2^-, meets a gas-phase molecule of interest in a chemical ionization region (a CI region) where electron transfer enables detection via the following reaction:

$$X^- + M \rightarrow X + M^- \qquad (1.20)$$

where X^- is the parent ion and M is a gas-phase molecule of interest. A series of lenses focuses the ionized species into a quadrupole mass analyzer for detection. The 'soft' ionization, which is specific for CIMS, minimizes fragmentation of the molecules resulting in enhancement of sensitivity and simplicity of analysis.

1.8. Thesis Outline

The main objective of this thesis is to understand how OH uptake by surfaces of tropospheric interest depends on relative humidity. This also includes the investigation of the reaction mechanism of the heterogeneous interaction of OH with a NaCl surface under dry and wet conditions. The information obtained contributes to better understanding the OH heterogeneous chemistry under realistic tropospheric conditions, thereby providing experimental data essential for improving the accuracy of atmospheric models.

Chapter 2 describes in detail the experimental setup used in the present study. The setup consists of a flow tube system with a reference and a reactor coupled to a CIMS. In addition, details about the path of the OH radical from its generation to detection are delineated.

In chapter 3, the dependence of the OH reaction probabilities on relative humidity of 0 to 48% is described for various organic and inorganic surfaces. Organic

surfaces studied in this work are paraffin wax, pyrene, and methane soot that served as proxies for hydrophobic aerosols, and glutaric acid ($C_3H_6(CO_2H)_2$) that served as proxy for hydrophilic ones. Inorganic surfaces, such as sodium chloride (NaCl), magnesium chloride ($MgCl_2$), sodium sulfate (Na_2SO_4), calcium chloride ($CaCl_2$), potassium chloride (KCl), and sea salt, are used as proxies for marine-originated sea salt aerosol, while silicon oxide and aluminum oxide are used to imitate mineral dust surfaces. A virtual tube approximation is proposed and successfully developed in the current study as a kinetics method employed to determine the OH reaction probability using a differential bead-packed flow tube.

Chapter 4 considers in detail the reaction mechanism of molecular chlorine formation in the heterogeneous OH + NaCl reaction. The obtained experimental data confirm that molecular chlorine detected in the gas-phase is a major product of the OH heterogeneous reaction with a NaCl surface. In addition, XPS experiments are carried out to study chemical composition transformation of the salt surface exposed to OH. The dependence of the efficiency of chlorine production on RH is also described.

The conclusion section (Chapter 5) summarizes the results and intermediate conclusions made in the previous chapters.

After the conclusion section (Chapter 6), recommendations for future studies are suggested: studies of heterogeneous HO_2 reactions on surfaces of tropospheric interest under humid conditions are also of atmospheric importance and would considerably complement the results of the current studies.

References for Chapter 1

S. T. Arnold and A. A. Viggiano, Turbulent ion flow tube study of the cluster-mediated reactions of SF_6^- with H_2O, CH_3OH, and C_2H_5OH from 50 to 500 Torr, *J. Phys. Chem. A*, 105, 3527-3531, 2001.

R. Atkinson, D. L. Baulch, R. A. Cox, J. N. Crowley, R. F. Hampson, R. G. Hynes, M. E. Jenkin, M. J. Rossi, J. Troe, Evaluated kinetic and photochemical data for atmospheric chemistry: Volume I - gas phase reactions of Ox, HOx, NOx and SOx species, *Atmos. Chem. Phys.*, **4**, 1461-1738, 2004.

Air Quality Criteria for Particulate Matter; United States Environmental Protection Agency, EPA/600/P-95/001, 1996.

A. K. Bertram, A. V. Ivanov, M. Hunter, L. T. Molina, and M. J. Molina, The reaction probability of OH on organic surfaces of tropospheric interest, *J. Phys. Chem. A*, **105**, 9415-9421, 2001.

R. L. Brown, Tubular flow reactors with first-order kinetics, *J. Res. Natl. Bur. Stand.*, **83**, 1-8, 1978.

N. Carslaw, D. J. Creasey, D. E. Heard, A. C. Lewis, J. B. McQuaid, M. J. Pilling, P. S. Monks, B. J. Bandy, and S. A. Penkett, Modeling OH, HO_2, and RO_2 readicals in the marine boundary layer: 1. Model construction and comparison with field measurements, *J. Geophys. Res.*, **104**, 30241-30255, 1999.

R. J. Cicerone, Halogens in the atmosphere, *Rev. Geophys. Space Phys.*, **19**, 123-139, 1981.

W. F. Cooke and J. J. N. Wilson, A global black carbon aerosol model, *J. Geophys. Res.*, **101**, 19395-19409, 1996.

P. L. Cooper and J. P. D. Abbatt, Heterogeneous interactions of OH and HO_2 radicals with surfaces characteristic of atmospheric particulate matter, *J. Phys. Chem.*, **100**, 2249-2254, 1996.

D. R. Crosley, The 1993 Tropospheric Chemistry Experiment: Preface, *J. Geophys. Res.*, **102**, 6169, 1997.

F. J. Dentener, G. R. Carmichael, Y. Zhang, J. Lelieveld, and P. J. Crutzen, Role of mineral aerosol as a reactive surface in the global troposphere, *J. Geophys. Res.*, **101**, 22,869-22,889, 1996.

L. D'Ottone, D. Bauer, P. Campuzano-Jost, M. Fardy, and A. J. Hynes, Vibrational deactivation studies of OH X $^2\Pi$(v = 1-5) by N_2 and O_2, *Phys. Chem. Chem. Phys.*, **6**, 4276-4282, 2004.

F. L. Eisele, G. H. Mount, F. C. Fehsenfeld, J. H. Edward Marovich, D. D. Parrish, J. Roberts, and M. Trainer, Intercomparison of tropospheric OH and ancillary trace gas measurements at Fritz Peak Observatory, Colorado, *J. Geophys Rev.*, 99, 18605-18626, 1994.

F. L. Eisele, D. J. Tanner, C. A. Cantrell, and J. G. Calvert, Measurements and steady state calculations of OH concentrations at Mauna Loa Observatory, *J. Geophys. Res.*, **101**, 14665-14679, 1996.

J. R. Ferraro, *Low-Frequency vibrations of inorganic and coordination compounds*, Plenum, New York, 1971.

B. J. Finlayson-Pitts, The Tropospheric chemistry of sea salt: A molecular-level view of the chemistry of NaCl and NaBr, *Chem. Rev.*, **103**, 4801-4822, 2003.

D. R. Hanson and A. R. Ravishankara, The reaction probabilities of $ClONO_2$ and N_2O_5 on polar stratospheric cloud materials, *J. Geophys. Res.*, **96**, 5081, 1991.

D. R. Hanson, J. B. Burkholder, C. J. Howard, and A. R. Ravishankara, Measurement of OH and HO_2 radical uptake coefficients on water an sulfuric acid surfaces, *J. Phys. Chem.*, **96**, 4979-4985, 1992

D. E. Heard and M. J. Pilling, Measurement of OH and HO_2 in the Troposphere, *Chem. Rev.*, **103**, 5163-5198, 2003.

J. C. Hemminger, Heterogeneous chemistry in the troposphere : a modern surface chemistry approach to the study of fundamental processes, *Int. Rev. Phys. Chem.*, **18**, 387-417, 1999.

I. S. A Isaksen and P. J. Crutzen, Uncertainties in calculated hydroxyl radical densities in the troposphere and stratosphere, *Geophys. Norvegica*, **31**, 1, 1977.

A. V. Ivanov, Y. M. Gershenzon, F. Gratpanche, P. Devolder, J. –P. Sawerysyn, Heterogeneous loss of OH on NaCl and NH_4NO_3 at tropospheric temperature, *Ann Geophys.*, **14**, 659-664, 1996.

C. E. Junge, Recent investigations in air chemistry, *Tellus*, **8**, 127-139, 1956.

W. C. Keene, A. A. P. Pszenny, D. J. Jacob, R. A. Duce, J. N. Galloway, J. J. Schultz-Tokos, H. Sievering, and J. F. Boatman, The geochemical cycling of reactive chlorine through the marine troposphere, *Global Biogeochem. Cycles*, **4**, 407-430, 1990.

C. E. Kolb, D. R. Worsnop, M. S. Zahniser, P. Davidovits, C. F. Keyser, M. T. Leu, M. J. Molina, D. R. Hanson, A. R. Ravishankara, L. R. Williams, and M. A. Tolbert, Laboratory studies of atmospheric heterogeneous chemistry, in *Current Problems and Progress in Atmopheric Chemistry* (edited by J. R. Barker), **3**, 771, World Scientific Publishing, 1995.

A. Laskin, T. W. Wietsma, B. J. Krueger, and V. H. Grassian, Heterogeneous chemistry of individual mineral dust particles with nitric acid: A combined CCSEM/EDX, ESEM, and ICP-MS study, *J. Geophys. Res.*, **110**, D10208, doi:10.1029/2004JD005206, 2005.

T. F. Lin, J. B. Gilbert, J. A. Naggar, and T. M. Imblum, Seawater conductivity enhancement by acid injection for the MHD thrusters, *Proceedings IEEE's OCEANS'91, Honolulu, Hawaii*, **3**, 1629-1635, 1991

J. B. Lipsion, T. W. Beiderhase, L. T. Molina, M. J. Molina, and M. Olzmann, Production of HCl in the OH + ClO reaction: Laboratory measurements and statistical rate theory calculations, *J. Phys. Chem. A*, **103**, 6540-6551, 1999.

B. J. Krueger, V. H. Grassian, A. Laskin, and J. P. Cowin, The transformation of solid atmospheric particles into liquid droplets through heterogeneous chemistry: Laboratory insights into the processing of calcium containing mineral dust aerosol in the troposphere, *Geophys. Res. Lett.*, **30**, 1148, doi:10.1029/2002GL016563, 2003.

K. Nakamoto, *Infrared and raman spectra of inorganic and coordination compounds*, Wiley-Interscience, New York, 1970.

J. Matthijse and D. L. Sedlak, Cloud model experiments of the effect of iron and copper on tropospheric ozone under marine and continental conditions, *Meteorol. Atmos. Phys.*, **57**, 43-60, 1995.

S. A. Mckeen, G. Mount, F. Eisele, E. Williams, J. Harder, P. Goldan, W. Kuster, S. C. Liu, K. Baumann, D. Tanner, A. Fried, S. Sewell, C. Cantrell, and R. Shetter, Photochemical modeling of hydroxyl and its relationship to other species during the Tropospheric OH Photochemistry Experiment, *J. Geophys. Res.*, **102**, 6467-6493, 1997.

L. M. Mclnnes, D. S. Covert, P. K. Quinn, and M. S. Germani, Measurements of chloride depletion and sulfur enrichment in individual sea-salt particles collected from the remote marine boundary layer, *J. Geophys. Res.*, **99**, 8257-8268, 1994.

M. J. Molina, L. T. Molina, and C. E. Kolb, Gas-phase and heterogeneous chemical kinetics of the troposphere and stratosphere, *Annu. Rev. Phys. Chem.*, **47**, 327-367, 1996.

H. Mouri and K. Okada, Shattering and modification of sea-salt particles in the marine atmosphere, *Geophys. Res. Lett.*, **20**, 49-52, 1993.

K. W. Oum, M. J. Lakin, D. O. DeHaan, T. Brauers, and B. J. Finlayson-Pitts, Formation of molecular chlorine from the photolysis of ozone and aqueous sea-salt particles, *science*, **279**, 74-77, 1998.

S. N. Pandis, J. H. Seinfeld, and C Pilinis, Chemical composition differences in fog and cloud droplets of different sizes, *Atomospheric Environment*, **24A**, 1957-1969, 1990.

S. N. Pandis, R. A. Harley, G. R. Cass, and J. H. Seinfeld, Secondary organic aerosol formation and transport, *Atmos. Environ.*, **26A**, 2269-2282, 1992.

J. –H. Park, H. Lee, H. –C. Kwon, H. –K. Kim, Y. –S. Choi, and J. –H. Choi, Atom-radical reaction dynamics of $O(^3P) + C_3H_5 \rightarrow C_3H_4 + OH$: Nascent rovibrational state distributions of products OH, *J. Chem. Phys.*, **117**, 2017-2029, 2002.

J. –H. Park, H. Lee, and J. –H. Choi, A theoretical study of the reaction of $O(^3P)$ with an allyl radical, C_3H_5, *J. Chem. Phys.*, **119**, 8966-8978, 2003.

S. J. Peters and G. E. Ewing, Water on salt: An infrared study of adsorbed H_2O on NaCl(100) under ambient conditions, *J. Phys. Chem. B*, **101**, 10880-10886, 1997.

D. Poppe, J. Zimmermann, R. Bauer, T. Brauers, D. Brűning, J. Callies, H.-P. Dorn, A. Hofzumahaus, F. –J. Johnen, A. Khedim, H. Koch, R. Koppmann, H. London, K. –P. Műller, R. Neuroth, C. Plass-Dűlmer, U. Platt, F. Rohrer, E. –P. Rőth, J. Rudolph, U. Schmidt, M. Wallasch, and D. H. Ehhalt, Comparison of measured OH concentrations with model calculations, *J. Geophys Res.*, **99**, 16633-16642, 1994.

U. Pöschl, M. Canagaratan, J. T. Jayne, L. T. Molina, D. R. Worsnop, C. E. Kolb, and M. J. Molina, Mass accommodation coefficient of H_2SO_4 vapor on aqueous sulfuric acid surfaces and gaseous diffusion coefficient of H_2SO_4 in N_2/H_2O, *J. Phys. Chem. A*, **102**, 10082-10089, 1998.

J. E. Penner, C. C. Chuang, and K. Grant, Climate forcing by carbonaceous and sulfate aerosols, *Clim. Dyn.*, **14**, 839-851, 1998.

J. M. Prospero, P. Ginoux, O. Torres, S. E. Nicholson, and T. E. Gill, Environmental characterization of global source of atmospheric soil dust identified with the Nimbus 7 total ozone mapping spectrometer (TOMS) absorbing aerosol product, *Rev. Geophys.*, **40**, 1002, doi:10.1029/2000RG000095, 2002.

J. A. Rau, Composition and size distribution of residual wood smoke particles, *Aerosol Sci. Technol.*, **10**, 181-192, 1989.

H. B. Ross, and K. J. Noone, A numerical investigation of the destruction of peroxy radical by Cu ion catalyzed reactions on aerosol particles, *J. Atmos. Chem.*, **12**, 121-136, 1991.

Y. Rudich, R. K. Talukdar, T. Imamura, R. W. Fox, and A. R. Ravishankara, Uptake of NO_3 on KI solutions: rate coefficient for the $NO_3 + I^-$ reaction and gas-phase diffusion coefficients for NO_3, *Chem. Phys. Lett.*, **261**, 467-473, 1996

D. Salcedo, P. W. Villalta, V. Varutbangkul, J. C. Wormhoudt, R. C. Miake-Lye, D. R. Worsnop, J. O. Ballenthin, W. F. Thorn, A. A. Viggiano, T. M. Miller, R. C. Flagan, and J. H. Seinfeld, Effect of relative humidity on the detection of sulfur dioxide and sulfuric acid using a chemical ionization mass spectrometer, *Int. J. Mass Spectrom.*, **231**, 17-30, 2004.

D. G. Sauder, J. C. Stephenson, D. S. King, and M. P. Casassa, Nascent product states in the photoinitiated reaction of O_3 and H_2O, *J. Chem. Phys.*, **97**, 952-961, 1992.

R. D. Saylor, And estimate of the potential significance of heterogeneous loss to aerosols as an additional sink for hydroperoxy radicals in the troposphere, *Atm. Environ.*, **31**, 3653-3658, 1997.

J. H. Seinfeld and S. N. Pandis. *Atmospheric Chemistry and Physics*. John Wiley & Sons, Inc., New York, 1998.

N. N. Semenov, Kinetics of complex homogeneous reactions *Acta Physicochimica U.R.S.S.*, **18**, 433-472, 1943.

J. V. Seeley, R. F. Meads, M. J. Elrod, and M. J. Molina, Temperature and pressure dependence of the rate constant for the $HO_2 + NO$ reaction, *J. Phys. Chem.*, **100**, 4026-4031, 1996.

T. R. Shirley, W. H. Brune, X. Ren, J. Mao, R. Lesher, B. Cardenas, R. Volkamer, L. T. Molina, M. J. Molina, B. Lamb, E. Velasco, T. Jobson, and M. Alexander, Atmospheric oxidation in the Mexico City Metropolitan Area (MCMA) during April 2003, *Atmos. Chem. Phys.*, **6**, 2753-2765, 2006.

A. Takami, S. Kato, A. Shimono, and S. Koda, Uptake coefficient of OH radical on aqueous surface, *Chem. Phys.*, **231**, 215-227, 1998.

P. A. Thiel and T. E. Madey, The interaction of water with solid surfaces: Fundamental aspects, *Surface Science Reports*, **7**, 211-385, 1987

P. W. Villalta, L. G. Huey, and C. J. Howard, A temperature-dependent kinetics study of the CH_3O_2 + NO reaction using chemical ionization mass spectrometry, *J. Phys. Chem.*, **99**, 12,829-12,834, 1995.

A. Vlasenko, S. Sjogren, E. Weingartner, K. Stemmler, H. W. Gäggeler, and M. Ammann, Effect of humidity on nitric acid uptake to mineral dust aerosol particles, *Atmos. Chem. Phys.*, **6**, 2147-2160, 2006.

P. P. Wickramanayake, G. J. Gardner, K. W. Michael Siu, and S. S. Berman, Ion/Molecule reaction between sulfur hexafluoride negative ion and water under atmospheric pressure ionization mass spectrometric conditions, *Int. J. Mass Spectrom. and Ion Proc.*, **69**, 39-43, 1986.

W. Wieprecht, K. Acker, S. Mertes, J. Collett Jr., W. Jaeschke, E. Brüggermann, D. Mőller, and H. Herrmann, Cloud physics and cloud water sampler comparison during FEBUKO, *Atmospheric Environment*, **39**, 4267-4277, 2005.

A. Y. Zasypkin, V. M. Grigor'eva, V. N. Korchak, and Y. M. Gershenson, A Formula for summing of kinetic resistances for mobile and stationary media: I. Cylindrical reaction, *Kinetics and Catalysis*, **38**, 772-781, 1997.

Chapter 2

Experimental

The experimental setup used in the present studies consists of parallel reactor tubes connected to a chemical ionization mass spectrometer. OH radicals are generated then exposed to surfaces of interest under dry and wet conditions in a flow tube system. Products of the heterogeneous reactions and OH radicals which have survived from heterogeneous losses are ionized for CIMS detection.

2.1. The Flow Tube System

The parallel flow tube design used in the present work is shown in detail in Figure 2.1. The flow tubes and the entire line of flow pathway made of borosilicate glass were completely coated with halocarbon wax (Halocarbon Inc., 600 series and 1500 series), to minimize unwanted heterogeneous reactions due to its low reactivity with OH, $\gamma_{OH} = 6\times10^{-4}$ [Bertram *et al.*, 2001]. The series numbers represent the average molecular weight of halocarbon wax wherein the higher molecular weight corresponds to greater inertness. No significant difference between 600 series and 1500 series halocarbon wax was observed under the experimental conditions employed in this work. Therefore, only 600 series halocarbon was used for convenience since it allowed for even coating at lower temperatures (~ 200℃).

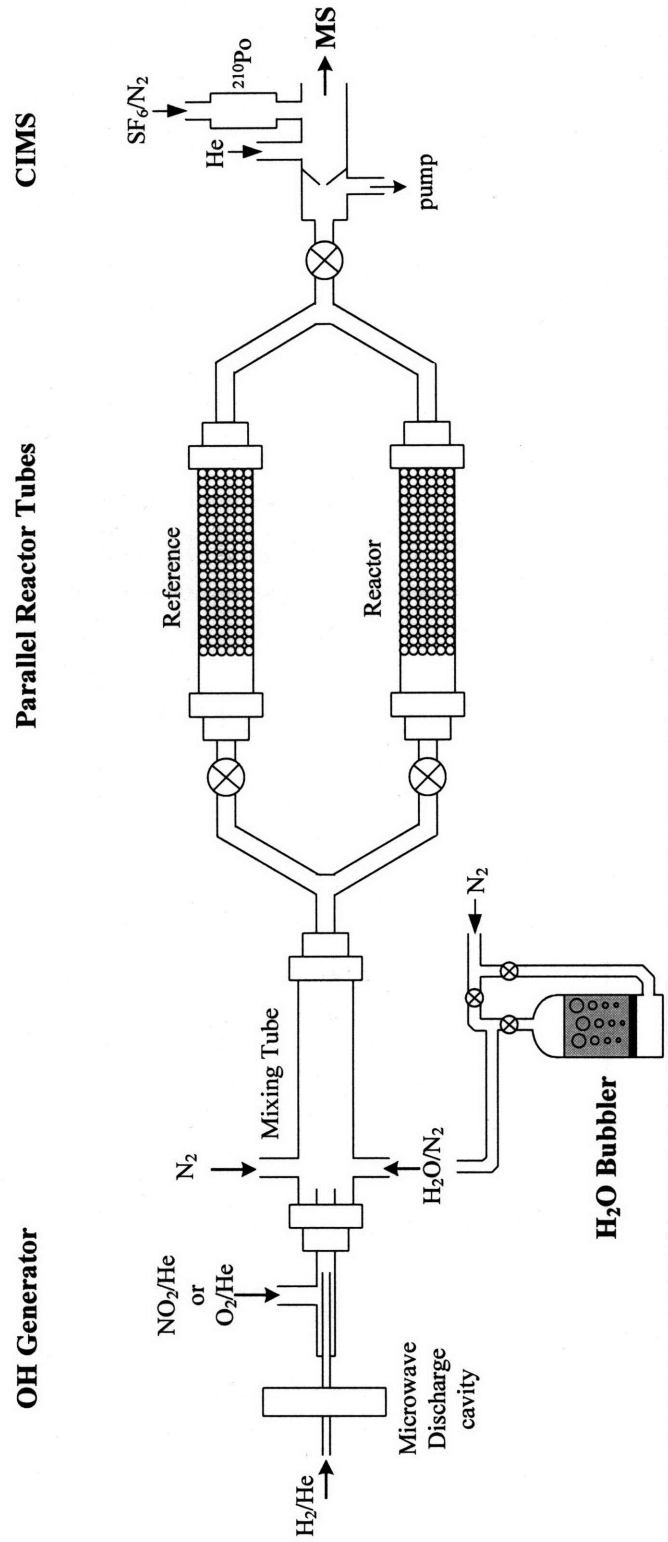

Figure 2.1 The flow tube system used in present work.

Gas flow rates were monitored with electronic mass flow meters (Millipore, Tylan). Since each flow meter was factory-calibrated by a specific gas flow, such as nitrogen or helium, a conversion factor is necessary when other gases are used in the experiments due to the different gas expansion. The conversion factor of He for N_2 calibrated mass flow meter is 1.45 [MKS Instruments].

For gas mixtures, gas correction factors (GCF) defined as following are necessary to determine the actual flow rate:

$$GCF = 0.3106 \frac{\sum a_i s_i}{\sum a_i d_i c_{pi}} \qquad (2.1)$$

where, a_i is the fractional flow of gas i (dimensionless), s_i is the molecular structure factor for gas i (dimensionless), d_i is the standard density for gas i (g/L), and c_{pi} is the specific heat capacity for gas i (cal/g℃). The molecular structure factors are 1.030 for monoatomic gases, 1.000 for diatomic gases, 0.941 for triatomic gases, and 0.880 for polyatomic gases [MKS Instruments].

For the diluted gas mixtures used in this work, which are 1% by volume (v/v) of NO_2 in He and 5% v/v O_2 in He, GCF were applied for He only since the contributions of NO_2 and O_2 were negligible. In the case of H_2/He and SF_6/N_2, the flow rates for the individual gases (H_2, He, SF_6, and N_2) were monitored by individual mass flow meters before mixing.

All glass and metal tubes in the flow system were connected through stainless steel Ultra-Torr vacuum fittings (Swagelok). Two direct type mechanical pumps (E2M-12 and E2M-80, BOC Edwards) maintained the base pressure of the flow system at 0.1 Torr, monitored by a pressure transducer (Baratron, MKS Instruments).

A decrease in temperature was expected inside the reduced pressure of flow

tube system due to gas expansion. The direct measurement of temperature inside the flow tube at 100 Torr was approximately one centigrade degree lower than the laboratory temperature.

2.2. OH Production and Calibration

Two different OH sources were used for OH production. The first source employed the following fast reaction ($k_{2.2}$ = 1.3×10^{-10} cm^3 $molecule^{-1}$ s^{-1}) [DeMore *et al.*, 1997] in an excess of H over NO_2:

$$H + NO_2 \rightarrow OH + NO \qquad (2.2)$$

A molecular hydrogen flow was diluted by helium (Airgas, UHP), then discharged inside a Beenaker microwave discharge cavity [Fehsenfeld *et al.*, 1965] operating at 30W to produce hydrogen atoms (~ 5×10^{12} molecule cm^{-3}) available to react with NO_2 (~ 1×10^{12} molecule cm^{-3}, Matheson Tri Gas, 99.5%) in the 0.400-cm i.d. tube. To prevent OH loss via self-recombination, the flow contained OH (~10^{11} molecule cm^{-3}) was expanded in a mixing tube (0.950-cm i.d.) and additionally diluted with nitrogen (N_2, PraxAir), the main carrier gas.

The second OH source used for a NO_x-free conditions follows a sequence of two reactions ($k_{2.3}$ = 1.9×10^{-13} cm^3 $molecule^{-1}$ s^{-1} at 100 Torr [DeMore *et al.*, 1997], $k_{2.4}$ = 7.2×10^{-11} cm^3 $molecule^{-1}$ s^{-1} [Atkinson *et al.*, 2001]) in excess of H radicals:

$$H + O_2 + M \rightarrow HO_2 + M \qquad (2.3)$$

$$H + HO_2 \rightarrow 2\ OH \qquad (2.4)$$

Initially produced HO_2 reacts promptly with the excess H radicals to generate OH. Since Reaction 2.4 is relatively fast, production of HO_2 was negligible (HO_2/OH ~ 1×10^{-2}).

Reaction 2.2 was also used to determine the CIMS sensitivity to OH. For calibration, the dependence of an OH signal was monitored upon introducing known amounts of NO_2, where the NO_2 mixing ratio in a prepared bulb was first verified by UV/Vis spectrometry. The same OH sensitivity was also applied to either production methods.

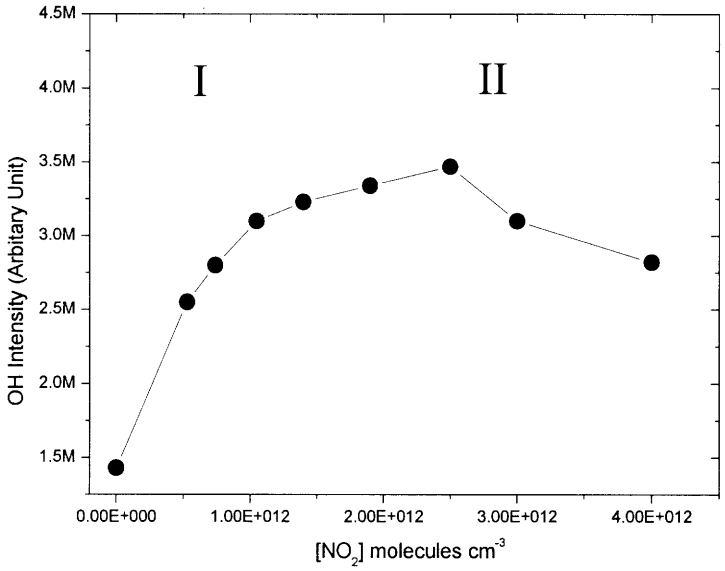

Figure 2.2 The OH intensity dependence on NO_2 concentration ($[NO_2]$). The OH intensity increases linearly in region I, finally reaching a plateau as NO_2 is consumed and secondary reaction take over.

Figure 2.2 shows how OH intensity depends on NO_2 concentrations ($[NO_2]$). At low $[NO_2]$, the OH intensity increased linearly as $[NO_2]$ increased (region I) in accordance with Reaction 2.2. However, at high $[NO_2]$, secondary chemistry of OH becomes important, significantly lowering the OH yield by the following reactions (region II):

$$OH + OH + M \rightarrow H_2O_2 + M \qquad (2.5)$$

$$OH + NO_2 + M \rightarrow HNO_3 + M \qquad (2.6)$$

where the termolecular rate constants ($k' = k[M]$) are 1.6×10^{-12} cm^3 $molecule^{-1}$ s^{-1} and 3.8×10^{-12} cm^3 $molecule^{-1}$ s^{-1} at 100 Torr, respectively. Therefore, the OH calibration was determined based on the experimental data taken from region I. Figure 2.3 shows that typical sensitivities of OH and NO_2 intensities were found to be 4.2 [$\pm$0.3] $\times10^7$ molecule cm^{-3} cps^{-1} and 1.07 [$\pm$0.02] $\times10^9$ molecule cm^{-3} cps^{-1}, respectively. The detection limit for OH was found at ~10^{10} molecule cm^{-3} at 100 Torr.

Since the OH intensity used in the flow tube was typically 20 kcps (kilocounts per second) under dry conditions, the concentration of OH ([OH]) in the flow tube was approximately 8×10^{11} molecule cm^{-3}. However, CIMS sensitivity decreased significantly under wet conditions due to water interference on the chemical ionization reactions as described in Chapter 1. For example, the OH sensitivity at 6% of RH was one order of magnitude smaller than that under dry conditions.

Measured OH reaction probabilities were independent of the OH sources used. However, it should be noted that NOx-free OH source (Reactions 2.3 and 2.4) typically resulted in a relatively higher OH yield, and therefore, was primarily used in our experiments to study the effects of relative humidity on OH uptake by surfaces of tropospheric importance (see Chapter 3). However, interference by secondary reactions between H, O_2, and HO_2 could be avoided by using the first source (Reaction 2.2) for the product study (see Chapter 4).

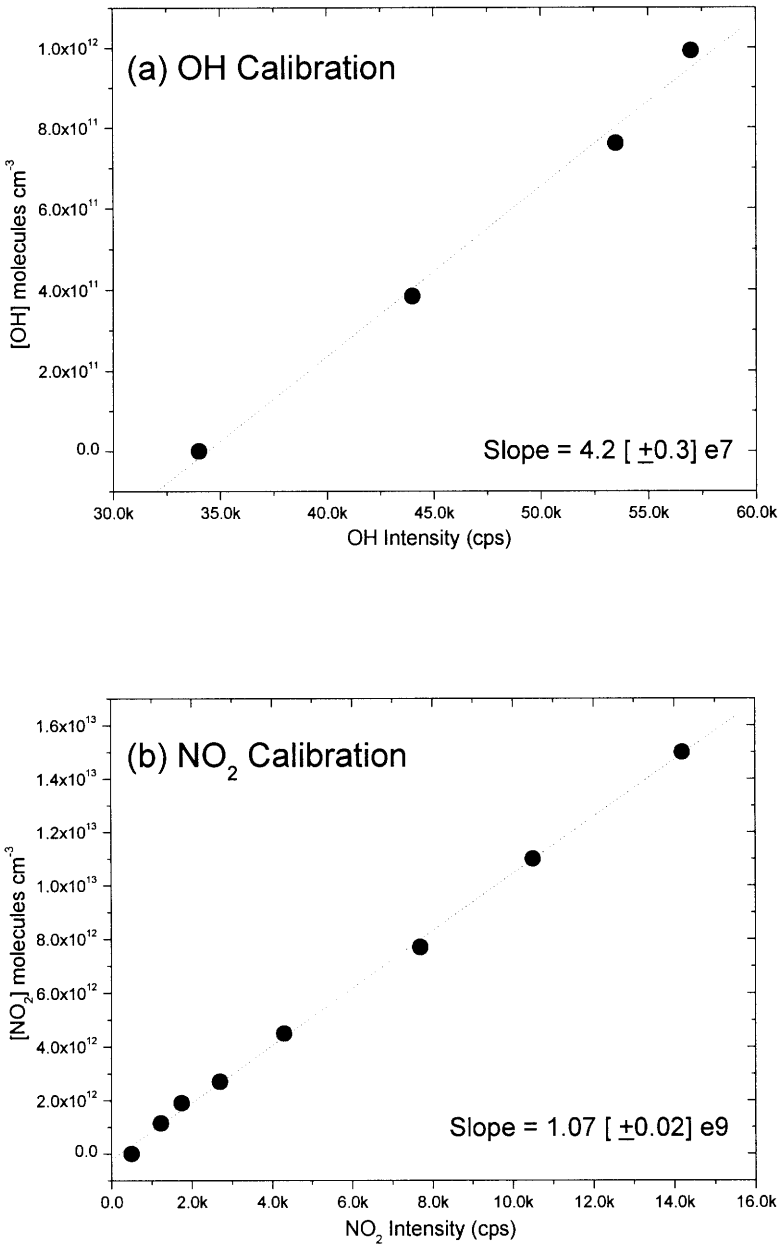

Figure 2.3 OH (a) and NO_2 (b) calibrations

2.3. Water Bubbler

Relative humidity of up to ~50% was produced in the flow tube system by

means of a water bubbler. An additional N_2 flow passed through a porous disk in a water bubbler (70 cm o.d.) to carry saturated water vapor as described in Figure 2.1 and Figure 2.4. The water vapor contained flow then was introduced to a mixing tube where it was mixed with a main carrier flow.

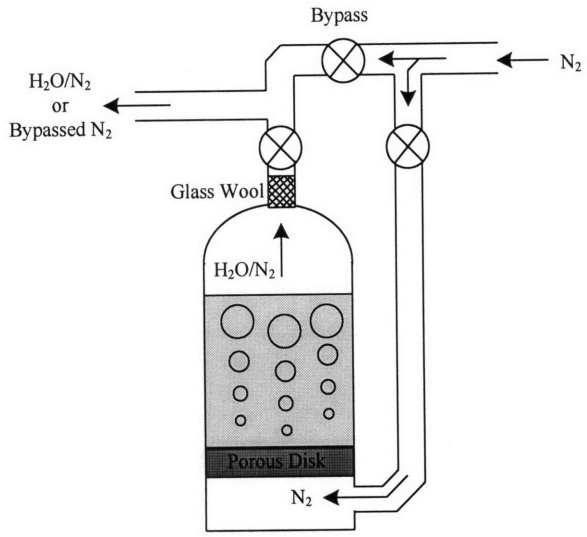

Figure 2.4 A schematic of the water bubbler

Glass wool was placed in the outlet of the water bubbler to refine the flow from water droplets coming from bubbling action at the interface. A total pressure of 100 Torr inside the flow tube was maintained by adjusting the main carrier gas flow. To estimate the partial pressure of water vapor, the same N_2 flow bypassed a water bubbler and the difference in pressures produced by the wet and dry N_2 flows was used based on the Dalton's law of partial pressures:

$$P_{H_2O} = P_{total} - P_{bypass} \qquad (2.7)$$

Then relative humidity was determined according to Equation 1.19 using the partial pressure of water and the saturated vapor pressure of water at given temperature as listed in Table 2.1 [Haar *et al.*, 1984; Lide *et al.*, 2007].

Table 2.1 Saturated water vapor pressure

Temperature ℃	Vapor Pressure Torr	Temperature ℃	Vapor Pressure Torr
18	15.5	22	19.8
19	16.5	23	21.1
20	17.5	24	22.4
21	18.7	25	23.8

2.4. Parallel Reactor Tubes

Two identical reactor tubes (0.950-cm i.d.) were placed downstream of the OH production region and mixing tube. The each reactor was filled with 60 borosilicate glass beads (3 mm o. d., Chemglass). To remove any organic and inorganic deposition, the beads were cleaned with sulfuric, nitric, and hydrofluoric (HF) acids prior to running an experiment. Exposure to HF for 10 seconds was sufficient to remove residual organic/inorganic material. The efficient reaction between HF and SiO_2 changed the roughness of the glass beads surface as can be seen in Figure 2.5.

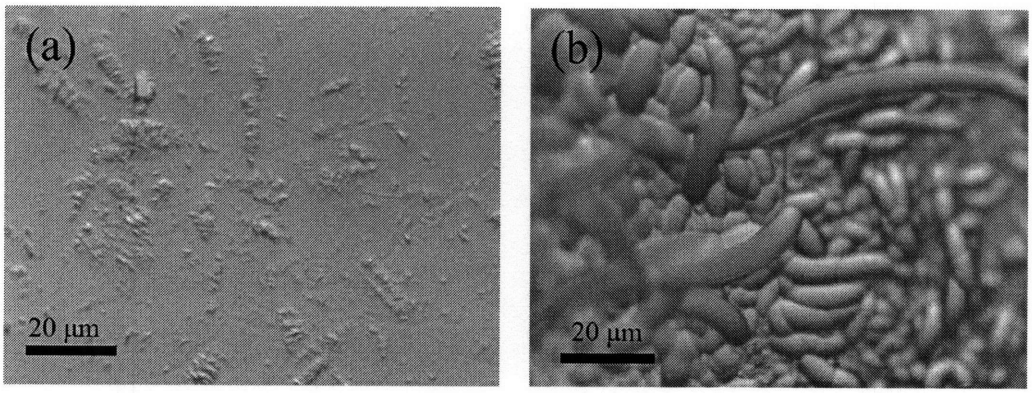

Figure 2.5 Optical microscopic images of raw borosilicate glass bead surface (a) and HF treated surface (b).

Nevertheless, testing both the untreated and HF-treated glass beads showed no difference in OH uptake, indicating that the pre-treatment did not affect reactivity measurements.

In our study, the glass beads were coated with the organic or inorganic materials and placed in the reactor tube, while beads in a reference tube were coated with halocarbon wax. Detailed description of the surface preparation is given in Section 2.2. It should be noted that the beads-packing caused a gas-dynamic resistance to a flow which led to a pressure gradient of 6-9 Torr. This pressure drop was neglected and the measured flow tube pressure (100 Torr) upstream of the beads was assumed to be accurate within ±5% error.

Using two stop valves, the total flow may be switched between the reactor tube and the reference tube to compare OH uptake on a reactive and inert surfaces. A parallel reactor tubes is particularly useful for the following reasons:

(1) Due to the beads packing design, the use of a movable injector that normally is employed as a movable radical source in kinetic studies to vary reaction time is not applicable in the present work and so the referencing OH heterogeneous loss on a reactive surface to that on an inert material seems to be the most appropriate way to determine the reaction probability, γ_{OH}. The detailed description of the routine used to determine γ_{OH} in a flow tube filled with beads is shown in Section 3.3.3.4. It should be noted that in our kinetics method, for a reference surface, such as halocarbon wax, a value of γ_{OH} should be known and measured accurately which is the case for halocarbon wax 600 series; the value of 6×10^{-4} was measured previously in many studies (see, for example, Bertram *et al.*, 2001).

(2) In fact, the reference technique does not require knowing the dependence of the CIMS sensitivity to OH on RH because of its subtraction when two OH signals are compared (see Chapter 3). The same is applied for by-products produced in the reaction of OH with flow tube walls coated with halocarbon wax: if Cl-contained species is formed upon the OH exposure of flow tube walls, it will be subtracted when both OH signals after reacting with reactive and inert surfaces are compared (see Chapter 4).

2.5. Flow Rates and Velocities

The two gas flows of N_2 and He formed a carrier gas flow in a flow tube with flow rates of 0.8 SLPM (standard liters per minute) and 1.75 SLPM, respectively, for a total flow rate of 2.55 SLPM. A linear transport velocity under the total flow (in cm s^{-1}) was determined as follows:

$$v = \frac{w}{s \cdot p} \cdot \frac{T}{273} \cdot \frac{1000}{60} \qquad (2.8)$$

where w is the total flow rate in L/min, T is the gas temperature in a flow tube in K, s is the cross section of a flow tube in cm^2, p is the pressure in a differential flow tube in Torr, and 1000 and 60 are the conversion factors of L to cm^3 and of minutes to seconds, respectively. Since the inner diameter of the reactor was 0.95 cm, v was calculated to be 480 cm/s.

Under given conditions, the Reynolds number as defined in Equation 2.9 was 341, corresponding to the laminar flow (Re << 2300)

$$\mathrm{Re} = \frac{2rv\rho}{\eta} \qquad (2.9)$$

where r is the radius of a flow tube, ρ is the gas density, and η is the gas viscosity.

As seen from Equations 2.8 and 2.9, flow velocity and the Reynolds number depend strongly on a radius of the flow tube. When the equations are applied for the beads-packing design, these equations produce different values of the parameters (see Section 3.3.3).

2.6. Pressure Reduction

At downstream of differential flow tube a total flux was then differentially pumped out so that only a small fraction (~1%) of the total flow was introduced via a skimmer of 1- mm I.D. to the chemical ionization region for further detection of OH; the rest of a total flow was pumped out by a mechanical pump (E2M-12, BOC Edwards). The differential pumping helped to reduce the pressure in the chemical ionization region and in addition to remove water vapors to minimize water-cluster formation influencing OH detection. Our experiments showed that the enhancement in OH sensitivity as a result of pumping ranged from 50% (at 4% RH) to a factor of 10 (at 48% RH).

For the product study under dry and low RH conditions (see Chapter 4), differential pumping was shut off to maintain high sensitivity to the gas-phase products, especially chlorine-containing species, enabling detection of the gas phase species without additional loss.

2.7. Detection Method

In the present studies, OH and gas-phase products were detected using chemical ionization mass spectrometry (CIMS). The chemical ionization mass spectrometer consists of a custom-built chemical ionization region (CI region) coupled to a

commercial quadrupole mass spectrometer (Extrel CMS) used for mass selection and electron multiplier (Channeltron) for ion detection. The schematic of the CIMS used in this work is shown in Figure 2.6.

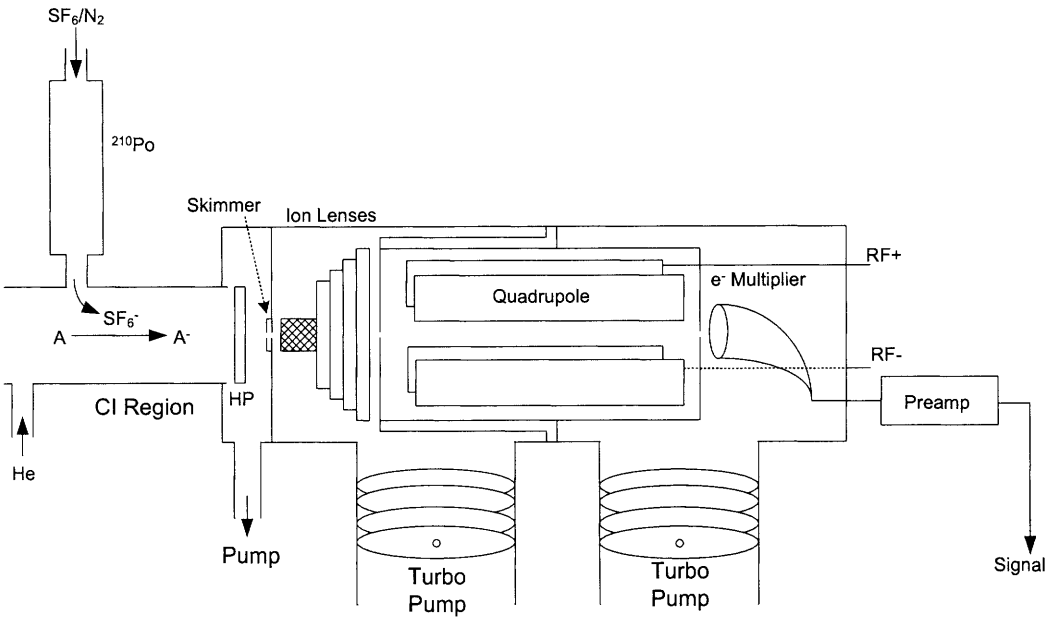

Figure 2.6 The schematic of the CIMS setup

2.7.1. CI region

To enable their detection, OH radicals and gas phase reaction products were ionized by charge transfer reactions with sulfur hexafluoride (SF_6^-) as the parent ion. To produce SF_6^- ions, a small flow of SF_6 (Matheson Tri Gas, 99.99%) was initially diluted with N_2 to 0.1% by volume and passed through a radioactive polonium source (NRD, ^{210}Po). The SF_6^-/N_2 flow (1.5 SLPM) was introduced to a stainless steel tube of 1-inch o.d. coated with halocarbon wax. In the CI region, SF_6^- was used to ionize the following species:

$$OH + SF_6^- \rightarrow OH^- + SF_6 \quad (2.10)$$

$$NO_2 + SF_6^- \rightarrow NO_2^- + SF_6 \quad (2.11)$$

$$Cl_2 + SF_6^- \rightarrow Cl_2^- + SF_6 \quad (2.12)$$

$$HCl + SF_6^- \rightarrow HClF^- + SF_5 \text{ (or } SF_5Cl^- + HF) \quad (2.13)$$

with the rate constants, $k_{2.10} = 2\times10^{-9}$ cm^3 molecule^{-1} s^{-1} [Lovejoy *et al.*, 1990], $k_{2.11} = 1.4\times10^{-10}$ cm^3 molecule^{-1} s^{-1} [Huey *et al.*, 1995], $k_{2.12} = 6.1\times10^{-11}$ cm^3 molecule^{-1} s^{-1} [Streit, 1982], and $k_{2.13} = 4.2\times10^{-10}$ cm^3 molecule^{-1} s^{-1} [Streit, 1982]. A negative potential of -10 V was applied to the CI region to prevent the loss of negative ions on a stainless steel surface, and to further accelerate the ions for detection.

As described in Chapter 1, water vapor interacts with SF_6^- by forming water complexes, such as $SOF_4^-(H_2O)_m$, $F^-(HF)_2(H_2O)_n$, and $F^-(HF)_n$ [Wickramanayake, 1986, Arnold *et al.*, 2001]. This loss of the parent ions would result in the significant lowering CIMS sensitivities to the detected species including OH. Moreover, in the CI region, water vapor readily forms water clusters with OH^-, such as $OH^-(H_2O)_n$, also reducing the OH sensitivity [Salcedo *et al.*, 2004]. The distribution of $F^-(HF)_n$ and SF_4O^- (a) and $OH^-(H_2O)_n$ (b) at various RH is shown in Figure 2.7.

To increase the CIMS sensitivity under wet conditions, an additional He flow of 2 SLPM was added to reduce cluster formation [Arnold *et al.*, 2001]. Although the He-buffer flow increased a total pressure in the CI region from 1.9 Torr to 10 Torr resulting in lowering OH sensitivity under dry condition as seen in Figure 2.8, however, the CIMS sensitivity increased significantly under wet conditions with He-buffer flow. Our experiments showed that for example, the OH intensity increased by factor of 17 with the He buffer flow at 38% RH, while it was barely observed without He buffer flow.

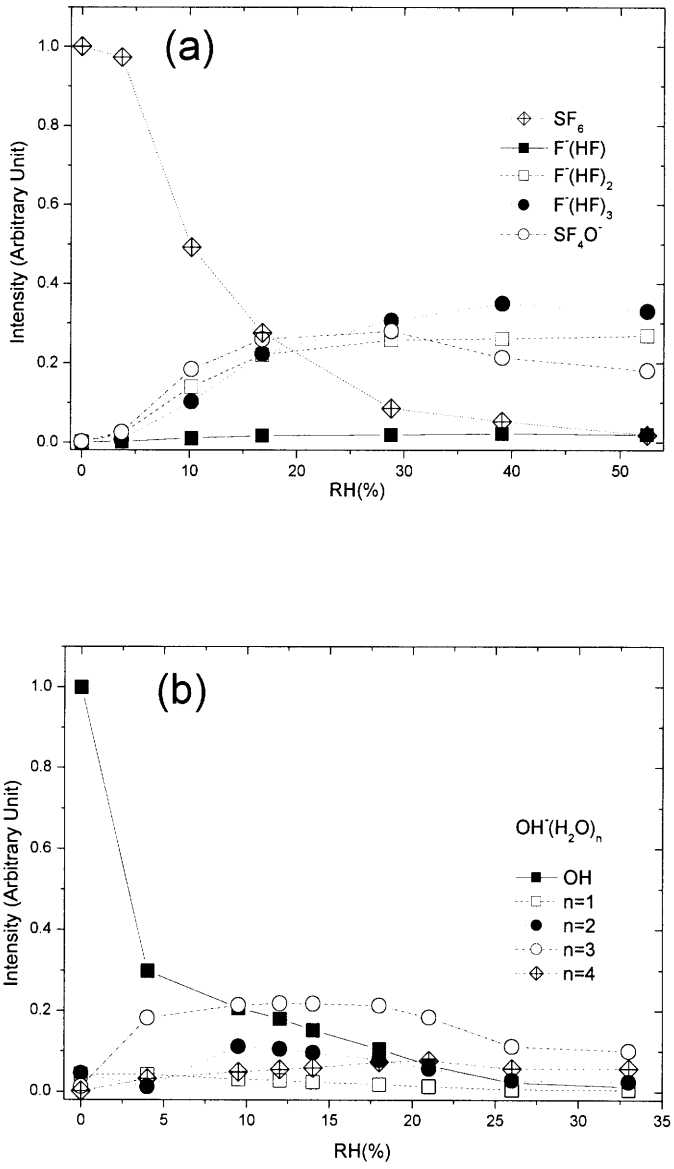

Figure 2.7 Distributions of $F^-(HF)_n$ and SF_4O^- (a), and $OH^-(H_2O)_n$ (b) in the presence of RH. There is no correlation in the arbitrary units between (a) and (b).

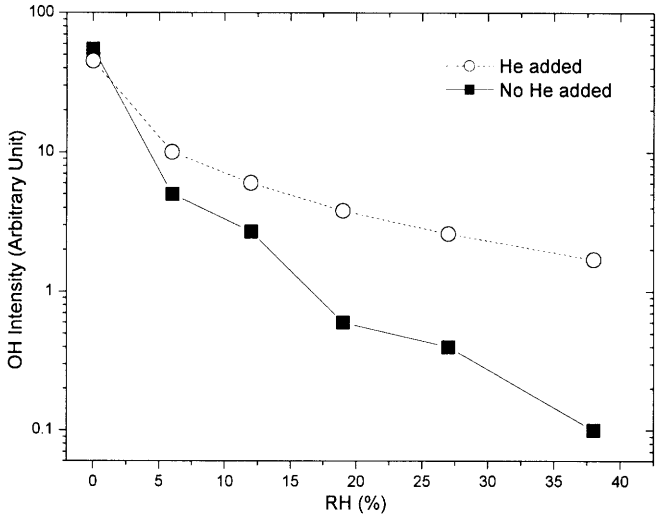

Figure 2.8 The OH intensity dependence on RH with (■) and without (○) He buffer flow

2.7.2. Mass Spectrometer

Only a small amount of a flow containing both neutral and ionized species was introduced to the mass spectrometer (MS) via a 100-μm pinhole skimmer biased at -5 V. Ions were focused into the MS through a negatively charged metal ring (high pressure lens) placed immediately after the CI region. In contrast, most amount of flow was pumped out by a mechanical pump (E2M-80, BOC Edwards) to maintain the low pressure of the MS, otherwise, the MS would be damaged.

An array of four ion lenses applied with different potentials, located just behind the pinhole and inside the MS chamber, was used to further focus ions into the quadrupole. A potential of approximately 3 kV impressed across the length of a continuous-dynode type electron multiplier (Channeltron 4870E, Burle Electro-Optics) induced a cascade of electrons by the strike of the analyzed ions with approximately 10^8

of gain. The resulting signal was pre-amplified (MTS-100, Advanced Research Instruments Corp.) then digitized and processed with a Merlin Automation System (Extrel).

Two turbo molecular pumps (360CSV, Leybold; STP-400, Seiko-Seiki) each with backing pumps (E2M-12, BOC Edwards; SD-450, Varian Inc.) were used to maintain the MS pressure below 8×10^{-6} Torr.

References for Chapter 2

S. T. Arnold and A. A. Viggiano, Turbulent ion flow tube study of the cluster-mediated reactions of SF_6^- with H_2O, CH_3OH, and C_2H_5OH from 50 to 500 Torr, *J. Phys. Chem. A*, 105, 3527-3531, 2001.

R. Atkinson, D. L. Baulch, R. A. Cox, J. N. Crowley, R. F. Hampson, Jr, J. A. Kerr, M. J. Rossi, and J. Troe, Summary of evaluated kinetic and photochemical data for atmospheric chemistry, IUPAC Subcommittee on Gas Kinetic Data Evaluation for Atmospheric Chemistry Web Version, 2001.

A. K. Bertram, A. V. Ivanov, M. Hunter, L. T. Molina, and M. J. Molina, The reaction probability of OH on organic surfaces of tropospheric interest, *J. Phys. Chem. A*, **105**, 9415-9421, 2001.

W. B. DeMore, S. P. Sander, C. J. Howard, A. R. Ravishankara, D. M. Golden, C. E. Kolb, R. F. Hampson, M. J. Kurylo, and M. J. Molina, *Chemical Kinetics and Phtochemical Data for Use in Stratospheric Modeling*, Evaluation Number 12, JPL Publication 97-4, NASA Jet Propulsion Laboratory, Pasadena, 1997.

F. C. Fehsenfeld, K. M. Evenson, and H. P. Broida, Microwave discharge cavities operation at 2450 MHz, *Rev. Sci. Instrum.*, **36**, 294-298, 1965.

L. Haar, J. S. Gallagher, and G. S. Kell, *NBS/NRC steam tables*, Hemisphere Publishing Corp., New York, 1984.

L. G. Huery, D. R. Hanson, and C. J. Howard, Reactions of SF_6^- and I^- with atmospheric trace gases, *J. Phys. Chem.*, **99**, 5001-5008, 1995.

E. R. Lovejoy, T. P. Murrells, A. R. Ravishankara, and C. J. Howard, Oxidation of CS2 by reaction with OH. 2. Yields of HO2 and SO2 in Oxygen, *J. Phys. Chem.*, **94**, 2386-2393, 1990.

D. R. Lide Ed., *CRC Handbook of Chemistry and Physics (88th Edition)*, CRC Press, Boca Raton, 2007.

D. Salcedo, P. W. Villalta, V. Varutbangkul, J. C. Wormhoudt, R. C. Miake-Lye, D. R. Worsnop, J. O. Ballenthin, W. F. Thorn, A. A. Viggiano, T. M. Miller, R. C. Flagan, and J. H. Seinfeld, Effect of relative humidity on the detection of sulfur dioxide and sulfuric acid using a chemical ionization mass spectrometer, *Int. J. Mass Spectrom.*, **231**, 17-30, 2004.

D. A. Skoog, F. J. Holler, and T. A. Nieman, *Principles of instrumental analysis (5th edition)*, Harcourt Brach & Company, Orlando, 1998.

G. E. Streit, Negative ion chemistry and the electron affinity of SF_6, *J. Chem. Phys.*, **77**, 826-833, 1982.

MKS Instruments, http://www.mksinst.com/docs/ur/flowfaq.aspx.

P. P. Wickramanayake, G. J. Gardner, K. W. Michael Siu, and S. S. Berman, Ion/Molecule reaction between sulfur hexafluoride negative ion and water under atmospheric pressure ionization mass spectrometric conditions, *Int. J. Mass Spectrom. and Ion Proc.*, **69**, 39-43, 1986.

CRC Handbook of Chemistry and Physics (88th Edition), CRC Press, Boca Raton, 2007.

Chapter 3

The Effects of Relative Humidity on OH Uptake by Surfaces of Tropospheric Importance

3. 1. Introduction

Due to its relatively large dipole moment and capability for strong hydrogen bonding, a water molecule may be taken up efficiently by surfaces with high surface tension [Liu *et al.*, 1996; Ball, 1999; Aloisio *et al.*, 2000; Staikova *et al.*, 2001; Mantz *et al.*, 2002]. Adsorbed water can efficiently affect, either inhibiting or enhancing, OH uptake through modifying the nature of surface active sites, which can in turn lead to different reaction mechanisms than under dry conditions. For instance, exposing OH to carbonaceous surfaces results in increased hydrophilicity with a greater water adsorption capacity [Bertram *et al.*, 2001, Zuberi *et al.*, 2005]]. A water adlayer can block active sites from further reaction [Remorrov *et al.*, 2002], or may enhance the chemical reactivity of active sites by increasing the coordination number and causing partial dissociation in the aqueous environment. For inorganic surfaces, adsorbed water can notably enhance the surface ionic mobility, thereby affecting ionic concentrations [Hemminger, 1999], as well as pH of an aerosol surface. All of these effects are expected to influence OH uptake, and in particular, the reaction mechanism. For example, segregation of halide ions observed at a surface of sea salt aerosol particles under wet conditions was found to be likely a key step in formation of gas-phase halogen-containing products [Dement'ev *et al.*, 2004].

To date, very little is known regarding the mechanism of OH uptake by aerosol surfaces under wet conditions. Only one study on OH uptake by organic surfaces reports direct measurement of the reaction probability, under conditions of low pressure and relative humidity (RH) < 1% [Molina *et al.*, 2004]. Results of this study showed that the OH reaction probability is independent of the presence of water vapor for initially hydrophobic organic surfaces, such as aliphatic, aromatic, and soot. OH

uptake measurements for deliquesced sea salt and its individual components have been performed at RH ≥ 80% [Oum *et al.*, 1998; Knipping *et al.*, 2002; Laskin *et al.*, 2006]. Results of these indirect measurements indicated noticeable enhancement in the OH uptake rate on the surfaces exposed to water vapor.

In this chapter, a new complementary approach has been developed and used to explore experimentally the RH effect on OH uptake by various organic and inorganic surfaces relevant to the troposphere. The new approach is based on the flow tube reactor system described previously (see Chapter 2), a virtual flow tube approximation and surface dilution technique that enables measurements of radical uptake with the initial probability near unity at high pressure and relative humidity.

3. 2. Experimental

The details of the experimental setup including the flow tube system equipped with CIMS were described in Chapter 2.

3.2.1. Radical Production

Among the two methods for OH production, the 'H + O_2 + M' scheme (Reaction 2.3 and 2.4) was employed due to its high radical yield.

$$H + O_2 + M \rightarrow HO_2 + M \qquad (2.3)$$

$$H + HO_2 \rightarrow 2\ OH \qquad (2.4)$$

where the rate constants are $k_{2.3} = 1.9\times10^{-13}$ cm^3 $molecule^{-1}$ s^{-1} at 100 Torr [DeMore *et al.*, 1997] and $k_{2.4} = 7.2\times10^{-11}$ cm^3 $molecule^{-1}$ s^{-1} [Atkinson *et al.*, 2001]. The sensitivity of OH was 4.2 [$\pm$0.3] $\times10^7$ molecule cm^{-3} cps^{-1} under dry conditions, while it

became smaller under wet conditions [Section 2.2].

3.2.2. Experimental Procedure

The system was normally allowed to stabilize under flow conditions for thirty minutes before acquiring data on OH concentration. The OH peak was integrated in each mass spectrum to determine a peak area, and then average ~ 200 points to obtain a median and a standard deviation. Once the signal intensity of OH was acquired upon exposing the OH to a material surface of interest, the gas flow was switched to a reference flow tube to acquire the reference signal for the comparison of which comprised a single experiment. A set of three to four experiments at each RH was repeated to confirm reproducibility of the data as well as for statistical considerations.

The RH was increased incrementally from 0% to 48%, followed by an extra measurement taken at 0% RH to evaluate possible aging of surface by OH-oxidation within the course of the experiments.

A main flow in the flow system was the mixture of N_2 , He, and water vapor with the flow rates 1.75 SLPM, 0.80 SLPM, and 0 SLPM, respectively, under dry conditions, and 1.45 SLPM, 0.80 SLPM, and 0.3 SLPM, respectively, at RH = 48%. Experiments were performed at room temperature with ±1 ℃ tolerance.

3.2.3. Surface Preparation

The surfaces of the glass beads were coated with the organic and inorganic materials of interest listed below.

(1) Reference : Halocarbon wax of a 600 series;

(2) Organic materials : paraffin wax, pyrene($C_{16}H_{10}$), glutaric acid ($C_5H_8O_4$),

methane soot;

(3) Inorganic materials:

(a) Sea salt compounds : NaCl, $MgCl_2$, Na_2SO_4, $CaCl_2$, KCl, Sea salt;

(b) Mineral dust compounds : SiO_2, Al_2O_3;

For the reference coating, we carefully controlled the temperature with a heat gun in order to melt halocarbon wax without its decomposition followed by adding it into a beaker with glass beads. The glass beads were vigorously stirred to ensure a thin and smooth coating as halocarbon wax solidified on the surface of the beads at room temperature. The coated surface was observed using an optical microscope (Zeiss Axioskop 20 microscope equipped with 50 x objectives). As shown in Figure 3.1 (a), the surface was evenly and completely covered.

The same method was applied to prepare paraffin wax (J.T. Baker), pyrene (99.5%, Sigma-Aldrich), and glutaric acid (99%, Sigma-Aldrich) coatings. The optical microscopic image shows that paraffin wax surface (Figure 3.1 (b)) was rougher than the halocarbon wax surface. However, it was shown that the difference in the surface roughness contributes negligibly to OH uptake (See Section 2.4). The pyrene surface shown in Figure 3.1 (c) was prepared from a mixture of halocarbon wax and pyrene in order to lower surface reactivity towards OH uptake (See Section 3.3.3.3).

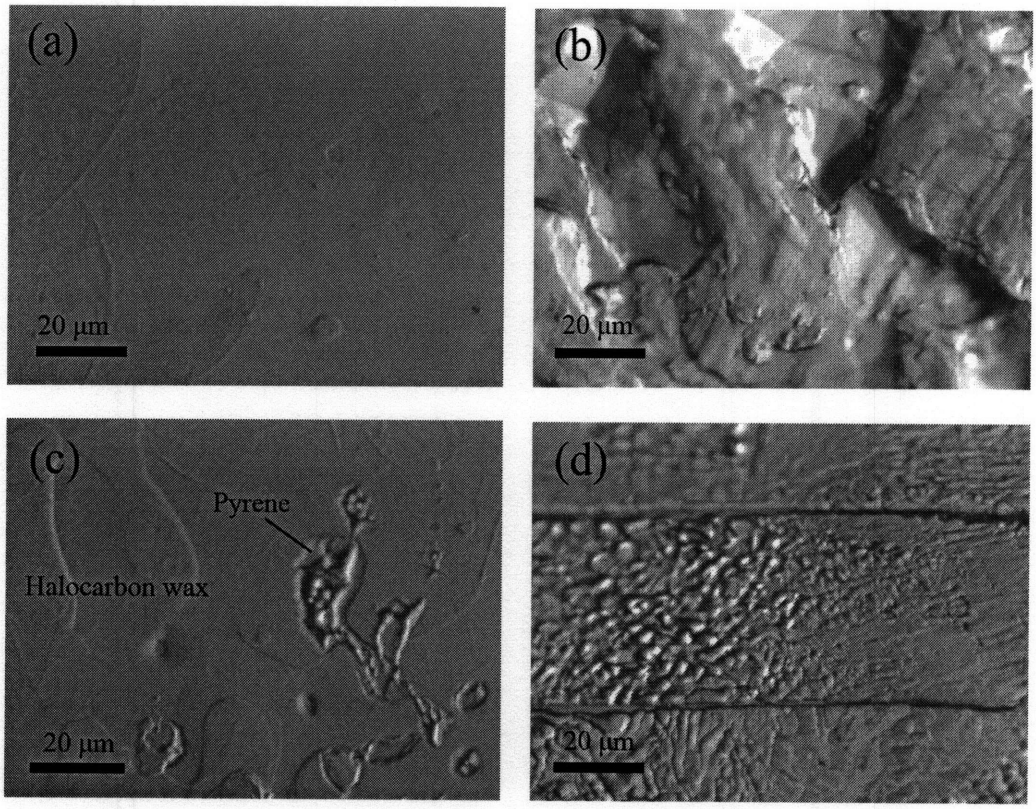

Figure 3.1. Optical microscopic images of halocarbon wax (a), paraffin wax (b), pyrene (c), and glutaric acid (d) coatings.

In other cases, NaCl for example, the surface coatings were prepared in the following way for homogeneous thin coating on the surface of a spherical shape. First, halocarbon wax was pre-coated on the glass beads as described above. Then, the pre-coated beads with the fine powder of materials in a Petri dish were shaken vigorously to coat the aerosol powder on the sticky surface. The coverage of material of interest was controlled by adding different amount of powder to the Petri dish.

A methane-soot surface was prepared using the above method by depositing soot collected from a methane-air flame produced with a standard torch. Figure 3.2 shows the optical microscopic image of methane soot coating on the halocarbon waxed beads.

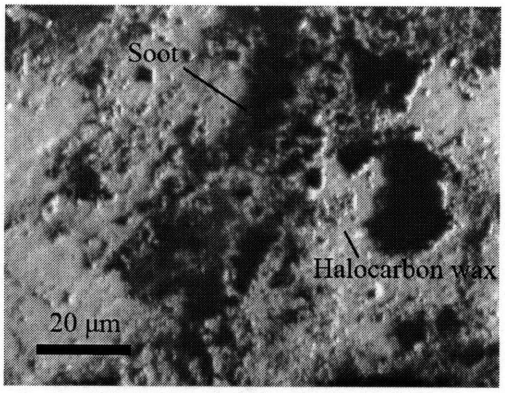

Figure 3.2. Optical microscopic image of methane soot. The soot was partially coated on the halocarbon wax pre-coated surfaces.

The aerosol materials in this work were NaCl (Mallinckrodt, 99.9%), $MgCl_2$ (Sigma-Aldrich, 99.5%), Na_2SO_4 (Sigma-Aldrich, ≥99.0%), KCl (Fisher Scientific, ACS grade), $CaCl_2$ (Mallinckrodt, 99%), Sea Salt (Sigma-Aldrich), SiO_2 (Sigma-Aldrich, 99.6%), and Al_2O_3 (Sigma-Aldrich, 99.9%). In addition, two mixtures were prepared: One was, so called, 'synthetic sea salt' which consisted of the same components in the same ratio as real sea salt. In the other mixture, so called, 'synthetic sea salt without $MgCl_2$', only $MgCl_2$ was removed from synthetic sea salt. The prepared aerosol surfaces were dried for overnight under vacuum (< 0.1 Torr) after being packed into the reactor. This process is required to evaporate water vapors adsorbed on the coatings during the surface preparation [Peters *et al.*, 1997].

Figure 3.3 shows the optical microscopic images for NaCl, Na_2SO_2, KCl, and sea salt, which were partially covered for lowering reactivity towards OH heterogeneous reaction (See Section 3.3.3.3 for details). Water absorption caused the inorganic crystals to appear more round since the images were taken under atmospheric conditions (RH = 50% - 70%). Images for $MgCl_2$ and $CaCl_2$ surfaces were unavailable to be taken within the certain time frame due to their extremely high hygroscopic properties.

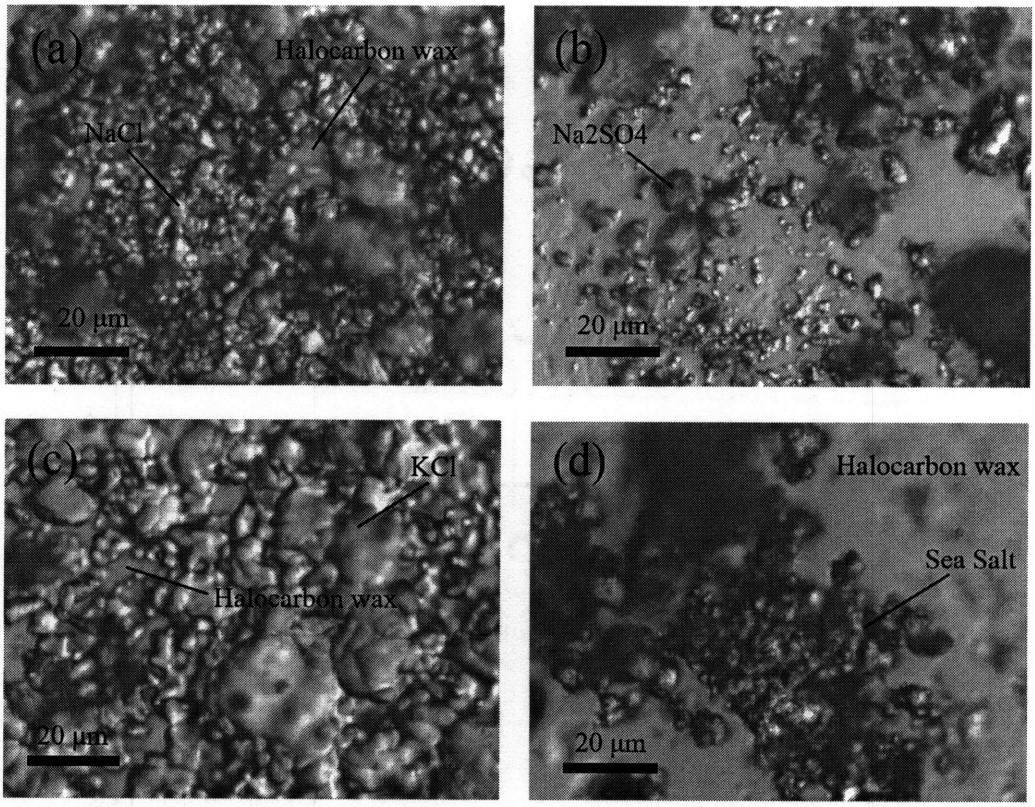

Figure 3.3. Optical microscopic images of NaCl (a), Na_2SO_4 (b), KCl (c), and Sea Salt (d). The inorganic aerosol surfaces were partially coated on the halocarbon wax pre-coated surfaces.

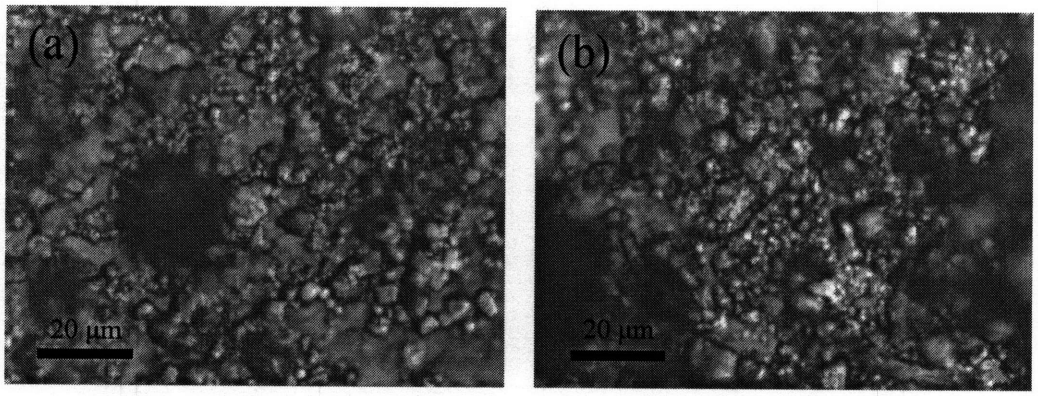

Figure 3.4. Optical microscopic images of synthetic sea salt (a) and synthetic sea salt without $MgCl_2$ (b). Some crystals were out of focus.

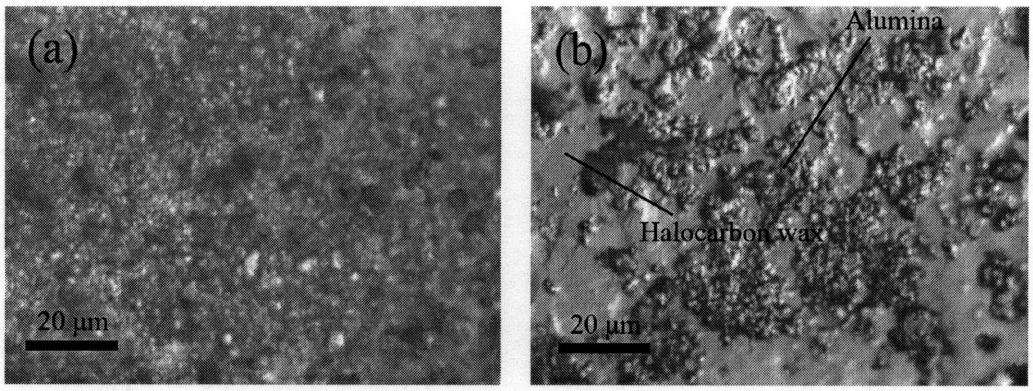

Figure 3.5. Optical microscopic images of SiO_2 (Silica) (a) and Al_2O_3 (Alumina) (b). Alumina was partially coated on the halocarbon wax pre-coated surfaces.

There was no significant difference in the appearances of the synthetic sea salt and the synthetic sea salt without $MgCl_2$ as seen in Figure 3.4. Figure 3.5 shows the optical microscopic images of SiO_2 and Al_2O_3.

Although the images shows increases in roughness caused from powder coatings, it is assumed that there is no significant effect from roughness changes in the same manner as paraffin wax coating discussed above.

3.2.4. Theoretical Method

To characterize $OH\text{-}(H_2O)_n$ and $OH^-\text{-}(H_2O)_n$ complexes, *ab initio* calculations were performed to obtain the global minima of these complexes. Geometries of the local minima of the complexes were optimized at the hybrid density functional B3LYP level of theory using a 6-31G(d,p) basis set. The energies for the optimized geometries of the complexes corrected by the zero-point energy (ZPE) were calculated using the same method and basis set. All calculations were carried out using GAUSSIAN 03 [Frisch et. al., 2003].

3. 3. Results and Discussion

3. 3. 1. Reaction Probability, γ

For first-order loss kinetics, the observed rate constant (k_{obs}) is determined by the following equation:

$$-\ln\frac{[OH]_t}{[OH]_0} = k_{obs}t \qquad (3.1)$$

where t is the reaction time, and $[OH]_0$ and $[OH]_t$ are the concentrations of OH initially and at time t, respectively. Since the concentration is proportional to the intensity of the detection signal, Equation 3.1 can be rewritten in the following way:

$$-\ln\frac{I_{OH}^t}{I_{OH}^0} = k_{obs}t \qquad (3.2)$$

where I_{OH}^0 and I_{OH}^t are the signal intensities of OH initially and at time t, respectively.

In a cylindrical flow tube, the additivity of kinetic resistances allows determination of the chemical kinetics rate constant (k_{kin}) from the observed rate constant of heterogeneous loss [Semenov, 1943; Brown, 1978; Zasypkin *et al.*, 1997; Bertram *et al.*, 2001]:

$$\frac{1}{k_{obs}} = \frac{1}{k_{kin}} + \frac{1}{k_{diff}} \qquad (3.3)$$

$$k_{kin} = \frac{\gamma \cdot c_{avg}}{(2-\gamma)\cdot r} \qquad (3.4)$$

$$k_{diff} = \frac{3.66 D_c}{r^2 P} \qquad (3.5)$$

where k_{diff} is the diffusion-controlled reaction rate constant (s^{-1}), r is the reactor radius (cm), D_c is the diffusion coefficient of the reactant in the carrier gas ($cm^2\ s^{-1}$ Torr), P is the pressure (Torr), and c_{avg} = 60,197 cm s^{-1} is the mean thermal velocity of OH at 293

K. Therefore the reaction probability, γ, is determined as follows:

$$\gamma = \frac{2rk_{kin}}{c_{avg} + rk_{kin}} \tag{3.6}$$

In the case of a carrier gas consisting of a mixture of different gases, D_c is determined by the combination rule for the diffusion coefficients of individual gases ($D_{OH\text{-}i}$) with a mixing ratio (α_i) according to the Blanc's law [Blanc, 1908; Fairbanks *et al.*, 1950; Hanson *et. al.*, 1992]:

$$D_c^{-1} = \sum_i \alpha_i \cdot D_{OH-i}^{-1} \tag{3.7}$$

The OH diffusion coefficients in N_2 and He ($D_{OH\text{-}N2}$ and $D_{OH\text{-}He}$) were reported at 163 ± 20 cm^2 Torr s^{-1} and 665 ± 35 cm^2 Torr s^{-1}, respectively [Bertram *et al.*, 2001; Ivanov *et. al.*, 2007]. In our studies, contribution of water vapor to net OH diffusion was assumed to be negligible since the OH diffusion coefficient in H_2O ($D_{OH\text{-}H2O}$ = 171 cm^2 Torr s^{-1} at 296 K) [Hanson *et al.*, 1992; Ivanov *et al.*, 2007] is very close to that in N_2. Moreover, the N_2 was the major gas in the flow even under high relative humidity. As shown in Appendix 3-I, for example, 12 Torr of water vapor corresponding to 50% of RH contributes only 1% to the net OH diffusion coefficient under typical experimental conditions.

3. 3. 2. The Relative Intensity of OH, $R_{surface}$

In kinetics studies, a movable injector is employed to vary a reaction time of heterogeneous reaction by changing the exposed fraction of a wall surface coated with material of interest to a reactive gas-phase species as it is schematically shown in Figure 3.6.

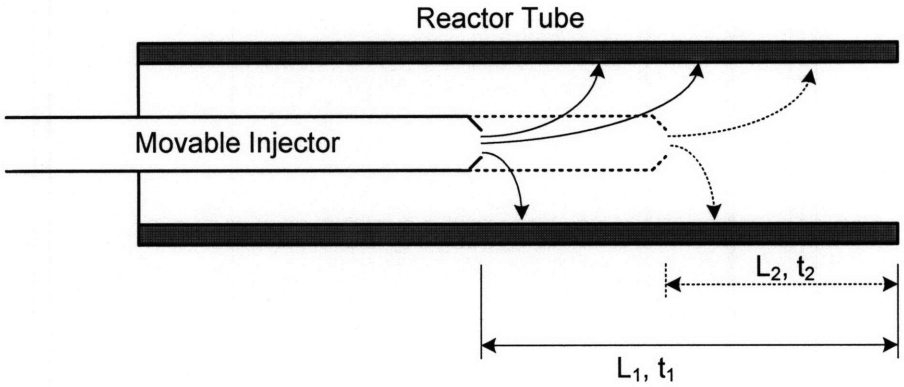

Figure 3.6. The schematic of a movable injector employed in kinetic studies of heterogeneous reactions. Gas-phase species of interest are effused from the end of a movable injector and react on the wall coated with material of interest. Variable positions of the movable injector change the fraction of a wall surface corresponding to different exposed lengths (L_1 and L_2) or different reaction times (t_1 and t_2).

However, use of a bead-packing reactor tube prohibits employment of a movable injector in the present work. Instead, two OH signals ($I^{OH}_{surface}$ and $I^{OH}_{reference}$) corresponding to the OH concentrations measured after exposure to the surface of interest and the reference (halocarbon wax) ($[OH]_{reaction}$ and $[OH]_{reference}$, respectively) are compared. The *relative intensity of OH for the heterogeneous reaction on the surface of interest*, R_{OH}, is defined in the present work as the ratio of OH signals measured when a OH-containing flow switched from a reaction flow tube to a reference tube:

$$R_{OH} = \frac{[OH]_{Surface}}{[OH]_{reference}} = \frac{I^{OH}_{Surface}}{I^{OH}_{reference}} \qquad (3.8)$$

Since each OH concentration is described in Equation 3.1, R_{OH} relates to the observed rate constants for each material as follows (See Appendix 3-II):

$$R_{OH} = \exp[-(k^{surface}_{obs} - k^{reference}_{obs}) \cdot t] \qquad (3.9)$$

Therefore, R_{OH} can be estimated based the known value of the OH reaction probabilities for a surface material and the halocarbon wax ($\gamma_{OH}^{\text{Halocarbon wax}} = 6\times10^{-4}$ [Bertram *et. al.*, 2001]) using Equations 3.8 and 3.9, and vice versa, any unknown OH reaction probability can be determined if R_{OH} is known.

To our knowledge, there is no theoretical consideration of heterogeneous radical loss in a flow tube packed with beads. In order to estimate k_{het} and t in a flow tube used in the present work, we simplified the reactor design by approximating the space between beads with a virtual cylindrical flow tube encompassing the same volume, with a wall surface area equal to the surface area of the beads

3. 3. 3. The Virtual Cylindrical Reactor (VCR) Approximation

The flow tubes used in the present study were packed with beads for two reasons: to increase a surface area for the heterogeneous reaction and to shorten the time necessary for OH diffusion to the surface. In the virtual cylindrical reactor (VCR) approximation, a flow tube packed with beads is virtually replaced for simplicity with a cylindrical reactor of radius, r_v, and length, l_v, chosen to correspond with the surface area of beads, S, and volume of space between the beads, V. Geometric parameters of such a virtual cylindrical reactor can be calculated as follows:

$$V = V_a = V_v = (\pi r_a^2 l_a) - \frac{4}{3}\pi r_b^3 n \tag{3.10}$$

$$S = S_a = S_v = 4\pi r_b^2 n \tag{3.11}$$

$$r_v = \frac{2V}{S} \tag{3.12}$$

$$l_v = \frac{V}{\pi r_v^2} \tag{3.13}$$

where

V : Volume of the space that the OH freely moves,

V_a : Volume of the actual reactor,

V_v : Volume of the VCR,

S : Surface area that the material is coated on,

S_a : Surface area of the actual reactor,

S_v : Surface area of the VCR,

r_v : Radius of the VCR,

l_v : Length of the VCR,

r_a : Radius of the actual tube,

l_a : Length of the actual tube,

r_b : Radius of the bead,

n : Number of beads packed.

Figure 3.7 illustrates the transfer from a flow tube packed with beads to a virtual cylindrical reactor. Therefore, the residence time (t) inside a virtual cylindrical flow tube can be determined as follows:

$$t = \frac{l_v}{v_v} = \frac{l_v \cdot \pi r_v^2}{W} = \frac{V}{W} \qquad (3.14)$$

where v_v is the gas convective velocity of the virtual flow with a total flow, W. The calculated Reynolds number of 1300 suggests that a virtual flow is laminar while it does not really imply the same for an actual flow.

There is an alternate approach to compute the mass transfer rate in a packed-bead reactor, described in the chemical engineering literature [e.g. Fogler, 1999]; it involves the Sherwood (Sh), Schmidt (Sc), and Reynold (Re) numbers, and the Colburn

J factor. In a future study, this approach will be compared to the VCR approximation.

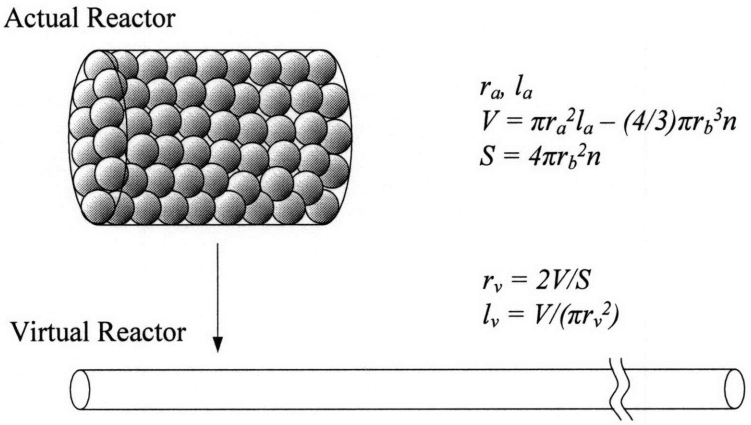

Figure 3.7. The schematic of conversion to a virtual reactor. The virtual reactor is typical cylindrical tube, while the actual reactor is filled with sixty beads, having the same volume and coated surface area as the actual reactor.

3.3.3.1. The Validity of the VCR Approximation

The validity of the VCR approximation was tested as follows. Paraffin wax was selected because of its well known reaction probability of OH [Bertram *et al.*, 2001]. In addition, its melting point is close to that of halocarbon wax (~ 58℃) so that two waxes mix together homogeneously when solidified, enabling to control the reactivity of the mixture properly. Since the average molecular weights of paraffin wax and halocarbon wax (600 series) used in this work are close to 600 g/mole, the ratio of number of reactive sites is considered to be equal to the weight ratio under the assumption that each wax molecule provides one reactive site. Therefore, the reaction probability of the mixture, γ^{mix}, is determined by the following equation:

$$\gamma_{OH}^{mix} = \sum_j \beta_j \gamma_{OH}^j \qquad (3.15)$$

where γ_j is the reaction probability of compound j in the mixture, and β_j is the fraction of compound j, which meets the condition of $\sum_j \beta_j = 1$ and $\beta_j = \frac{n_j}{\sum nj}$, where n_i is the number of active sites of compound j.

We prepared four different mixtures of paraffin wax and halocarbon wax, which were 1/130, 1/43, 1/20, and pure paraffin wax corresponding to 0.0012, 0.0037, 0.008, and 0.16 of reaction probabilities, respectively. The relative intensities of OH from these mixtures obtained from the experiment (■) are in agreement with the results of the virtual reactor approximation (solid line) as shown in Figure 3.8.

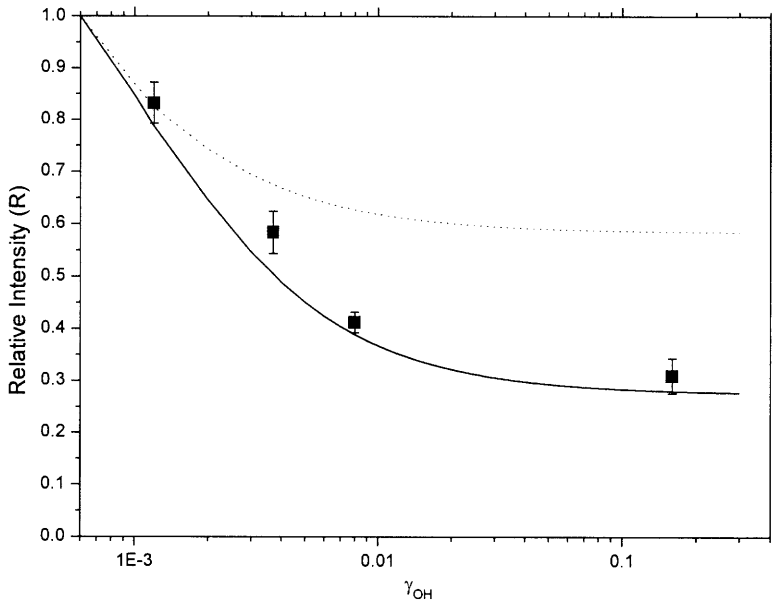

Figure 3.8. The estimated relative intensity of OH in a beads-packed reactor (solid line) and the experimental relative intensities of various mixtures of paraffin wax and halocarbon wax (■). The reaction probabilities of the mixtures are 0.16 (pure paraffin wax), 0.008 (1/20 paraffin wax), 0.0037 (1/43), and 0.0012 (1/130). The estimated relative intensity of OH in a conventional cylindrical tube (dashed line) was included for a comparison with a beads-packed system.

3.3.3.2. Beads-Packing Technique (Revisited)

The estimated relative OH intensity in a cylindrical tube without beads-packing (dashed line) is included in Figure 3.8 to confirm the necessity of beads-packing technique in this work (Section 2.4). Note that coating with a material of interest only on the wall of a flow tube resulted in a small probability for OH to collide with the walls at high pressure. The change in the relative intensity of OH in the beads-packing system was doubled when compared to that in a flow tube within the same change in γ_{OH}. This illustrates how the beads-packing technique enhances the sensitivity of $R_{surface}$ by increasing the surface area.

3.3.3.3. Technique of Dilution for Better Sensitivity

For the highly reactive surface to OH resulting high value of k_{kin}, the additivity of kinetic resistances (Equation 3.3) expects that k_{obs} is mainly determined by the relatively low value of k_{dif}. In other words, the OH heterogeneous reactions on the highly reactive surface are screened by the diffusion of the radical to the wall even in our beads-packed system. As seen in Figure 3.8, the estimated relative intensity (R_{est}) converges fast as γ_{OH} increases, especially from 0.01. For example, R_{est} changes only 0.016 in the range between γ_{OH} = 0.02 and 0.03, while 0.1 in the range between γ_{OH} = 0.002 and 0.003. Taking our systematic error in $R_{surface}$ (~ $\pm$5%) into account, any changes in the reactions of high uptakes, even if any, are totally screened by diffusion. Therefore, we are not expected to observe any water effects on the OH heterogeneous reactions on the highly reactive materials due to the diffusion limitation.

Diluting materials with halocarbon wax (in the case of organic materials) or partial coating (in the case of inorganic materials in powder) enabled to escape from the

diffusion limitation. It was already shown above (Figure 3.8) that dilution of the material of interest effectively reduces the uptake of OH on the surface. This decrease in the uptake does not indicate a change in the chemistry, but rather a decrease in the extent of heterogeneous loss of OH on the surface. In other words, heterogeneous reactions of OH on the surface in the influence of RH take place for a reduced amount so that the chemistry is out of the diffusion limitation while the original values of γ_{OH} for the pure surface are still able to recover by considering the degree of dilution and/or surface coverage.

By this approach, the reaction probabilities of highly reactive materials were controlled to comparable values with diffusion, or approximately $\gamma_{OH} = 0.001 \sim 0.002$, corresponding to $R_{surface} = 0.6 \sim 0.8$. The specific example of the technique of dilution for better sensitivity is shown in Section 3.3.5.2.

3.3.3.4. Determination of γ_{OH} from $R_{surface}$

As discussed above, the reaction probability of OH, γ_{OH}, may be determined from the $R_{surface}$ obtained using the r_v and t obtained from the VCR approximation, even though the experimental reaction time is fixed. An example for the determination of γ_{OH} from $R_{surface}$ is shown in Appendix 3-III. In addition, the errors arising in the calculations propagated from the errors of measurements are shown in Appendix 3-IV.

3. 3. 4. OH-H_2O Complexes

Due to its ability to form hydrogen bonds, water vapor clusters readily with various gaseous species in the atmosphere [Aloisio *et al.*, 2000; Hansen *et al.*, 2002; Sennikov *et al.*, 2005]. For example, much attention, both experimental and

theoretical, has been paid to the water dimer [Dyke *et al.*, 1977; Newton *et al.*, 1983; Feyereisen *et al.*, 1996]. On the other hand, the complex between OH and water molecule has been rarely studied. Experimental evidence for the existence of such complex has been rarely reported, while theoretical studies have only succeeded in estimating the structure and energy of the complex [Kim *et al.*, 1991; Dubey *et al.*, 1997; Wang *et al.*, 1999; Aloisio *et al.*, 2002; Karakus *et al.*, 2005; Sennikov *et al.*, 2005]. Although our study is focused on heterogeneous processes, it is worth considering $OH\text{-}H_2O$ complex formation through a gas-phase reaction since the two species were abundant in the gas phase, and therefore, the water complexes can affect our experimental observations [Hansen *et al.*, 2002].

In fact, the $OH\text{-}H_2O$ complex is an intermediate in the proton transfer reaction between OH and H_2O [Dubey *et. al.*, 1997]:

$$OH + H_2O \rightarrow OH\text{-}H_2O \qquad (3.16)$$

$$OH\text{-}H_2O \rightarrow [OH\text{-}H\text{-}OH]^{\ddagger} \rightarrow H_2O\text{-}OH \rightarrow H_2O + OH \qquad (3.17)$$

where the double dagger stands for the transition state. The theoretically calculated rate constant for the proton exchange reactions (3.16 ~ 3.17) is reported at 2.94×10^{-17} cm^3 $molecule^{-1}$ s^{-1} at 300 K [Uchimaru *et. al.*, 2003]:

$$HO + HOH \rightarrow HOH + OH, \qquad k_{3.17} = 2.94 \times 10^{-17} \qquad (3.18)$$

Additional complexes with additional water molecules, $OH\text{-}(H_2O)_n$, can be formed under conditions when $OH\text{-}H_2O$ collides with another water molecule before its self-dissociation or isomerization:

$$OH\text{-}H_2O + H_2O \rightarrow OH\text{-}(H_2O)_2 \qquad (3.19)$$

$$OH\text{-}(H_2O)_2 + H_2O \rightarrow OH\text{-}(H_2O)_3 \qquad (3.20)$$

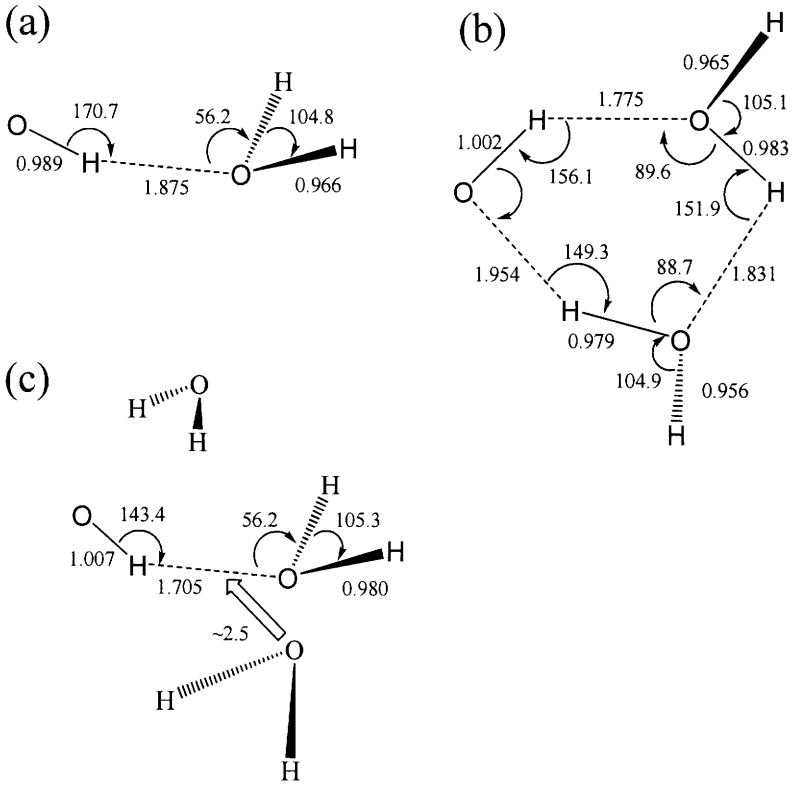

Figure 3.9. The structures of OH-H_2O (a), OH-$(H_2O)_2$ (b), and OH-$(H_2O)_3$ (c) optimized with the B3LYP method and 6-31G(d,p) basis set. The structures of (a) and (b) belong to the C_s point group.

Ab initio calculations for the three complexes between OH and water molecules, OH-H_2O, OH-$(H_2O)_2$, and OH-$(H_2O)_3$, were performed in the present work to obtain their geometries and energy states. Geometries of the water complexes optimized at the global minima are shown in Figure 3.9. OH-H_2O and OH-$(H_2O)_3$ belong to the Cs point group while OH-$(H_2O)_2$ has no symmetry. The structure of OH-H_2O is consistent with results of the previous works [Kim *et al.*, 1991; Xie *et al.*, 1993; Dubey *et al.*, 1997; Wang *et a.l,* 1999; Aloisio *et al.*, 2002; Karakus *et al.*, 2005; Sennikov *et al.*, 2005]. The hydrogen bond is formed between the hydrogen atom of OH and the oxygen atom of H_2O because OH accepts readily the electronic density. In OH-$(H_2O)_3$,

two additional water molecules form efficiently hydrogen bonds with OH-(H_2O) from out of plane directions with approximately 2.5Å distance to the C_s plane. OH-$(H_2O)_2$ consists of a six-membered ring formed by the OH radical and two OH groups from the water molecules through hydrogen bonding.

3.3.4.1. Energy States of Water Complexes

The total energies and the Gibbs free energies of the reactants and the complexes at global minima are listed in Table 3.1. The binding energy of OH-H_2O complex (-6 kcal/mol) is consistent with the results of previous works [Nanayakkara *et al.*, 1992; Xie *et al.*, 1993]. Further hydration with hydrogen bonding is expected to stabilize the complex with negative enthalpy changes ($\Delta H_{n-1\rightarrow n} < 0$) apart from how fast they proceed before a OH-H_2O complex is dissociated.

Table 3.1. Summary of the energies of the various species (in Hartree)

Species	Total Energy [a]	Gibbs Free Energy	$\Delta H_{n-1\rightarrow n}$ [b] (kcal/mol)
OH	-75.720061	-75.736997	
H_2O	-76.398364	-76.416020	
OH-H_2O	-152.127950	-152.153581	-6.0 (-5.7) [c]
OH-$(H_2O)_2$	-228.546261	-228.575091	-12.5
OH-$(H_2O)_3$	-304.956232	-304.989515	-7.3
$OH\cdots H_2O$ [d]	-152.118299[e]	-152.146902[e]	

[a] Corrected by zero-point energy

[b] Enthalpy change for water hydration ($OH\text{-}(H_2O)_{n-1} + H_2O \rightarrow OH\text{-}(H_2O)_n$)

[c] Nanayakkara *et al.*, 1992; Xie *et al.*, 1993

[d] Loose complex for the substitution of a transition state. Details are described in Appendix 3-V.

[e] One imaginary frequency was ignored from the energy corrections.

3.3.4.2. Fraction of OH-H_2O in the System

The information about the rates for the forward ($k_{3.16}$) and the backward ($k^{-1}_{3.16}$) reactions is necessary to determine the fraction of a OH-H_2O complex gas phase; it can be estimated using the following equilibrium constant, $K^{3.16}$:

$$K_{3.16} = \frac{[OH \cdot H_2O]}{[OH][H_2O]} = \frac{k_{3.16}}{k^{-1}_{3.16}} \qquad (3.21)$$

Since the rate constants for the reactions have not been determined, *ab initio* calculations were used to obtain the rate constants theoretically. At the level of B3LYP and MP2 theories, the transition state for Reaction 3.16 was not found, implying that an entrance barrier is extremely shallow or zero. Therefore, the reaction was assumed to proceed whenever the reactants collide together in a proper orientation. The rate constant of Reaction 3.16 ($k_{3.16}$) within the reactive hard-sphere model was estimated to be 1.1×10^{-16} cm^3 $molecule^{-1}$ s^{-1} at 298 K. Due to the low binding energy of the water complex and the shallow barrier, the lifetime of the water complex is extremely short (1.9×10^{-10} s) with $k^{-1}_{3.16} = 5.3 \times 10^9$ s^{-1} at 298 K.

Since the equilibrium constant ($K_{3.16}$) was determined as 2.1×10^{-26} cm^3 $molecule^{-1}$ using $k_{3.16}$ and $k^{-1}_{3.16}$, the concentration of OH-H_2O complex was estimated to be 5.3×10^2 molecule cm^{-3} corresponding 6.6×10^{-10} as the fraction of the water complex in the gas-phase. The possibility of the existence for a OH-$(H_2O)_n$ complex in the gas phase was excluded due to its negligible fraction and the extremely short life time of the complex. The details about the determination of the rate constants are described in Appendix 3-V.

In fact, OH^--$(H_2O)_n$ complexes was observed as RH increased as mentioned in Section 2.1.7. Although a possible origin of the water clusters can have two reasons, the first one (Reactions 3.16 and 3.22) should be excluded for the reason stated above.

$$OH + H_2O \rightarrow OH\text{-}H_2O \quad (3.16)$$

$$OH\text{-}H_2O + SF_6^- \rightarrow OH^-\text{-}(H_2O) + SF_6 \quad \text{(at CI region)} \quad (3.22)$$

or,

$$OH + SF_6^- \rightarrow OH^- + SF_6 \quad \text{(at CI region)} \quad (3.23)$$

$$OH^- + H_2O \rightarrow OH^-\text{-}(H_2O) \quad (3.24)$$

The equilibrium in the Reaction 3.24 is believed to shift to the left because of thermodynamically deep wells of the complexes (-36.5 kcal/mol). The results of the *ab initio* calculations for the energy of the $OH^-\text{-}(H_2O)_n$ complexes are listed in Table 3.2.

Table 3.2. The summary of the energies of the species (in Hartree) (B3LYP)

Species	Total Energy [a]	$\Delta H_{n-1\rightarrow n}$ [b] (kcal/mol)
OH^-	-75.718319	-
H_2O	-76.398364	-
$OH^-\text{-}H_2O$	-152.174882	-36.5
$OH^-\text{-}(H_2O)_2$	-228.633088	-37.6
$OH^-\text{-}(H_2O)_3$	-305.057267	-16.2

[a] Corrected by zero-point energy

[b] Enthalpy change for water hydration ($OH^-\text{-}(H_2O)_{n-1} + H_2O \rightarrow OH^-\text{-}(H_2O)_n$)

3. 3. 5. Organic Surfaces

3.3.5.1. Determination of γ_{OH} under Dry Conditions

We first determined the OH reaction probabilities for pure organic surfaces, such as paraffin wax, pyrene, glutaric acid, and methane-soot, under dry conditions for verification of the suggested VCR method. First, the relative intensity of OH, R_{OH}, for the pure organic surfaces was experimentally measured followed by determining γ_{OH} as

described in Section 3.3.3.4. Results of the uptake measurements are shown in Table 3.3; for comparison, literature values for the same organic surfaces are shown as well. As seen from the table, the experimental results obtained based on the VCR approximation reproduce reasonably well the literature values, although the range of the measured reaction probability values is wider due to the worse sensitivity of the VCR method to high uptake values, as discussed above.

Table 3.3. The OH reaction probability for the organics under the dry condition.

surface	R	γ_{OH}	references
paraffin wax	0.281 ± 0.016	0.03 - 1	present work
		0.16 – 1	[Bertram *et al.*, 2001]
pyrene	0.270 ± 0.008	0.03 - 1	present work
		0.15 – 1	[Bertram *et al.*, 2001]
glutaric acid	0.277 ± 0.006	0.03 – 1	present work
methane-soot	0.285 ± 0.010	0.02 – 1	present work
		0.5 - 1	[Bertram *et al.*, 2001]

3.3.5.2. The Effect of Relative Humidity

The effect of water vapor on OH uptake by organic materials was studied for the pure and diluted surfaces. As most of the organics studied are highly reactive to OH, resulting in a high value for k_{kin} due to the diffusion limitation, a water effect on OH uptake was not expected. For this reason, the organic surfaces were diluted with halocarbon wax to give a net γ_{OH}-value in the region of (1-2) × 10^{-3} that corresponds to $R_{surface}$ = 0.6 - 0.8 where the sensitivity of the VCR method is the best (See Section 3.3.3.3).

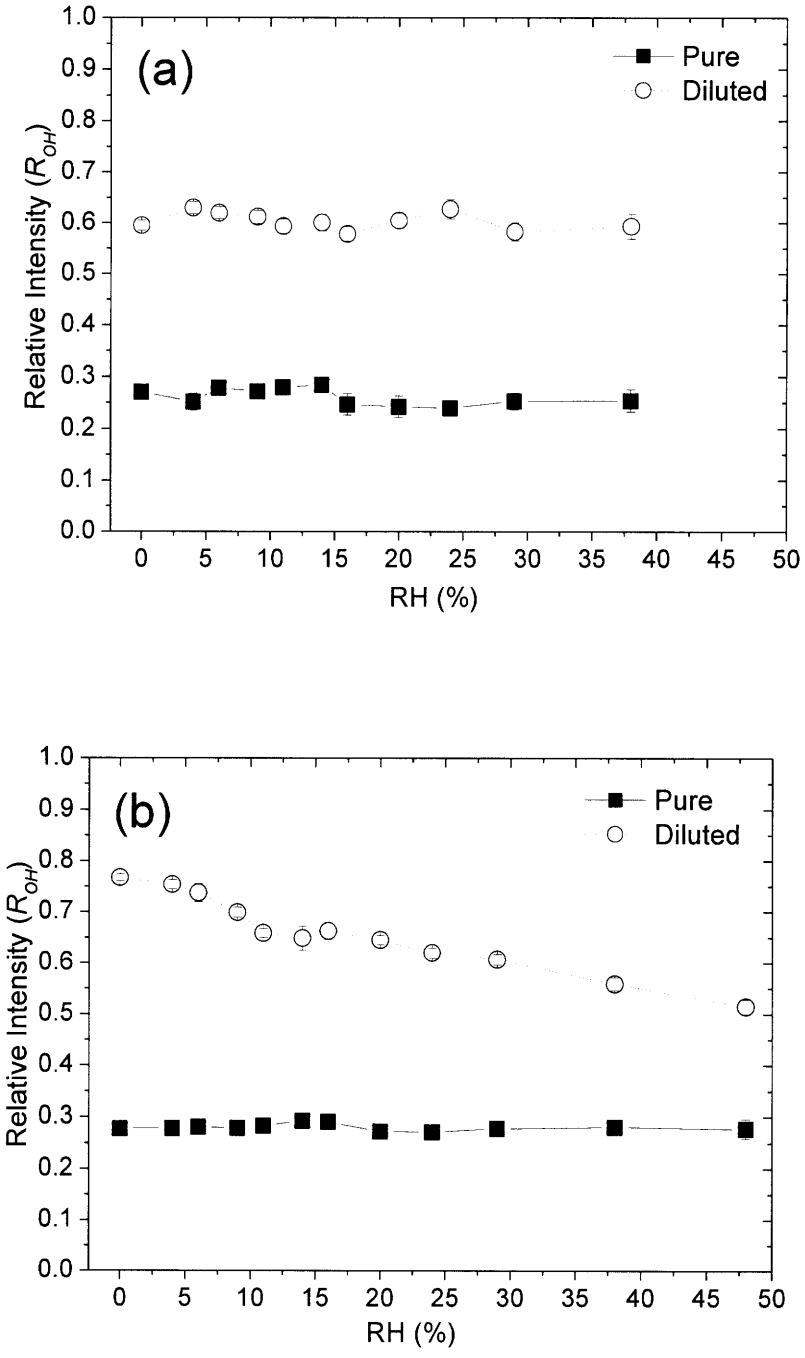

Figure 3.10. The relative intensities of OH (R_{OH}) for pure (■) and diluted (○) surfaces of pyrene (a), and glutaric acid (b) under various relative humidity conditions. There are no changes in R_{OH} on both pure organic surfaces, whereas only the diluted surface of glutaric acid changed.

Figure 3.10 illustrates how the surface dilution technique works. No changes in R_{OH} under wet conditions were observed for pure surfaces of pyrene (a) and glutaric acid (b). However, it appears ambiguous that no change on highly reactive surface implies no water effect since the diffusion of OH limits our observation as described above. The observation becomes much clearer for the diluted surfaces. We observed a decrease in R_{OH} on the diluted surface of glutaric acid, whereas still no change on that of pyrene. (Controlling the net OH reaction probability by dilution was applied not only to highly reactive organic materials, but also to most materials studied, except $CaCl_2$, $MgCl_2$, and sea salt, used in this work to increase sensitivity.)

The effect of relative humidity on R_{OH} for the diluted paraffin wax and methane soot surfaces of known composition was also studied. Subsequently applied Equation 3.9 and 3.15, we were able to retrieve the OH reaction probability values for the pure organic and methane soot surfaces. The details about the determination of γ_{OH} for the pure organic surfaces based on measurements of R_{OH} for diluted surfaces are described in Appendix 3-VI.

The results of these experiments are shown in Figure 3.11 and Table 3.4. Only an initially hydrophilic organic surface, such as glutaric acid, shows the enhancement in its reactivity towards OH, whereas for paraffin wax and pyrene surfaces no noticeable changes in γ_{OH} within experimental error were observed under wet conditions. More attention is required for methane soot since only small decrease in γ_{OH}^{soot} was observed at low RH. Focused on the region of small RH change (RH < 9%), γ_{OH} on the methane soot surface (γ_{OH}^{soot}) dropped by approximately 40%. In constrast, further increase in RH was relatively insensitive for change in OH uptake.

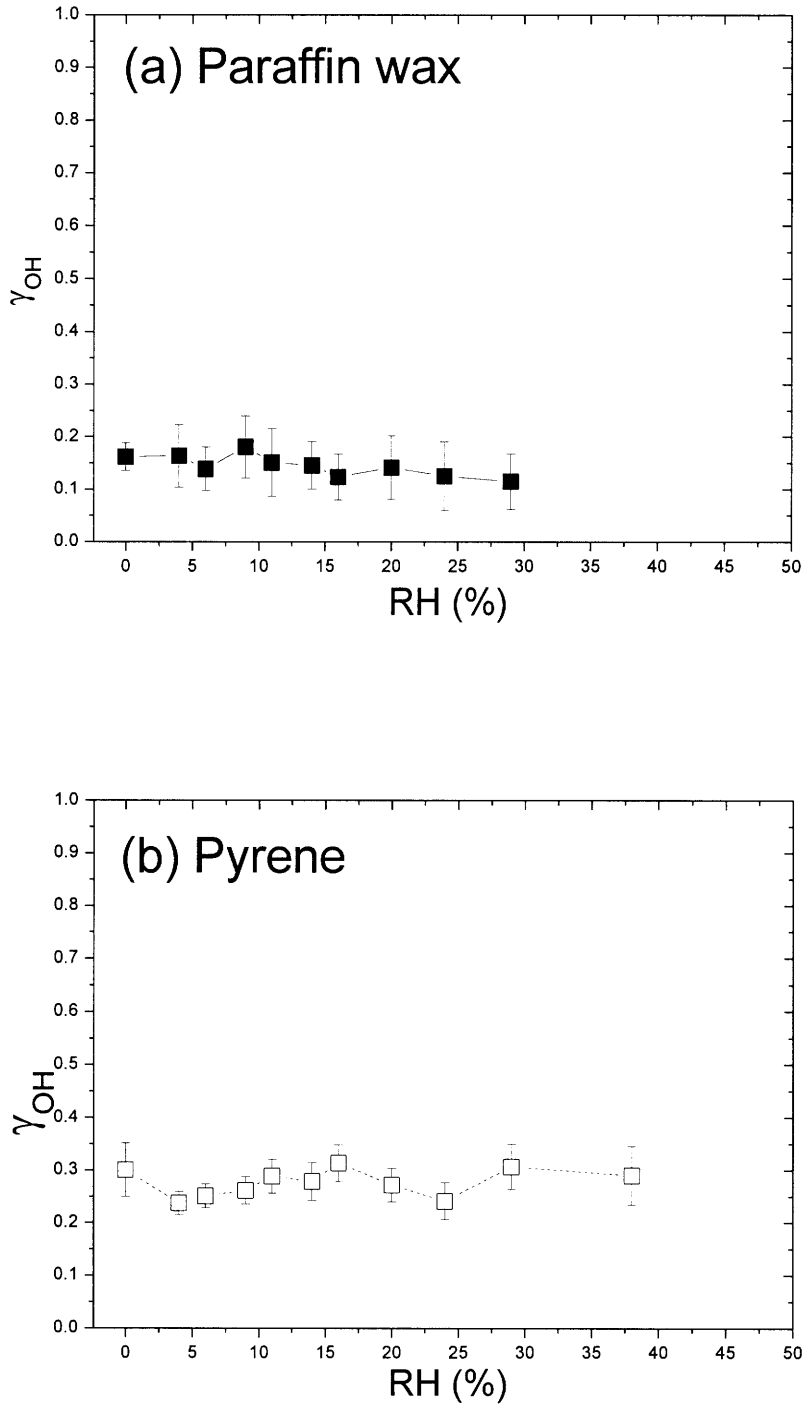

Figure 3.11. The dependences of γ_{OH} for paraffin wax (a), pyrene (b), glutaric acid (c), and methane soot (d) on RH.

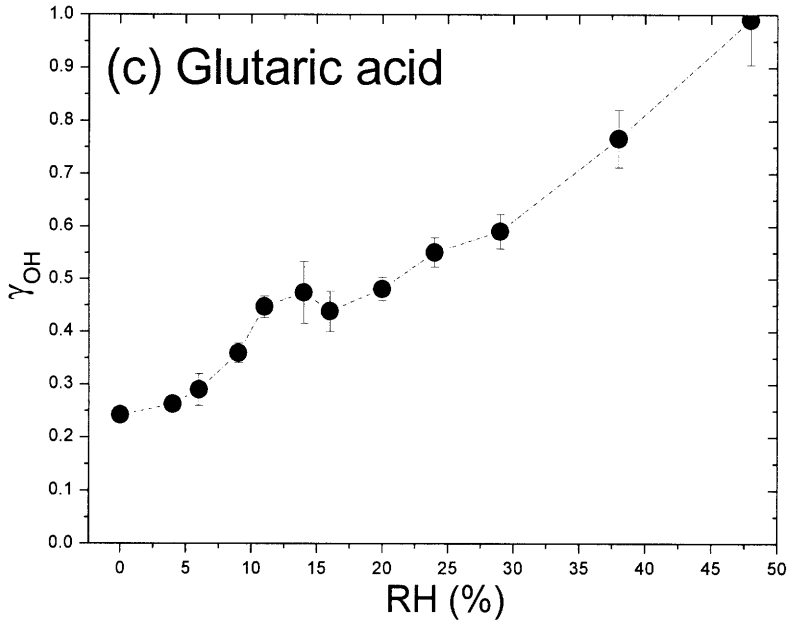

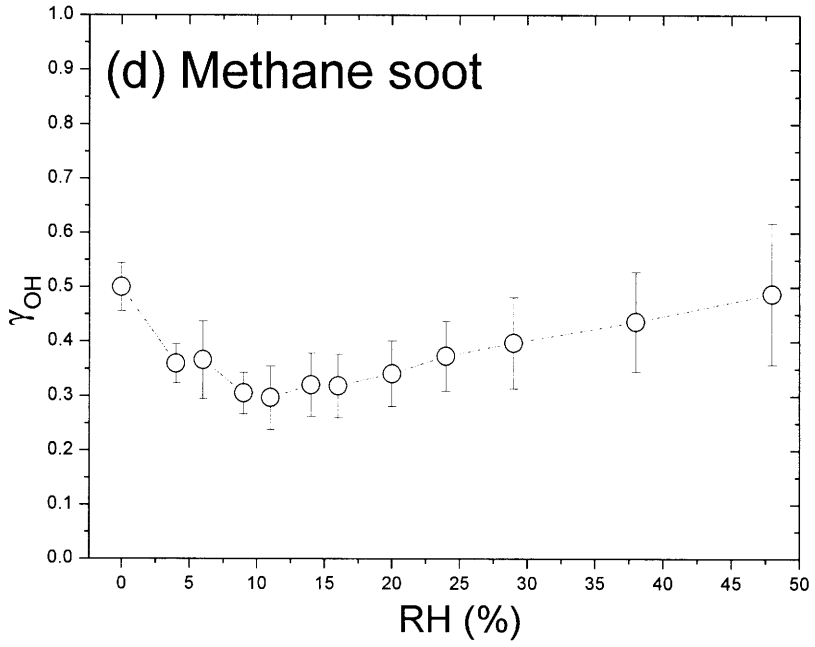

Figure 3.11. Continued

Table 3.4. The OH reaction probability for organics under various RH conditions

RH (%)	γ_{OH}			
	Paraffin wax	Pyrene	Glutaric acid	Methane Soot
0	0.16 ± 0.03	0.30 ± 0.05	0.24 ± 0.01	0.50 ± 0.04
4	0.16 ± 0.06	0.24 ± 0.02	0.26 ± 0.01	0.36 ± 0.04
6	0.14 ± 0.04	0.25 ± 0.02	0.29 ± 0.03	0.37 ± 0.07
9	0.18 ± 0.06	0.26 ± 0.03	0.36 ± 0.02	0.30 ± 0.04
11	0.15 ± 0.06	0.29 ± 0.03	0.45 ± 0.02	0.30 ± 0.06
14	0.15 ± 0.05	0.28 ± 0.04	0.47 ± 0.06	0.32 ± 0.06
16	0.12 ± 0.04	0.31 ± 0.04	0.44 ± 0.04	0.32 ± 0.06
20	0.14 ± 0.06	0.27 ± 0.03	0.48 ± 0.02	0.34 ± 0.06
24	0.12 ± 0.07	0.24 ± 0.04	0.55 ± 0.03	0.37 ± 0.06
29	0.11 ± 0.05	0.31 ± 0.04	0.59 ± 0.03	0.40 ± 0.83
38	-[a]	0.29 ± 0.06	0.77 ± 0.05	0.44 ± 0.09
48	-[a]	-[a]	0.99 ± 0.09	0.49 ± 0.13

[a] γ_{OH} were not measured at these RH conditions.

Whereas fresh soot is extremely hydrophobic and repels water, soot becomes hydrophilic due to the formation of oxygen-containing groups on the surface upon OH exposure [Molina *et al.*, 2004; Zuberi *et al.*, 2005]. Since the freshly prepared soot surface was pre-treated by OH for an hour before our measurements, the aged soot surface was believed to allow for water adsorption on the surface. Therefore, there is the possibility that adsorbed water adlayer will cover surface active sites, resulting in their screening from OH, and lowering γ_{OH}^{soot} under wet conditions, which can be responsible for the decrease in γ_{OH}^{soot} at low RH. However, in fact, the extent of changes in the hydrophilicity of a soot surface upon OH exposure is small [Zuberi *et. al.*, 2005], making this explanation less plausible. In the range of the RH (0 - 50%) in our

experiments, even aged soot takes up only a small amount of water [Zuberi *et. al.*, 2005] which is not enough to screen surface site available for OH uptake.

Coming back to Figure 3.11 (d), the first change in γ_{OH}^{soot} was 40%. Considering that the possible uncertainty of ~ 25% in γ_{OH} arising from error propagation is approximately 25% (Appendix 3-IV), a 40% change is not sufficient to determine the water effect on γ_{OH}^{soot}. Moreover, the uncertainty in the γ_{OH}^{soot} value obtained at 48% RH overlaps with the whole range of the change in γ_{OH}^{soot}. Therefore, additional study on this issue with enhanced sensitivity and accuracy is required to determine the water effect on γ_{OH}^{soot}.

The obtained results on the change in γ_{OH} on paraffin wax, pyrene, and methane soot (Figure 3.11 (a), (b), and (d)) suggest that OH exposure does not alter the hydrophilicity of organic and soot surfaces to such extent to influence OH uptake. Therefore, water molecules in a humid environment are not adsorbed efficiently on the carbonaceous surfaces in order to noticeably affect OH uptake. This conclusion is in agreement with results previous results from our laboratory on the OH-initiated oxidation of organic and soot surfaces [Molina *et al.*, 2004].

On the other hand, a hydrophilic organic surface with a relatively higher water adsorption capacity may exhibit a change in OH reactivity in a different (liquid) environment. Glutaric acid, a dicarboxylic acid, can be an example of such initially hydrophilic organic surface (Figure 3.11 (c)). The first step of the OH heterogeneous interaction with organic materials is the H-abstraction reaction [Bertram *et al.*, 2001].

$$R\text{-}H + \cdot OH \rightarrow R\cdot + H_2O \qquad (3.26)$$

where R-H is a alkane and R· is a alkyl group. As the C—H bond in alkane becomes

less strong, a lower activation energy for hydrogen abstraction could be caused for a faster reaction rate. Although the rest of the C—H bonds in glutaric acid are not expected to be influenced by water adsorption, O—H bonds in carboxylic functional groups may weaken through electron density stabilization by surrounding water [Reichardt, 1994; Woods III *et al.*, 2005]. As a result, the carboxylic H may be more easily abstracted, leading to higher OH uptake.

The reaction mechanism for OH uptake at higher RH conditions may change from radical to ionic. For example, assuming that water molecules are preferentially adsorbed on carboxylic functional groups, as more water is taken up by a surface, a higher degree of dissociation of glutaric acid can occur. OH may react more efficiently with dissolved ions: for example, OH uptake was enhanced by a factor of 25 on sulfuric acid as compared to that on pure water [Hanson *et al.*, 1992]. Therefore, weakening an O—H bond in carboxylic groups and the acidic dissociation can be responsible for the observed enhancement by a factor of 4 in the OH reaction probability at 48% of RH (Figure 3.11 (c)).

3. 3. 6. Inorganic Surfaces

We have also measured the relative OH intensity (R_{OH}) for inorganic materials of tropospheric importance followed by determining the reaction probabilities of OH under dry conditions as shown in Table 3.5. For direct measurements, the pure surface material was used (no dilution). Few studies have been carried out on the heterogeneous reactions of OH with inorganic salts up to date; to our knowledge, our study presents the first reported OH reaction probabilities on $MgCl_2$, Na_2SO_4, $CaCl_2$, and KCl. Consistency of γ_{OH} for NaCl, sea salt and Al_2O_3 with the literature values

provides support for our experimental approach [Ivanov *et al.*, 1996; Gratpanche *et al.*, 1996; Bertram *et al.*, 2001].

Table 3.5. The OH reaction probability for inorganic materials under dry conditions.

Surface	R	γ_{OH} ($\times 10^{-3}$)
NaCl	0.469 ± 0.012	4.6 [±0.7] 4 [a]
$MgCl_2$	0.428 ± 0.008	6.1 [±1.2]
Na_2SO_4	0.523 ± 0.008	3.5 [±0.3]
$CaCl_2$	0.500 ± 0.015	3.9 [±0.4]
KCl	0.443 ± 0.010	5.5 [±1.0]
Sea Salt	0.524 ± 0.010	3.3 [±0.3] 5 [b]
SiO_2	0.305 ± 0.020	0.019 ~ 0.085 2×10^{-3} [c]
Al_2O_3	0.295 ± 0.012	0.028 ~ 0.10 0.11 ~ 0.44 [d]

[a] Ivanov *et al.*, 1996 [b] Gratpanche *et al.*, 1996
[c] Suh *et al.*, 2000 [d] Bertram *et al.*, 2001

Approximately one order of magnitude difference in γ_{OH} on SiO_2 from the reported value obtained on fused quartz [Suh *et al.*, 2000] was observed. The variation possibly arised from the origin of SiO_2 as Suh and the coworkers explained for their unexpected small value.

3.3.6.1. Sea Salt and its Components

The VCR method together with a surface dilution technique was successfully applied in the present uptake experiments for sea salt and its five major components, NaCl (68%), $MgCl_2$ (14%), Na_2SO_4 (11%), $CaCl_2$ (4%), and KCl (2%), to investigate the effect of relative humidity on the heterogeneous reaction of OH. The OH reaction probabilities for the salts measured under dry and wet conditions (0 to 48% of RH) are shown in Figure 3.12 and also listed in Table 3.6.

The reaction probability values for the hygroscopic salts ($MgCl_2$, $CaCl_2$, and sea salt) are not available at high RH conditions because the salts were deliquesced before reaching those RH. Deliquescence is a phase transformation whereby a solid absorbs water vapor from the atmosphere, leading to the dissolution of the solid. It occurs at deliquescence relative humidity point (DRH), when the RH is equal to the vapor pressure of the corresponding solution. The DRH's of $CaCl_2$ (hexahydrate, $CaCl_2 \cdot 6H_2O$) and $MgCl_2$ (hexahydrate, $MgCl_2 \cdot 6H_2O$) are 29% RH and 33% RH, respectively [Linke, 1965; Wagman *et al.*, 1982; Lide, 2007]. However, the observed DRH of $CaCl_2$ and $MgCl_2$ were found to be 24% RH and 35% RH, respectively, explained by the fact that the hydration was incomplete in short time frames resulting in mixtures of tetra- and hexa-hydrates. The DRH of sea salt was observed at ~40%, which is consistent with the recent report for the deliquescence in binary mixtures [Salameh *et al.*, 2005]. Since the deliquesced solution could not stay on a bead surface under a fast flow environment, the salt was washed out from the beads causing irreversible changes in salt-coating morphology.

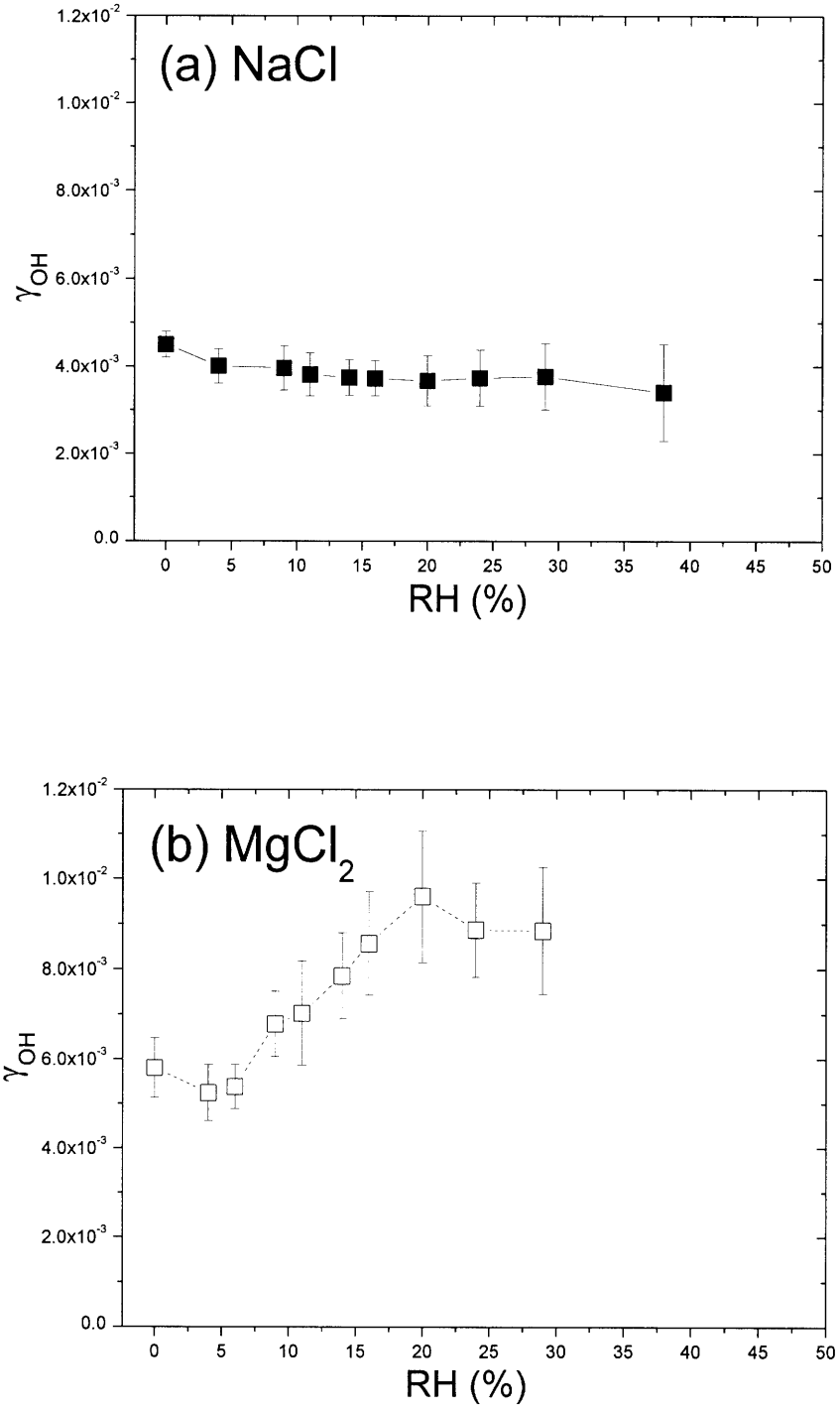

Figure 3.12. The dependences of γ_{OH} for NaCl (a), $MgCl_2$ (b), Na_2SO_4 (c), $CaCl_2$ (d), KCl (e), and sea salt (f) on RH.

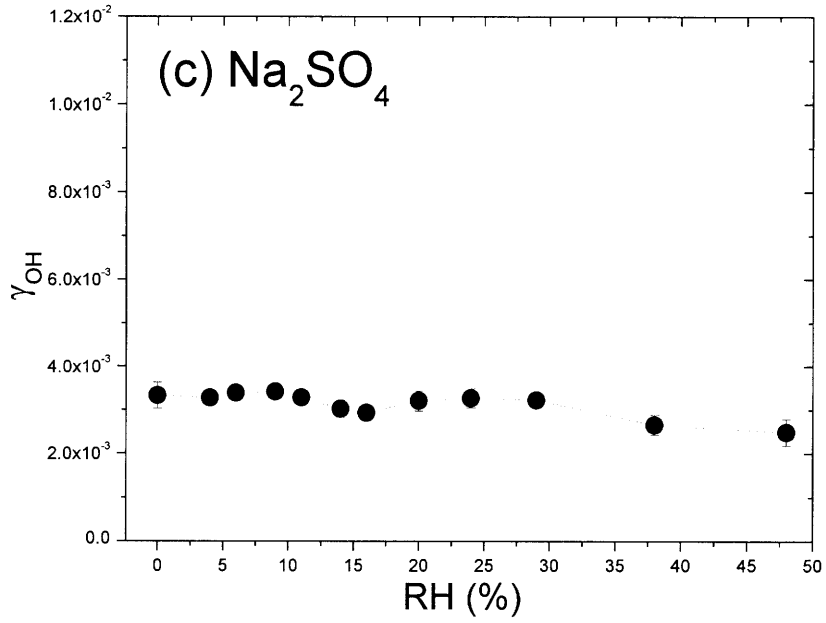

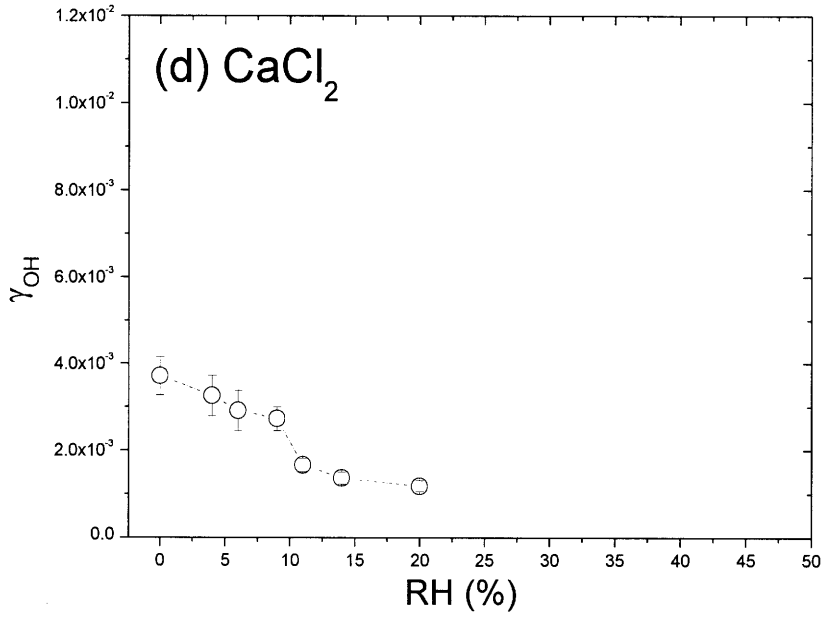

Figure 3.12. Continued

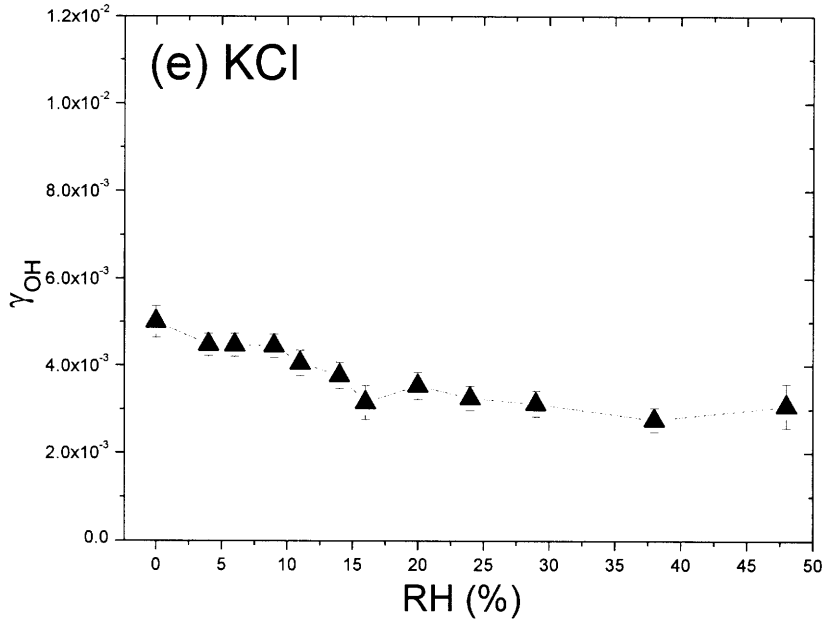

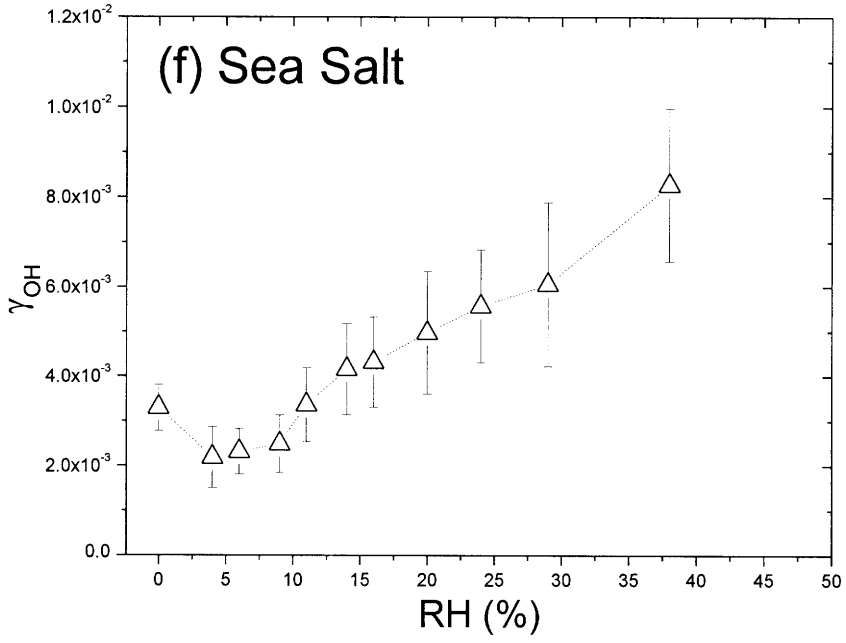

Figure 3.12. Continued

Table 3.6. The OH reaction probability for salts under various RH conditions

RH (%)	γ_{OH} ($\times 10^{-3}$)					
	NaCl	$MgCl_2$	Na_2SO_4	$CaCl_2$	KCl	Sea Salt
0	4.5 ± 0.3	5.8 ± 0.7	3.3 ± 0.3	3.7 ± 0.4	5.0 ± 0.4	3.3 ± 0.5
4	4.0 ± 0.4	5.2 ± 0.6	3.3 ± 0.2	3.3 ± 0.5	4.5 ± 0.3	2.2 ± 0.7
6	-[a]	5.4 ± 0.5	3.4 ± 0.2	2.9 ± 0.5	4.5 ± 0.3	2.3 ± 0.5
9	4.0 ± 0.5	6.8 ± 0.7	3.4 ± 0.2	2.7 ± 0.3	4.5 ± 0.3	2.5 ± 0.6
11	3.8 ± 0.5	7.0 ± 1.1	3.3 ± 0.2	1.7 ± 0.2	4.1 ± 0.3	3.4 ± 0.8
14	3.7 ± 0.4	7.9 ± 0.9	3.0 ± 0.2	1.4 ± 0.2	3.8 ± 0.3	4.2 ± 1.0
16	3.7 ± 0.4	8.6 ± 1.2	2.9 ± 0.2	-[a]	3.2 ± 0.4	4.3 ± 1.0
20	3.7 ± 0.6	9.6 ± 1.5	3.2 ± 0.2	1.2 ± 0.1	3.5 ± 0.3	5.0 ± 1.4
24	3.7 ± 0.6	8.9 ± 1.0	3.3 ± 0.2	-[b]	3.3 ± 0.3	5.6 ± 1.3
29	3.8 ± 0.8	8.9 ± 1.4	3.2 ± 0.2	-[b]	3.1 ± 0.3	6.1 ± 1.8
38	3.4 ± 1.1	-[b]	2.7 ± 0.2	-[b]	2.8 ± 0.3	8.3 ± 1.7
48	-[a]	-[b]	2.5 ± 0.3	-[b]	3.1 ± 0.3	-[b]

[a] γ_{OH} were not measured at these RH conditions.
[b] The salts were deliquesced.

Noticeable changes in the OH reaction probability were observed at 0 - 48% of RH for the highly hygroscopic salts ($MgCl_2$, $CaCl_2$, and sea salt), but not for less hygroscopic salts (NaCl, Na_2SO_4, and KCl). We observed that as RH increases, γ_{OH} on $MgCl_2$ increased by factor of 1.7 at 20% of RH as compared to the dry condition value. However, $CaCl_2$ showed opposite changes in γ_{OH}. The γ_{OH} value for $CaCl_2$ decreased by factor of 3.2 at 20% RH as compared to dry conditions. Although a small decrease in γ_{OH} was observed for KCl as well, the water effect is uncertain due to the same reason as the case of methane soot (Section 3.3.5.2). Interestingly, sea salt showed a positive effect of water on γ_{OH} following $MgCl_2$, rather than NaCl, its major component.

3.3.6.1.1. Redistribution of ions at the surface

Absorbed water can influence OH uptake by salt materials due to a surface redistribution effect of salt ions. It has been reported that large polarizable anions are more readily available at a surface than relatively small and less polarizable cations [Jarvis *et al.*, 1968; Petersen *et al.*, 1999; Knipping *et al.*, 2000; Ghosal *et al.*, 2005]. Cations are thought to fit more easily into the hydrogen-bonded water structure upon solvation, whereas anions are too large [Knipping *et al.*, 2000]. Therefore, water extracts the small nonpolarizable cations to the bulk from the interface (surface). As a result, ions are redistributed near the surface according to their size and polarizability.

At this point, attention needs to be paid to define the surface and the bulk since it determines the way of the redistribution of the surface ions. In a solution, the bulk is the side that is abundant in water, while the surface is the other side exposed to the gas-phase. Therefore, due to its larger size and higher polarizability, anions are pushed out from the bulk to the surface interface while cations stay in the bulk [Jarvis *et al.*, 1968].

In our system of present work, however, the bulk is defined as inside of the salt solid, which is dry, whereas the surface is relatively abundant in water. As a consequence, water in the surface extracts cations from the bulk making them abundant on the surface interface under wet conditions.

The redistribution of surface ions is not limited to the fully wetted conditions at RH higher than their deliquescence. Even at low RH (~ 2%), ionic mobility is found to be enhanced, leading to the efficient redistribution of the surface ions [Hemminger, 1999] even though the extent of ion redistribution is a strong function of RH. It was found that the following factors are important in characterization of the surface ion redistribution:

(1) The size of ion

(2) The polarizability of ion

(3) Relative humidity

The radii and polarizabilities of ions in NaCl, $MgCl_2$, KCl, and $CaCl_2$ are summarized in Table 3.6. Since $MgCl_2$ and $CaCl_2$ exist as hydrated complexes under wet conditions, ionic radii for the higher coordination number (CN) are also listed. The order of ionic radii for ions with CN = 6 is $Mg^{2+} < Na^+ \sim Ca^{2+} < K^+ < Cl^-$. As can be seen from the ionic radius order, Mg^{2+} is expected to be the most active in the surface ion redistribution. Although K^+ is the least favorable ion due to its large ionic size, it is still more abundant on a wet surface as compared to even larger anions, such as Cl^-.

The ion radii of Na^+ and Ca^{2+} with CN = 6 are very close to each other. However, accounting for its higher coordination number and higher polarizability, Ca^{2+} is less favorable to be extracted by water from the bulk to the surface as compared to

Mg^{2+} or Na^{+}. Therefore, the efficiency of the surface ion redistribution at given RH is thought to follow the following order:

$$Surface \leftarrow Mg^{2+} < Na^{+} < Ca^{2+} < K^{+} < Cl^{-} \rightarrow Solid\ Bulk$$

This order can be applied not only to and individual salt, but also to a salt mixture, such as sea salt, leading to segregation effect as discussed in Section 3.3.6.1.3.

Table 3.7. Ionic radii and polarizabilities

Ion	Na^{+}	Mg^{2+}	K^{+}	Ca^{2+}	Cl^{-}
Ionic radius (Å)[a]	1.02[c]	0.72[c] 0.89[d]	1.38[c]	1.00[c] 1.34[e]	1.81[c]
Polarizability ($\times 10^{-24}$ cm^3)[b]	0.179	0.094	0.83	0.47	3.66

[a] Shannon *et al.*, 1976
[b] Jaswal *et al.*, 1973
[c] Coordination number : 6
[d] Coordination number : 8
[e] Coordination number : 12

3.3.6.1.2. The effect of the surface ion redistribution on OH uptake

The change in a cation surface concentration can influence OH uptake due to the following surface effects:

(1) Screening the available site for OH uptake (F1)

(2) Acidification of the surface (F2)

The first effect (*F1*) reduces γ_{OH}, while the second effect (*F2*) increases γ_{OH} as RH increases. These two opposite factors compete with each other, and therefore, the net effect is determined by the type of ions in the salt molecule, and by the RH condition.

The OH radical is an electron acceptor for which it is favorable to fill its π

orbital. The OH electron affinity is 1.828 eV [Goldfarb *et al.*, 2005], which is greater than that of O (1.461 eV [Neumark *et al.*, 1982]) and a half of that of Cl (3.613 eV) [Berzinsh *et al.*, 1995]. This implies that OH prefers an anion to an electron-deficient cation as an uptake site. Therefore, as anions are deficient in the surface, less OH uptake occurs on those sites.

The redistribution of ions results in an anion deficiency near the surface. The molecular dynamics simulations for a model salt surface $(NaCl)_{96}(H_2O)_{864}$ by Knipping et. al. [2000] showed the significant separation of the anion and the cation on the gas-wet solid interface, indicating that the surface cation concentration prevails over of the surface anion concentration depending on the degree of redistribution of the surface ions. As a consequence, the active sites available for OH uptake, ie, Cl^-, are screened by abundant cations and/or adsorbed water molecules decreasing γ_{OH}.

A similar effect was observed by Remorov *et al.* (2002) in a study of HO_2 uptake on NaCl. They reported a decrease in the HO_2 uptake on NaCl at a pressure of 0.1 Torr. Although the redistribution of ions was not taken into account, they successfully explained that the phenomenon by inhibition of water vapor reducing the number of the free sites available for adsorption of HO_2.

According to the reaction mechanism proposed early [Oum *et al.*, 1998; Finlayson-Pitts *et al.*, 2000], OH uptake on NaCl is extremely sensitive to surface pH since the reaction with H^+ (Reaction 3.28) is involved, which is considered to be the rate determining step:

$$OH + Cl^- \leftrightarrow HOCl^- \qquad (3.27)$$

$$HOCl^- + H^+ \rightarrow Cl + H_2O \qquad (3.28)$$

The detailed reaction mechanism is described in Appedix 3-VII.

The ion redistribution changes the surface pH with the efficiency dependant on the cation. To explain this dependence, other related facts must be taken into consideration. It has been reported that a water molecule can efficiently dissociate upon its adsorption on a surface with defects to form surface OH^- [Fölsch *et al.*, 1991; Dai *et al.*, 1995; Hemminger, 1999; Ghosal *et al.*, 2004] although the mechanism is still unknown. The surface remains neutral as H^+ and OH^- are produced together.

$$H_2O \rightarrow OH^- + H^+ \quad \text{(at surfaces with defects)} \qquad (3.29)$$

Also, it should be mentioned that water dissociates in the liquid bulk to produce the same products with $K_w = 1.0 \times 10^{-14}$, where K_w is the dissociation constant.

$$H_2O \rightarrow OH^- + H^+ \qquad (3.30)$$

Magnesium hydroxide ($Mg(OH)_2$) and calcium hydroxide ($Ca(OH)_2$) are insoluble in water with the solubility product constants (K_{sp}) of 5.61×10^{-12} mole^3 L^{-3} and 5.02×10^{-6} mole^3 L^{-3}, respectively [Wagman *et al.*, 1982; Lide, 2007].

$$K_{sp}(Mg(OH)_2) = [Mg^{2+}]\cdot[OH^-]^2 = 5.61\times10^{-12} \qquad (3.31)$$

$$K_{sp}(Ca(OH)_2) = [Ca^{2+}]\cdot[OH^-]^2 = 5.02\times10^{-6} \qquad (3.32)$$

Therefore, cations at high concentrations precipitate due to their reaction with OH^- produced from Reactions 3.29 and 3.30. As OH^- is removed from the surface interface according to Le Châtelier's Principle, surface pH decreases.

Although it is assumed that $K_w = 1.0 \times 10^{-14}$ is valid for Reaction 3.30 at the macroscopic scale (several water monolayers), the surface concentration of OH^- produced on surface defects (Reaction 3.29) is not known. Assuming that the two reactions are comparable, $[OH^-]$ can be estimated at 2×10^{-7} mole L^{-1}, and using this value in Reactions 3.31 and 3.32, the surface Mg^{2+} and Ca^{2+} concentrations to be precipitated can be estimated at 140 mole L^{-1} and 1.26×10^8 mole L^{-1}, respectively.

Since the latter is highly unlikely, it may be concluded that Ca^{2+} does not noticeably change the surface pH. Moreover, the degree of surface Ca^{2+} and Cl^- redistribution is much less than that for Mg^{2+} and Cl^- ions due to the larger size of Ca^{2+} (Section 3.3.6.1.1), implying $[Ca^{2+}] < [Mg^{2+}]$.

Due to the uncertainties in $[OH^-]$ and $[Mg^{2+}]$, it is difficult to determine if Mg^{2+} precipitates efficiently with OH^- ions. A concentration of $[Mg^{2+}] = 140$ mole L^{-1} is unlikely because the $MgCl_2$ solubility is 5.9 mole L^{-1} [Lide, 2007; Phase diagrams for ceramists, Volumes 1-8; ACerS-NIST Phase equilibrium diagrams, 1964-2001]. If significant relocation of Mg^{2+} into the surface by the redistribution of the surface ions is taken into account, however, an order of magnitude increase in its concentration may be possible.

Although precipitation does not occur, OH^- may still be removed via the following extremely favorable reaction ($K_{3.33} = 380$) [Stock *et al.*, 1948; Harris, 1991]:

$$Mg^{2+} + OH^- \leftrightarrow MgOH^+ \qquad (3.33)$$

As a result, the surface pH is lowered, favored by Reaction 3.28, causing an enhancement of OH uptake. In addition, this effect becomes greater at higher RH since the degree of the redistribution of the surface ions depends on RH.

Unfortunately, quantification of $[H^+]$ and the resulting change in γ_{OH} cannot be done accurately since the production rate in Reaction 3.29 is unknown. Additionally, the mechanism of OH uptake on a salt surface (Appendix 3-VII) is not yet well understood, although the qualitative estimation for change in γ_{OH} under wet conditions depending on salt is enabled as described above.

Recalling the beginning of this section, the overall relative humidity effect on OH uptake is determined by two competing factors (*F1* and *F2*), and depends on nature

of a salt surface. For $MgCl_2$, the surface acidification (*F2*) prevails over the screening by water adsorption the surface sites available for OH uptake (*F1*). As a result, γ_{OH} on $MgCl_2$ was enhanced as RH increased (Figure 3.12 (b)). In contrast, *F2* does not work for $CaCl_2$, while *F1* does, and therefore, OH uptake on $CaCl_2$ is decreased under wet conditions (Figure 3.12 (d)).

The same consideration can be applied to NaCl and KCl. As NaOH and KOH are extremely soluble, precipitation is not expected. However, the amount of adsorbed water on NaCl and KCl available to screen the surface sites from OH uptake is less than that on $CaCl_2$ at given RH due to the lower hydrophilicity of $CaCl_2$. Indeed, no noticeable change in γ_{OH} was observed (Figures 3.12 (a) and (e)). Assuming that the DRH is an appropriate measure of hydrophilicity, NaCl and KCl are less sensitive to change within a factor of 2.5 in RH than $CaCl_2$ since the DRH values for NaCl, KCl and $CaCl_2$ are 75%, 84% and 29%, respectively [Linke, 1965; Wagman *et al.*, 1982; Lide, 2007]. Although any noticeable change in γ_{OH} for NaCl and KCl were not observed in the range of 0 - 48% RH, lowering γ_{OH} is still anticipated in accordance with *F2* as RH approaches DRH.

The fact that a cation determines the water effect on OH uptake for its salt was confirmed by the observation for the two pairs of salts mixtures: $MgCl_2$-$MgSO_4$, and NaCl-Na_2SO_4. In addition to the five major components of sea salt, we performed additional uptake measurements for magnesium sulfate ($MgSO_4$) to study the role of cations in the effect of RH on OH uptake. As seen in Figure 3.13, γ_{OH} on $MgSO_4$ increased with RH, which is the similar effect as for $MgCl_2$. Recalling Figure 3.12 (a) and (c) for the other salt pair, Na_2SO_4 showed no change as the same was observed for NaCl. Based on the results of these experiments, we conclude the following:

(1) Cations are more important in determining the effect of relative humidity on OH uptake by a salt surface.

(2) Anions provide the reaction sites for OH uptake.

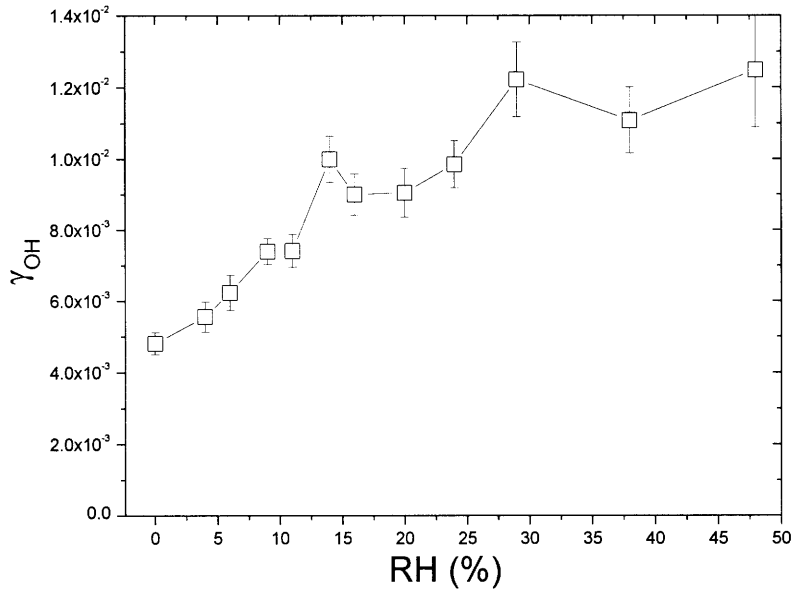

Figure 3.13. The dependence of γ_{OH} for $MgSO_4$ on RH. Note that the scale for the *x* axis (γ_{OH}) is wider than those in Figure 3.12 to show the full range of change.

3.3.6.1.3. Sea Salt

The most interesting observation was sea salt, a mixture of different salt components. As shown in Figure 3.12 (f), the water effect on OH uptake by sea salt followed patterns specific for $MgCl_2$ rather than its major constituent, NaCl. The enhancement by a factor of 2.7 in γ_{OH} for sea salt was observed at 0-38% of RH.

To determine which component(s) drive this reactivity, we studied two different salt mixtures. One was, so called, 'synthetic sea salt' which consisted of the same components in the same ratio as the real sea salt. In the other mixture, so called,

'synthetic sea salt without $MgCl_2$', only $MgCl_2$ was removed from the synthetic sea salt. As shown in Figure 3.14, the synthetic sea salt reproduced the sea salt regarding water effect on OH uptake, while the other without $MgCl_2$ followed NaCl reactivity with no changes observed. Therefore, $MgCl_2$ is likely responsible for the observed effect of water vapor on γ_{OH} for sea salt.

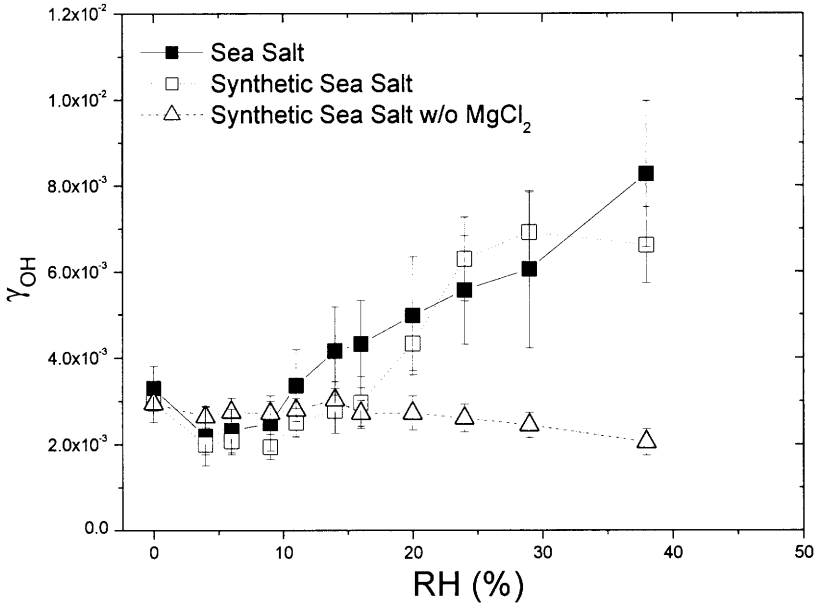

Figure 3.14. The dependence of γ_{OH} for sea salt (■), synthetic sea salt (□), and synthetic sea salt without $MgCl_2$ (△) on RH.

This may be explained by the segregation effect due to surface ion redistribution. In a multicomponent salt, such as sea salt, cations are redistributed by adsorbed water according to the order described in Section 3.3.6.1.1. For example, Dementiev *et al.* [2004] observed a similar segregation effect in a mixture of $MgCl_2 \cdot 6H_2O$ and NaCl. After exposure to water vapor for 10-15 min, the

$[Mg2^+]/[Na^+]$ molar ratio on the surface was enhanced from 0.043 to 1.2, which is quite consistent with the concept of the ion redistribution described in Section 3.3.6.1.1. As a result, Mg^{2+} becomes the most abundant cation on the sea salt surface under wet conditions, regardless of the average fraction in the bulk determining the overall effect of water on OH uptake by sea salt.

3.3.6.2. Mineral Dust Particles

Figure 3.15 and Table 3.7 show the observed enhancement in γ_{OH} for SiO_2 (silica) and Al_2O_3 (alumina) with increasing RH. The observed enhancement for silica and alumina are factors of 3 and 2, respectively, at RH of up to 38%.

A reaction mechanism for OH uptake on silica and alumina has not been proposed yet. However, surface-catalyzed bimolecular reactions following the Langmuir-Hinshelwood (L-H) and Eley-Rideal (E-R) mechanisms [Steinfeld *et al.*, 1998] may be involved. The extremely strong covalent bonding network in silica and alumina do not allow any direct abstractions (as in the reactions of OH on organics) or substitutions through reaction steps (as in the reactions of OH on inorganic salts) by the OH radical. It should be noted that the melting points of silica and alumina are 1722℃ (cristobalite) and 2054℃ (α type), respectively, whereas those of NaCl and $MgCl_2$ are much lower at 800℃ and 822℃, respectively

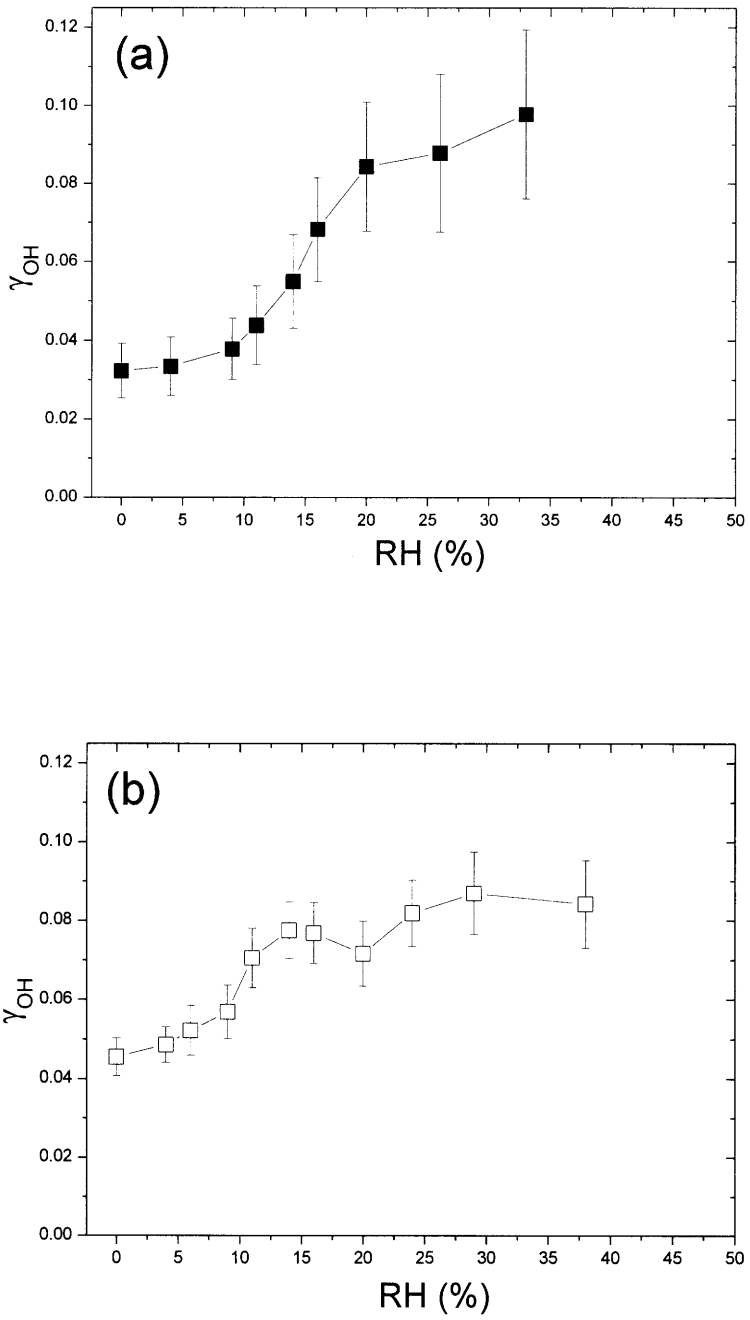

Figure 3.15. The dependence of γ_{OH} for SiO_2 (a) and Al_2O_3 (b) on RH

Table 3.8. The OH reaction probability for SiO_2 and Al_2O_3 under various RH conditions

RH (%)	γ_{OH} ($\times 10^{-2}$)	
	SiO_2	Al_2O_3
0	3.2 ± 0.7	4.5 ± 0.5
4	3.3 ± 0.7	4.9 ± 0.4
6	-[a]	5.2 ± 0.6
9	3.8 ± 0.8	5.7 ± 0.7
11	4.4 ± 1.0	7.0 ± 0.8
14	5.5 ± 1.2	7.8 ± 0.7
16	6.8 ± 1.3	7.7 ± 0.8
20	8.4 ± 1.7	7.2 ± 0.8
24	-[a]	8.2 ± 0.8
26	8.8 ± 2.0	-[a]
29	-[a]	8.7 ± 1.0
33	9.8 ± 2.2	-[a]
38	-[a]	8.4 ± 1.2

[a] γ_{OH} were not measured at these RH conditions.

(1) Langmuir-Hinshelwood (L-H) Mechanism

$$A + S \leftrightarrow A \cdot S \tag{3.34}$$

$$B + S \leftrightarrow B \cdot S \tag{3.35}$$

$$A \cdot S + B \cdot S \rightarrow \text{products} \tag{3.36}$$

$$R_{L-H} = \frac{k_{3.35} K_{3.33}[A] K_{3.34}[B] S_0^2}{\left(1 + K_{3.33}[A] + K_{3.34}[B]\right)^2} \tag{3.37}$$

(2) Eley-Rideal (E-R) Mechanism

$$A + S \leftrightarrow A \cdot S \tag{3.34}$$

$$A \cdot S + B \rightarrow \text{products} \tag{3.38}$$

$$R_{E-R} = \frac{k_{3.37} K_{3.33}[A] p_B S_0}{1 + K_{3.33}[A]} \tag{3.39}$$

where, A and B are the reactants (may be the same species), S is a site on the surface, R is the rate of product formation, k is the rate constant, K is the equilibrium constant for the adsorption process, S_0 is the number of available binding sites, and p_B is the gas pressure of B [Steinfeld *et al.*, 1998].

It has been known that the surface of silica and alumina are hydroxylated upon the dissociation of the adsorbed water leading to formation of surface Si-OH and Al-OH [Schaefer *et al.*, 1984; Nishijima *et al.*, 1986; Chen *et al.*, 1986; Thiel *et al.*, 1987; Elam *et al.*, 1998; Fu *et al.*, 2006]. Si-H formation upon water dissociation was also observed [Schaefer *et al.*, 1984; Nishijima *et al.*, 1986] while no observation for Al-H was reported.

The formation of Si-OH and Al-OH (and Si-H in the case of silica) upon the dissociation of adsorbed water molecules provides a higher probability for reaction with OH via the L-H or E-R process. More specifically, formation of Si-OH and Al-OH increases the amount of A·S due to Reaction 3.34, leading to a higher value of $K_{3.34}[A]$ in Equations 3.37 and 3.39. As a consequence, the product formation rate ($R_{L\text{-}H}$ and $R_{E\text{-}R}$) is enhanced although it still depends on the steps involving OH, such as Reactions 3.35, 3.36, and 3.38. Unfortunately, the estimation of the water effect on γ_{OH} for silica and alumina by quantification of the variables in the two catalytic mechanisms is not available. However qualitatively, it can be expected that the hydroxylation of silica and alumina by the adsorbed water causes increases in OH loss by its uptake on silica and alumina under wet conditions.

The products of the OH surface-catalyzed bimolecular reactions with the mineral dust surfaces likely include water and hydrogen peroxide (H_2O_2). The H_2O_2 released from the surface can further react with OH in the gas-phase:

$$H_2O_2 + OH \rightarrow H_2O + HO_2 \qquad (3.40)$$

with the rate constant $k_{3.40}$ = 1.7 $\times 10^{-12}$ cm^3 $molecule^{-1}$ s^{-1} [Atkinson *et al.*, 2004]. While OH loss in Reaction 3.40 is negligible at [OH] = 8 $\times 10^{-12}$ molecule cm^{-3}, H_2O_2 was not detected in the gas phase likely because of the slow rate of electron transfer from SF_6^-. Therefore, switching the reagent ion to O_2^+ for a higher CIMS sensitivity would increase the ability to detect H_2O_2.

$$O_2^+ + H_2O_2 \rightarrow O_2 + H_2O_2^+ \qquad (3.41)$$

with $k_{3.41}$ = 1.5 $\times 10^{-9}$ cm^3 $molecule^{-1}$ s^{-1} [Lindinger *et al.*, 1975]

We observed that γ_{OH} on alumina reached a maximum at approximately 14% RH as seen in Figure 3.15 (b). Coming back to the expression of the rate of product formation (Equations 3.37 and 3.39), the efficient hydroxylation of silica and alumina by water adsorption (corresponding A·S in Reaction 3.34), $K_{3.34}[A] \gg 1$, can lead to this saturation effect for since the adsorption of OH corresponding to Reactions 3.35, 3.36, and 3.38 is relatively slow. Therefore, it is suggested that the water adsorption on alumina is faster than that on silica, and hence becomes saturated at 14% RH.

3. 4. Atmospheric Implications

The results obtained show that the OH reaction probability is RH dependent for both initially hydrophilic organic surfaces and inorganic surfaces reaching higher values in comparison with those measured early under dry conditions. These high γ_{OH}-values become important for atmospheric modeling in which interactions with aerosol particles are included. A mechanism of such interactions and the RH effect can vary depending on the chemical composition and a mixed state of aerosol particles and a gas-phase environment but it is clear that it does not change a concentration level of OH in the

troposphere. Meanwhile, OH exposure can initiate and be ultimately responsible for chemical aging of atmospheric aerosol particles modifying their physical and chemical properties. It can lead to change in cloud condensation nuclei (CCN) ability of aerosols and their radiative forcing as well as to produce and release photochemically active gas-phase products.

The reactivity of sea salt under wet conditions was observed in the present study to be determined by its lower deliquesced component, namely $MgCl_2$. On the other hand, the efficiency of Cl_2 production in the reaction of OH with the deliquesced NaCl was found to be much higher than under dry conditions due to pronounced segregation of Cl^- to the surface interface. We can therefore conclude that the presence of a $MgCl_2$ component extracted to a sea-salt surface under subsaturated conditions will likely extend the reactivity of a sea-salt aerosol to lower relative humidity conditions increasing its contribution to Cl_2 production in the marine boundary layer.

3.5. Summary

We have investigated the effect of relative humidity on OH uptake by surfaces of tropospheric importance, such as organic compounds, sea-salt components, and mineral dust. In order to surmount diffusion limitations resulting from the introduction of high water vapor, the flow tube setup incorporated three techniques: i) beads-packing, ii) parallel reactor tubes with a reference, and iii) surface dilution. The virtual cylindrical reactor approximation successfully quantified the reaction probability of OH for the surfaces of interest.

The OH exposure of the hydrophobic organic surfaces (paraffin wax, pyrene, and methane soot) did not result in a measurable change to their hydrophilicities.

However, water vapor was observed to enhance the OH reactivity on a glutaric acid surface, a hydrophilic organic compound. The humidity effect on OH uptake by sea salt and its components was dependent on the nature of the cation of the salts. A redistribution of surface ions under humid environments caused changes in the proton concentration on a surface, influencing the rate determining step in the reaction mechanism of OH uptake. The segregation effect, a derivative effect from the redistribution of ions, explains why the RH effect on OH uptake by sea salt is determined by $MgCl_2$ rather than NaCl. Adsorbed water molecules on the surfaces of SiO_2 and Al_2O_3 provide sites for OH radicals to react through the surface-catalyzed bimolecular reactions resulting in the enhancement of the OH reactivity to a mineral dust surface under wet conditions.

Appendix 3-I. The Diffusion Coefficient of OH in a Mixture of Gases

The diffusion coefficient of OH in the flow of the mixture (D_c) was determined based on equation 3.7.

$$D_c^{-1} = \sum_i \alpha_i \cdot D_{OH-i}^{-1} \tag{3.7}$$

where α_i is the mixing ratio of the ith flow, and $D_{OH\text{-}i}$ is the diffusion coefficient of OH in the ith flow. When W_{mix} and W_i are the flow rates of the mixture and i, respectively, α_i was calculated as following:

$$\alpha_i = \frac{W_i}{W_{mix}} = \frac{W_i}{\sum_i W_i} \tag{3.40}$$

Under dry conditions, the mixed flow consists mainly of N_2 and He with W_{N2} = 1.75 SLPM and W_{He} = 0.80 SLPM, corresponding to α_{N2} = 0.686 and α_{He} = 0.314. Therefore, D_c was calculated as 213 [± 17] cm^2 Torr s^{-1}.

The 50% RH condition generated the water vapor flow with W_{H2O} = 0.30 SLPM to the system, and adjusted the N_2 flow to W_{N2} = 1.45 SLPM for a constant pressure. Under this condition, the mixing ratios were α_{N2} = 0.569, α_{He} = 0.314, and α_{H2O} = 0.118, with D_c = 215 [± 30] cm^2 Torr s^{-1}. 50% RH contributes only 1% of difference in the diffusion of OH in the flow.

Appendix 3-II. The Relative Intensity of OH, $R_{surface}$

$[OH]_t$, the concentration of OH at time t, is expressed as Equation 3.41 using Equation 3.1.

$$-\ln\frac{[OH]_t}{[OH]_0} = k_{obs}t \tag{3.1}$$

$$[OH]_t = [OH]_0 \cdot \exp(-k_{obs} \cdot t) \tag{3.41}$$

in turn, $[OH]_{surface}$ and $[OH]_{reference}$, which are the concentrations of OH measured after exposure to the organic and inorganic surfaces of interest and the reference (halocarbon wax), respectively, are expressed as follows:

$$[OH]_{surface} = [OH]_0 \cdot \exp(-k_{obs}^{surface} \cdot t) \tag{3.42}$$

$$[OH]_{reference} = [OH]_0 \cdot \exp(-k_{obs}^{reference} \cdot t) \tag{3.43}$$

The relative intensity of OH for the heterogeneous reaction on the aerosol surface of interest, R_{OH}, is defined by Equation 3.13 as discussed in Section 3.3.2:

$$R_{OH} = \frac{[OH]_{Surface}}{[OH]_{reference}} = \frac{I_{Surface}^{OH}}{I_{reference}^{OH}} \tag{3.8}$$

where $I^{OH}_{surface}$ and $I^{OH}_{reference}$ are the signal intensities of OH in detection from the reactor and the reference, respectively. Using Equations 3.42 and 3.43, R_{OH}, is related to the observed rate constants for each material as follows:

$$R_{OH} = \frac{[OH]_{Surface}}{[OH]_{reference}} = \frac{[OH]_0 \cdot \exp(-k_{obs}^{surface} \cdot t)}{[OH]_0 \cdot \exp(-k_{obs}^{reference} \cdot t)} \tag{3.44}$$

$$R_{OH} = \exp[-(k_{obs}^{surface} - k_{obs}^{reference}) \cdot t] \tag{3.9}$$

Appendix 3-III. Determination of γ_{OH} from $R_{surface}$

The following is an example of the determination of γ_{OH} on pure paraffin wax surface from $R_{paraffin\ wax}$ using the following given values.

$l_a = 2.6$ cm $= 2.6 \times 10^{-2}$ m

$r_a = 0.474$ cm $= 4.74 \times 10^{-3}$ m

n = 60

$r_b = 0.149$ cm $= 1.49 \times 10^{-3}$ m

p = 100 Torr

T = 293 K

Therefore, the following may be calculated,

$$V = (\pi r_a^2 l_a) - \frac{4}{3}\pi r_b^3 n = 1.01 \times 10^{-6} m^3 \quad \text{(Equation 3.10)},$$

$$S = 4\pi r_b^2 n = 1.66 \times 10^{-3} m^2 \quad \text{(Equation 3.11)}$$

$$r_v = \frac{2V}{S} = 1.22 \times 10^{-3} m \quad \text{(Equation 3.12)}$$

$$l_v = \frac{V}{\pi r_v^2} = 2.16 \times 10^{-1} m \quad \text{(Equation 3.13)}$$

$$t_v = \frac{V}{W} = 3.13 \times 10^{-3} s \quad \text{(Equation 3.14)}$$

$$c_{OH} = 1.45 \times 10^2 \cdot \sqrt{\frac{T}{\mu_{OH}}} = 602 m \cdot s^{-1}$$

Since, D_c was calculated as 213 [± 17] cm^2 Torr s^{-1} in Appendix 3-I,

$$k_{diff} = \frac{3.66 D_c}{r^2 P} = 528.8 s^{-1} \quad \text{(Equation 3.4)}.$$

For halocarbon wax as a reference, $\gamma_{OH} = 6\times10^{-4}$ [Bertram *et al.*, 2001], therefore,

$$k_{kin}^{halo} = \frac{\gamma_{OH}^{halo} \cdot c_{OH}}{2 \cdot r_v} = 148.3s^{-1} \text{ and } k_{obs}^{halo} = (\frac{1}{k_{diff}} + \frac{1}{k_{kin}^{halo}})^{-1} = 115s^{-1}.$$

The upper limit of the relative intensity of OH for paraffin wax obtained experimentally was 0.297. Therefore, $k_{obs}^{paraffin}$ for paraffin wax is calculated using Equation 3.9, followed by determining $k_{kin}^{paraffin}$.

$$k_{obs}^{paraffin} = k_{obs}^{reference} - \frac{\ln(R_{paraffin})}{t} = 503.3s^{-1}$$

$$k_{kin}^{paraffin} = (\frac{1}{k_{obs}^{paraffin}} - \frac{1}{k_{diff}})^{-1} = 1.04\times10^{4}s^{-1}$$

Finally, the reaction probability of OH on paraffin wax is determined as follows:

$$\gamma_{OH}^{paraffin} = \frac{2r \cdot k_{kin}^{paraffin}}{c_{avg} + r \cdot k_{kin}^{paraffin}} = 0.041$$

The uncertainty of γ_{OH} is obtained from the upper and lower limits of R_{OH}, rather than from the error propagation described in Appendix 3-IV. For example, the lower limit of R_{OH} on paraffin wax is 0.265, which corresponds $\gamma_{OH}^{paraffin}$=1. Therefore, the possible range of $\gamma_{OH}^{paraffin}$ is 0.04 - 1.

Appendix 3-IV. Errors in the VCR Approximation

A. 3-IV. 1. The basic rules of error propagation

$$z = x \pm y, \qquad \Delta z = \sqrt{(\Delta x)^2 + (\Delta y)^2} \tag{3.45}$$

$$z = x \cdot y, \qquad \frac{\Delta z}{z} = \sqrt{\left(\frac{\Delta x}{x}\right)^2 + \left(\frac{\Delta y}{y}\right)^2} \tag{3.46}$$

$$z = x^m \cdot y^n, \qquad \frac{\Delta z}{z} = \sqrt{\left(\frac{m \cdot \Delta x}{x}\right)^2 + \left(\frac{n \cdot \Delta y}{y}\right)^2} \tag{3.47}$$

$$z = f(x,y), \qquad \Delta z = \left(\frac{\partial f}{\partial x}\right) \cdot \Delta x + \left(\frac{\partial f}{\partial y}\right) \cdot \Delta y \tag{3.48}$$

A. 3-IV. 2. The Initial Errors in Measurements

l_a = 2.6 [± 0.1] cm $\qquad$ r_a = 0.474 [± 0.005] cm

r_b = 0.149 [± 0.002] cm $\qquad$ p = 100 [± 1] Torr

T = 293 [± 1] K $\qquad$ W = 2.55 [± 0.04] SLPM.

A. 3-IV. 3. Errors in V, S, l_v, r_v, and t

The volume of the space in which OH can freely move (V) is the difference between V_{tube} and the total volume of the beads packed in a flow tube.

$$V = V_{tube} - V_{bead} \cdot n \tag{3.49}$$

where V_{tube} and V_{bead} are the volume of a tube and the volume of a bead, respectively. Since $V_{tube} = l_a \cdot \pi \cdot r_a^2$, the propagated error in V_{tube} is

$$\frac{\Delta V_{tube}}{V_{tube}} = \sqrt{\left(\frac{\Delta l_a}{l_a}\right)^2 + \left(\frac{2\Delta r_a}{r_a}\right)^2} = \sqrt{\left(\frac{0.1}{2.6}\right)^2 + \left(\frac{0.01}{0.474}\right)^2} = 4\%$$

For $V_{bead} = \frac{4}{3}\pi \cdot r_b^3$, $\frac{\Delta V_{bead}}{V_{bead}} = \sqrt{\left(\frac{3\Delta r_b}{r_b}\right)^2} = \sqrt{\left(\frac{0.006}{0.149}\right)^2} = 4\%$.

Therefore, $\Delta V = \sqrt{(4\% \times V_{tube})^2 + (4\% \times V_{bead} \cdot n)^2} = 8.04 \times 10^{-8} m^3$, since V_{tube} = 1.84×10^{-6} m^3 and $V_{bead} = 1.37\times10^{-8}$ m^3. This corresponds 7% error in V.

For S, $\frac{\Delta S}{S} = \frac{\Delta r_b^2}{r_b^2}$, as $S = 4\pi r_b^2 n$. Therefore, $\frac{\Delta S}{S} = 3\%$.

For l_v, r_v, and t,

$$\frac{\Delta l_v}{l_v} = \sqrt{\left(\frac{\Delta V}{V}\right)^2 + \left(\frac{\Delta S}{S}\right)^2} = 8\% \quad (\because \; l_v = \frac{V}{S}),$$

$$\frac{\Delta r_v}{r_v} = \sqrt{\left(\frac{\Delta V}{V}\right)^2 + \left(\frac{\Delta S}{S}\right)^2} = 8\% \quad (\because \; r_v = \frac{2V}{S}), \text{ and}$$

$$\frac{\Delta t}{t} = \sqrt{\left(\frac{\Delta V}{V}\right)^2 + \left(\frac{\Delta W}{W}\right)^2} = 7\% \quad (\because \; t = \frac{V}{W}).$$

A. 3-IV. 4. Errors in Diffusion Coefficients

The errors in the diffusion coefficients of OH in N_2 and He in the mixtures are 5% and 12%, respectively [Bertram *et al.*, 2001; Ivanov *et al.*, 2007; Section 3.3.1]. Since the errors in the flow rates are 2%, the propagated error in the mixing ratio (α_i) is calculated to be 3%.

For $D_c^{-1} = \alpha_{N_2} \cdot D_{OH-N_2}^{-1} + \alpha_{He} \cdot D_{OH-He}^{-1}$,

$$\frac{\Delta(\alpha_{N_2} \cdot D_{OH-N_2}^{-1})}{\alpha_{N_2} \cdot D_{OH-N_2}^{-1}} = \sqrt{\left(\frac{\Delta\alpha_{N_2}}{\alpha_{N_2}}\right)^2 + \left(\frac{\Delta(D_{OH-N_2}^{-1})}{D_{OH-N_2}^{-1}}\right)^2} = \sqrt{(0.03)^2 + (0.12)^2} = 12\%,$$

and, $\frac{\Delta(\alpha_{He} \cdot D_{OH-He}^{-1})}{\alpha_{He} \cdot D_{OH-He}^{-1}} = \sqrt{(0.03)^2 + (0.05)^2} = 6\%$. Therefore, $\frac{\Delta D_c}{D_c} = 11\%$.

Since $k_{diff} = \frac{3.66 D_c}{r^2 P}$,

$$\frac{\Delta k_{diff}}{k_{diff}} = \sqrt{\left(\frac{\Delta D_c}{D_c}\right)^2 + \left(\frac{2\Delta r_v}{r_v}\right)^2 + \left(\frac{\Delta P}{P}\right)^2} = \sqrt{(0.11)^2 + (2 \times 0.08)^2 + (0.01)^2} = 19\%$$

.

A. 3-IV. 5. Errors in Kinetics

The error in k_{kin} depends on the heterogeneous reactivity of OH to the surface material. Therefore, in the case of k_{kin} and γ_{OH}, only approximate estimations of the errors under certain assumptions are available.

Assuming that the errors in $k_{kin}^{reference}$ are determined by the error in r_v= 8%, the error in $k_{obs}^{reference}$ is calculated to be 10% based on the additivity of kinetic resistances (Equation 3.3).

In the modified Equation 3.9, $k_{obs}^{surface} = k_{obs}^{reference} - \frac{\ln(R_{surface})}{t}$, $\Delta\left(\ln(R_{surface})\right) = \left(\frac{1}{R_{surface}}\right) \cdot \Delta R_{surface}$ is calculated to be 0.05 since the error in $R_{surface}$ is 5%. Accounting for 7% error in t, the error in $k_{obs}^{surface}$ is estimated to be 14% approximately at $R_{surface} = 0.50 \pm 0.05$.

Under the assumption $\frac{\Delta k_{kin}^{surface}}{k_{kin}^{surface}} = \sqrt{\left(\frac{\Delta k_{obs}^{surface}}{k_{obs}^{surface}}\right)^2 + \left(\frac{\Delta k_{diff}}{k_{diff}}\right)^2}$, the error in $k_{kin}^{surface}$ is estimated as 24%. Errors in the OH reaction probability are calculated based on Equation 3.6.

$$\frac{\Delta \gamma_{OH}}{\gamma_{OH}} = \sqrt{\left(\frac{\Delta r_v}{r_v}\right)^2 + \left(\frac{\Delta k_{kin}^{surface}}{k_{kin}^{surface}}\right)^2} = \sqrt{(0.07)^2 + (0.24)^2} = 25\%$$

However, note that the uncertainties of γ_{OH} are obtained from the upper and lower limits of R_{OH}, but not from the error propagation described above in Appendix 3-III. In other words, only random errors in measurements were accounted. However, the uncertainty from error propagation can be used to determine how much change in γ_{OH} may be considered experimentally significant.

Appendix 3-V. Determination of the fraction of OH-H_2O complex

A.3-V.1. $k_{3.16}$

The transition state in Reaction 3.16 could not be determined at a level of B3LYP and MP2 theory, implying the energy barrier is extremely shallow or zero. Therefore, the reaction is assumed to proceed whenever the reactants collide with each other with the proper orientation. The rate constant within the reactive hard-sphere model is calculated by the collision frequency (Z) and the activation energy (E*) as follows [Steinfeld *et al.*, 1998] :

$$k = Z \cdot p \cdot e^{-E^*/k_BT} = \pi d^2 \left(\frac{8k_BT}{\pi\mu} \right)^{1/2} p \cdot e^{-E^*/k_BT} \qquad (3.50)$$

where

d : hard sphere minimum approach distance (m)

k_B : Boltzmann constant (1.381×10^{-23} J K^{-1})

T : Temperature (298 K)

μ : Reduced mass (kg)

p : Steric factor

The distance d was set as that between two oxygen atoms in the complex, d = 2.86×10^{-10} m, because the centers of mass are close to the oxygen atoms in OH and H_2O. Since no entrance barrier (E* = 0) was assumed, the rate constant was calculated as $2.18 \times10^{-16} \cdot p$ cm^3 $molecule^{-1}$ s^{-1}. Therefore, the steric factor, p, is the last variable to be determined.

The steric factor p corresponds to the relative orientation of the reacting

molecules, a deviation of the reactive hard-sphere model from the observed gas-kinetic collision rate [Levine, 1990, Akins, 1990, Laidler *et al.*, 1992, Steinfeld *et. al.*, 1998]. Since the quantitative determination of p is beyond the scope of this thesis and the transition state was not optimized, an approximate value was estimated by scanning the potential energy surface through the variables in Figure 3.16.

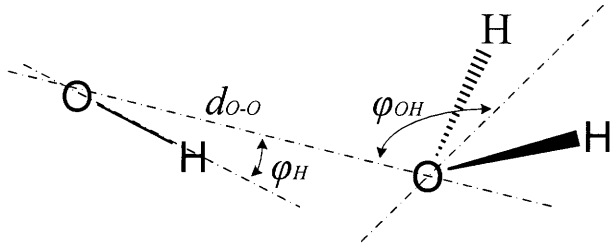

Figure 3.16. Variables to scan the potential energy surface of OH-H_2O complex.

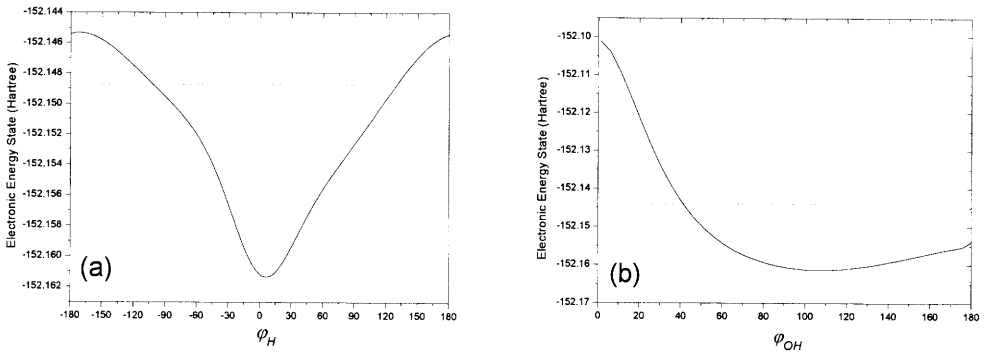

Figure 3.17. The energy dependence on the orientation of the molecules. The dotted line is the total energy of the reactants.

φ_H is the angle of the hydrogen atom in OH to the of two oxygen atoms representing the orientation of OH, φ_{OH} is the angle of OH to the plane consisting of H_2O representing the orientation of H_2O, and $d_{O\text{-}O}$ is the distance between two oxygen with fixed O—H distance in OH. Although the energy dependence on φ_H and φ_{OH} did not cover the entire orientation of the two molecules, it provided an approximation for p.

The energy dependence on the angle variables for angles (φ_H (a) and φ_{OH} (b)) is shown in Figure 3.17.

According to Figure 3.17, most orientations were favorable for the reaction. When φ_H was in the range -90° to 120°, the energy of the complex was below than that of the reactants, implying 60% of OH orientation is favorable for the reaction. In the case of φ_{OH}, 80 % is proper for the reaction. Therefore, p is roughly estimated as 0.5 giving $k_{3.16} = 1.1 \times 10^{-16}$ cm^3 molecule^{-1} s^{-1}.

A.3-V.2. $k^{-1}_{3.16}$

For the reverse of Reaction 3.16, self-dissociation of OH-H_2O, a loose complex of OH and H_2O (OH$\cdots$$H_2O$ in Table 3.1) was assumed to represent the transition state in the reaction although no optimized transition state was found. The structures of OH and H_2O at their individual global minima were retained in the loose complex while the distance between them was long enough not to interrupt the stability of each species. Figure 3.18 shows how the total energy of the complex depends on $d_{O\text{-}O}$. Since the energy started converging at the distance of 5.5 Å, $d_{O\text{-}O}$ was set at 5.5 Å.

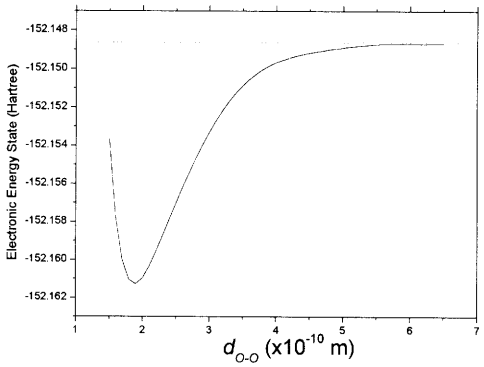

Figure 3.18. The energy dependence on $d_{O\text{-}O}$ in the OH$\cdots$$H_2O$ complex.

The rate constant for the reverse reaction, $k^{-1}_{3.16}$, was determined using the loose

complex ($OH\cdots H_2O$) and $OH\text{-}H_2O$ complex through the Eyring equation [Atkins, 1990; Laidler *et al.*, 1995].

$$k = \frac{k_B T}{h} e^{\Delta^* S^o / R} e^{-\Delta^* H^o / RT} = \frac{k_B T}{h} e^{\Delta^* G^o / RT} \qquad (3.51)$$

where

h : Planck's constant (6.626×10^{-34} J s)

R : Gas constant (8.315 J K^{-1} mol^{-1})

$\Delta^* S^o$: Entropy change between a reactant and a transition state

$\Delta^* H^o$: Enthalpy change between a reactant and a transition state

$\Delta^* G^o$: Gibbs free energy change between a reactant and a transition state.

The Gibbs free energies of the two complexes (Table 3.1) gave a rate constant $k^{-1}_{3.16}$ = 5.3×10^9 s^{-1} at 298 K. Since this reaction is first order, the lifetime of the complex could be determined as the inverse of the rate constant, or 1.9×10^{-10} s.

A.3-V.3. Fraction of a $OH\text{-}H_2O$ complex in the Gas-phase

Using Equation 3.21 and the rate constants obtained above, the equilibrium constant was determined as follows:

$$K_{3.15} = \frac{k_{3.15}}{k^{-1}_{3.15}} = \frac{1.1 \times 10^{-16} cm^3 molecule^{-1} s^{-1}}{5.3 \times 10^9 s^{-1}} = 2.1 \times 10^{-26} cm^3 molecule^{-1}.$$

Since the concentrations of OH and H_2O are 8×10^{11} molecule cm^{-3} and 3.2×10^{17} molecule cm^{-3}, respectively, at 40% RH, the concentration of $OH\text{-}H_2O$ complex was calculated as follows:

$$[OH - H_2O] = K_{3.15} \cdot [OH] \cdot [H_2O] = 5.3 \times 10^2 \text{ molecule cm}^{-3}$$

Therefore, the fraction of $OH\text{-}H_2O$ complex in the gas phase was estimated at 6.6×10^{-10}.

Appendix 3-VI. Determination of γ_{OH} on the pure organic surfaces from $R_{surface}$ for diluted surfaces

A.3-VI.1. The material with known γ_{OH} (Pyrene as an example)

$R_{surface}$ = 0.571 was measured on a diluted pyrene surface under dry conditions, which corresponds to γ_{OH} = 0.0027 (See Appendix 3-II). As the reaction probability of OH on pyrene was known to be 0.30 [Bertram *et. al.*, 2001], the fraction of pyrene in the diluted mixture, denoted β_{pyrene}, was determined as follows with Equation 3.15:

$$\gamma_{OH}^{mix} = \sum_j \beta_j \gamma_{OH}^j = \beta_{pyrene}\gamma_{OH}^{pyrene} + (1-\beta_{pyrene})\gamma_{OH}^{reference} \qquad (3.15)$$

$$\beta_{pyrene} = \frac{\gamma_{OH}^{mix} - \gamma_{OH}^{reference}}{\gamma_{OH}^{pyrene} - \gamma_{OH}^{reference}} = 0.0070 \qquad (3.52)$$

Since β_{pyrene} is independent of dry or wet conditions, it was possible to retrieve the γ_{OH}^{mix} under wet conditions for the pure pyrene surface (γ_{OH}^{pyrene}) using the same value of β_{pyrene} according to Equation 3.53:

$$\gamma_{OH}^{pyrene} = \frac{\gamma_{OH}^{mix} - (1-\beta_{pyrene})\gamma_{OH}^{reference}}{\beta_{pyrene}} \qquad (3.53)$$

A.3-VI.2. The material on unknown γ_{OH} (Glutaric acid as an example)

Since γ_{OH} on glutaric acid was unknown, R_{OH} on pure glutaric acid was first measured under dry conditions. Based on the obtained R_{OH} we were able to estimate γ_{OH} of 0.24 for glutaric acid following the procedure described in the Section A.3-VI.1.

Appendix 3-VII. Reaction Mechanism of OH Uptake by NaCl

Keene *et al.* [1993], Oum *et al.* [1998] and Finalyson-Pitts *et al.* [2000] suggested the following reaction mechanism of OH uptake by NaCl:

$$OH + Cl^- \leftrightarrow HOCl^- \quad (3.27)$$

$$HOCl^- + H^+ \rightarrow Cl + H_2O \quad (3.28)$$

$$Cl + Cl \rightarrow Cl_2 \quad (3.54)$$

$$Cl + Cl^- \rightarrow Cl_2^- \quad (3.55)$$

$$Cl_2^- + Cl_2^- \rightarrow Cl_2 + 2Cl^- \quad (3.56)$$

$$Cl_2 + H_2O \rightarrow HOCl + H^+ + Cl^- \quad (3.57)$$

$$HOCl + H^+ + Cl^- \rightarrow Cl_2 + H_2O \quad (3.58)$$

Reaction 3.28 is assumed to be the rate-determining step. At a high pH, i.e. low $[H^+]$, the dissociation of $HOCl^-$ in Reaction 3.27 is faster than Reaction 3.28, such that the reaction mechanism is pH sensitive.

References for Chapter 3

S. Aloisio and J. S. Francisco, Radical-water complexes in earth's atmosphere, *Acc. Chem. Res.*, **33**, 825-830, 2000.

P. W. Atkins, Physical Chemistry (4th Edition), Oxford University Press, Oxford, 1990.

R. Atkinson, D. L. Baulch, R. A. Cox, J. N. Crowley, R. F. Hampson, Jr, J. A. Kerr, M. J. Rossi, and J. Troe, Summary of evaluated kinetic and photochemical data for atmospheric chemistry, IUPAC Subcommittee on Gas Kinetic Data Evaluation for Atmospheric Chemistry Web Version, 2001.

R. Atkinson, D. L. Baulch, R. A. Cox, J. N. Crowley, R. F. Hampson, R. G. Hynes, M. E. Jenkin, M. J. Rossi, and J. Troe, Evaluated kinetic and photochemical data for atmospheric chemistry: Volume I – Gas phase reactions of O_x, HO_x, NO_x and SO_x species, *Atmos. Chem. Phys.*, **4**, 1461-1738, 2004.

D. W. Ball, DFT and G2 calculations on the NO2-H2O molecular complex, *Chem. Phys. Lett.*, **312**, 306-310, 1999.

A. K. Bertram, A. V. Ivanov, M. Hunter, L. T. Molina, and M. J. Molina, The reaction probability of OH on organic surfaces of tropospheric interest, *J. Phys. Chem. A*, **105**, 9415-9421, 2001.

U. Berzinsh, M. Gustafsson, D. Hanstorp, A. Klinkmüller, U. Ljungblad, and A. –M. Maartensson-Pendrill, Isotope shift in the electron affinity of chlorine, *Phys. Rev. A*, **51**, 231-238, 1995.

A. Blanc, *J. Phys.*, 7, 825, 1908.

R. L. Brown, Tubular flow reactors with first-order kinetics, *J. Res. Natl. Bur. Stand.*, **83**, 1-8, 1978.

J. G. Chen, J. E. Crowell, and J. T. Yates, Jr., Assignment of a surface vibrational mode by chemical means: Modification of the lattice modes of Al_2O_3 by a surface reaction with H_2O, *J. Chem. Phys.*, **84**, 5906-5909, 1986.

A. P. Dement'ev, V. V. Zelenov, E. V. Aparina, D. V. Shestakov, S. D. Il'in, and Yu. M. Gershenzon, Kinetics mechanisms of the capture of atomospheric gases on the surfaces of marine salts. VI. Segregation of $MgCl_2 \cdot 6H_2O$ on the surface of NaCl salt doped with $MgCl_2 \cdot 6H_2O$ and its effect on the rate of heterogeneous reaction with NO_3, *Khimicheskaya Fizika*, **23**, 54-59, 2004.

M. K. Dubey, R. Mohrschladt, N. M. Donahue, and J. G. Anderson, Isotope specific kinetics of hydroxyl radical (OH) with water (H_2O): Testing models of reactivity and atmospheric fractionation, *J. Phys. Chem. A*, **101**, 1494-1500, 1997.

T. R. Dyke, K. M. Kack, and J. S. Muenter, Microwave-spectrum and structure of hydrogen-bonded water dimer, *J. Chem. Phys.*, **66**, 492-497, 1977.

D. F. Fairbanks and C. R. Wilke, Diffusion Coefficients in multicomponent gas mixtures, *Ind. Eng. Chem.*, **42**, 471-475, 1950.

J. W. Elam, C. E. Nelson, M. A. Cameron, M. A. Tolbert, and S. M. George, Adsorption of H_2O on a single-crystal α-Al_2O_3(0001) surface, *J. Phys. Chem. B*, **102**, 7008-7015, 1998.

M. W. Feyereisen, D. Feller, and D. A. Dixon, Hydorgen bond energy of the water dimer, *J. Phys. Chem.*, **100**, 2993-2997, 1996.

B. J. Finlayson-Pitts and J. C. Hemminger, Physical chemistry of airborne sea salt particles and their components, *J. Phys. Chem. A*, **104**, 11463-11477, 2000.

H. S. Fogler, *Elements of chemical reaction engineering (3rd Edition)*, Prentice Hall, Upper Saddle River, N.J., 1999.

M. J. Frisch, G. W. Trucks, H. B. Schlegel, G. E. Scuseria, M. A. Robb, , J. R. Cheeseman, J. A. Montgomery, Jr., T. Vreven, K. N. Kudin, J. C. Burant, J. M. Millam, S. S. Iyengar, J. Tomasi, V. Barone, B. Mennucci, M. Cossi, G. Scalmani, N. Rega, G. A. Petersson, H. Nakatsuji, M. Hada, M. Ehara, K. Toyota, R. Fukuda, J. Hasegawa, M. Ishida, T. Nakajima, Y. Honda, O. Kitao, H. Nakai, M. Klene, X. Li, J. E. Knox, H. P. Hratchian, J. B. Cross, C. Adamo, J. Jaramillo, R. Gomperts, R. E. Stratmann, O.

Yazyev, A. J. Austin, R. Cammi, C. Pomelli, J. W. Ochterski, P. Y. Ayala, K. Morokuma, G. A. Voth, P. Salvador, J. J. Dannenberg, V. G. Zakrzewski, S. Dapprich, A. D. Daniels, M. C. Strain, O. Farkas, D. K. Malick, A. D. Rabuck, K. Raghavachari, J. B. Foresman, J. V. Ortiz, Q. Cui, A. G. Baboul, S. Clifford, J. Cioslowski, B. B. Stefanov, G. Liu, A. Liashenko, P. Piskorz, I. Komaromi, R. L. Martin, D. J. Fox, T. Keith, M. A. Al-Laham, C. Y. Peng, A. Nanayakkara, M. Challacombe, P. M. W. Gill, B. Johnson, W. Chen, M. W. Wong, C. Gonzalez, and J. A. Pople, Gaussian 03, Revision B.01, Gaussian, Inc., Pittsburgh PA, 2003.

Q. Fu, T. Wagner, and M. Rűhle, Hydroxylated α-$Al_2O_3(0001)$ surfaces and metal/α-$Al_2O_3(0001)$ interfaces, *Surf. Sci.*, **600**, 4870-4877, 2006.

S. Ghosal and J. C. Hemminger, Surface adsorbed water on NaCl and its effect on nitric acid reactivity with NaCl powders, *J. Phys. Chem. B*, **108**, 14102-14108, 2004.

S. Ghosal, J. C. Hemminger, H. Bluhm, B. S. Mun, E. L. D. Hebenstreit, G. Ketteler, D. F. Ogletree, F. G. Requejo, and M. Salmeron, Electron spectroscopy of aqueous solution interfaces reveals surface enhancement of halides, *Science*, **307**, 563-566, 2005.

F. Goldfarb, C. Drag, W. Chaibi, S. Kröger, C. Blondel, and C. Delsart, Photodetachment microscopy of the P, Q, and R branches of the OH^- (v = 0) to OH (v = 0) detachment threshold, *J. Chem. Phys.*, **122**, 014308, 2005.

F. Gratpanche, A. Ivanov, P. Devolder, Y. Gershenzon, and J. –P. Sawerysyn, Uptake coefficients of OH and HO_2 radicals on material surfaces of atmospheric interest, *in 14th International symposium on gas kinetics book of abstracts*, edited by the University of Leeds, abstract **A12**, Leeds, 1996.

J. C. Hansen and J. S. Francisco, Radical-molecule complexes: Changing our perspective on the molecular mechanisms of radical-molecule reactions and their impact on atmospheric chemistry, *Chem. Phys. Chem.*, **3**, 833-840, 2002.

D. R. Hanson, J. B. Burkholder, C. J. Howard, and A. R. Ravishankara, Measurement of OH and HO_2 radical uptake coefficients on water a sulfuric acid surfaces, *J. Phys. Chem.*, **96**, 4979-4985, 1992.

D. C. Harris, *Quantitative chemical analysis (3rd Edition)*, W. H. Freeman and Company, New York, 1991.

J. C. Hemminger, Heterogeneous chemistry in the troposphere: a modern surface chemistry approach to the study of fundamental processes, *Int. Rev. Phys. Chem.*, **18**, 387-417, 1999.

A. V. Ivanov, S. Trakhtenberg, A. K. Bertram, Y. M. Gershenzon, and M. J. Molina, OH, HO_2, and ozone gaseous diffusion coefficients, *J. Phys. Chem. A*, **111**, 1632-1637, 2007.

N. L. Jarvis and M. A. Scheiman, Surface potentials of aqueous electrolyte solutions, *J. Phys. Chem.*, **72**, 74-78, 1968.

S. S. Jaswal and T. P. Sharma, Electronic polariabilities of ions in alkali halide crystals, *J. Phys. Chem. Solids*, **34**, 509-511, 1973.

N. Karakus and R. Ozkan, *Ab initio* study of atmospheric reactions of the hydroxyl radical-water complex ($OH\text{-}H_2O$) with saturated hydrocarbons (methane, ethane and propane), *Theochem.*, **724**, 39-44, 2005.

W. C. Keene, J. R. Maben. A. A. P. Pszenny, and J. N. Galloway, Measurement technique for inorganic chlorine gases in the marine boundary layer, *Environ. Sci. Technol.*, **27**, 866-874, 1993.

E. M. Knipping, M. J. Lakin, K. L. Foster, P. Jungwirth, D. J. Tobias, R. B. Gerber, D. Dabdub, B. J. Finlayson-Pitts, Experiments and simulations of ion-enhanced interfacial chemistry on aqueous NaCl aerosols, *Science*, **288**, 301-306, 2000.

K. S. Kim, H. S. kim, J. H. Jang, H. S. Kim, and B. Mhin, Hydrogen bonding between the water molecule and the hydroxyl radical ($H_2O{\cdot}OH$): The $^2A''$ and $^2A'$ minima, *J. Chem. Phys.*, **94**, 2057-2061, 1991.

K. J. Laidler and J. H. Meiser, *Physical Chemistry (2nd Edition)*, Houghton Mifflin Co., Boston, 1995.

A. Laskin, H. Wang, W. H. Robertson, J. P. Cowin, M. J. Ezell, and B. J. Finlayson-Pitts, A new approach to determining gas-particle reaction probabilities and application to the heterogeneous reaction of deliquesced sodium chloride particles with gas-phase hydroxyl radicals, *J. Phys. Chem. A*, **110**, 10619-10627, 2006.

R. D. Levine, The steric factor in transition state theory and in collision theory, *Chem. Phys. Lett.*, **175**, 331-337, 1990.

W. Lindinger, D. L. Albritton, C. J. Howard, F. C. Fehsenfeld, and E. E. Ferguson, Flow-drift tube measurements of hydrogen peroxide(+) ion reactions with water, ammonia, nitrogen monoxide, and carbon monoxide and charge transfer of molecular oxygen(+) ion with hydrogen peroxide, *J. Chem. Phys.*, **63**, 5220-5222, 1975.

W. F. Linke, *Solubilities inorganic and metal-organic compounds (4^{th} edition)*, American Chemical Society, Washington DC, 1965.

K. Liu, M. G. Brown, M. R. Viant, J. D. Cruzan, and R. J. Saykally, Far-infrared VRT spectroscopy of two water trimer iotopomers: Vibrationally averaged structures and rearrangement dynamics. *Mol. Phys.*, **89**, 1373-1396, 1996.

Y. A. Mantz, F. M. Geiger, L. T. Molina, M. J. Molina, B. L. Trout, A theoretical Study of the Interaction of HCl with Crystalline NAT, *J. Phys. Chem. A*, **106**, 69972-6981, 2002.

M. J. Molina, A. V. Ivanov, S. Trakhtenberg, and L. T. Molina, Atmospheric evolution of organic aerosol, *Geophys. Res. Lett.*, **31**, L22104, doi:10.1029/2004GL020910, 2004.

A. A. Nanayakkara, G. G. Balint-Kurti, and I. H. Williams, Barrier heights for hydrogen atome transfer reactions. Evaluation of *ab initio* molecular orbital methods for the degenerate exchange $HO^{\cdot} + H_2O \rightarrow H_2O + {}^{\cdot}OH$, *J. Phys. Chem.*, **96**, 3662-3669, 1992.

D. M. Neumark, K. R. Lykke, T. Andersen, and W. C. Lineberger, Laser photodetachment measurement of the electron affinity of atomic oxygen, *Phys. Rev. A*, **32**, 1890-1892, 1985.

M. D. Newton and N. R. Kestner, The water dimer: Theory versus experiment. *Chem.*

Phys. Lett., **94**, 198-201, 1983.

M. Nishijima, K. Edamoto, K. Kubota, S. Tanaka, and M. Onchi, Vibrational electron energy loss spectroscopy of the Si(111)(7×7)-$H_2O(D_2O)$ system, *J. Chem. Phys.*, **84**, 6458-6465, 1986

K. W. Oum, M. J. Lakin, D. O. DeHaan, T. Brauers, and B. J. Finlayson-Pitts, Formation of molecular chlorine from the photolysis of ozone and aqueous sea-salt particles, *Science*, **279**, 74-77, 1998.

S. J. Peters and G. E. Ewing, Water on salt: An infrared study of adsorbed H_2O on NaCl(100) under ambient conditions, *J. Phys. Chem. B*, **101**, 10880-10886, 1997.

C. P. Petersen and M. S. Gordon, Solvation of sodium chloride: An effective fragment study of $NaCl(H_2O)_n$, *J. Phys. Chem. A*, **103**, 4162-4166, 1999.

C. Reichardt, Solvatochromic dyes as solvent polarity indicators, *Chem. Rev.*, **94**, 2319-2358, 1994.

R. G. Remorov, Y. M. Gershenzon, L. T. Molina dnd M. J. Molina, *J. Phys. Chem. A*, **106**, 4558-4565, 2002.

A. K. Salameh and L. S. Taylor, Deliquescence in binary mixtures, *Pharm. Res.*, **22**, 318-324, 2005.

J. A. Schaefer, F. Stucki, D. J. Frankel, W. Göpel, and G. J. Lapeyre, Adsorption of H, O, and H_2O at Si(100) and Si(111) surfaces in the monolayer range: A combined EELS, LEED, and XPS study, *J. Vac. Sci. Technol. B*, **2**, 359-365, 1984.

P. G. Sennikov, S. K. Ignatov, and O. Schrems, Complexes and clusters of water relevant to atmospheric chemistry: H_2O complexes with oxidants, *Chem. Phys. Chem.*, **6**, 392-412, 2005.

N. N. Semenov, Kinetics of complex homogeneous reactions *Acta Physicochimica U.R.S.S.*, **18**, 433-472, 1943.

R. D. Shannon, Revised effective ionic radii and systematic studies of interatomic distances in halides and chalcogenides, *Acta Crystallogr. A.*, **32**, 751-767, 1976.

M. Staikova and D. J. Donaldson, *Ab initio* investigation of water complexes of some atmospherically important acid: HONO, HNO_3 and HO_2NO_2, *Phys. Chem. Chem. Phys.*, **3**, 1999-2006, 2001.

M. Staikova and D. J. Donaldson, Water complexes as catalysts in atmospheric reactions, *Phys. Chem. Earth. (C)*, **26**, 473-478, 2001.

J. I. Steinfeld, J. S. Francisco, and W. L. Hase, *Chemical Kinetics and Dynamics (2nd Edition)*, Prentice Hall, Upper Saddle River, N.J., 1998.

D. I. Stock, and C. W. Davies, Second dissociation constant of magnesium hydroxide, *Trans. Faraday. Soc.*, **44**, 856-859, 1948.

M. Suh, P. S. Bagus, S. Pak, M. P. Rosynek, and J. H. Lunsford, Reactions of hydroxyl radicals on titania, silica, alumina, and gold surfaces, *J. Phys. Chem. B*, **104**, 2736-2742, 2000.

I. N. Tang, A. C. Tridico, and K. H. Fung, Thermodynamic and optical properties of sea salt aerosols, *J. Geophys. Res.*, **102**, 23269-23275, 1997.

P. A. Thiel and T. E. Madey, The interaction of water with solid surfaces: Fundamental aspects, *Surface Science Reports*, **7**, 211-385, 1987

T. Uchimaru, A. K. Chandra, S. Tsuzuki, M. Sugie, and A. Sekiya, *Ab initio* investigation on the reaction path and rate for the gas-phase reaction of $HO + H_2O \leftrightarrow H_2O + OH$, *J. Comput. Chem.*, 24, 1538-1548, 2003.

B. Wang, H. Hou, and Y. Gu, Density functional study of the hydrogen bonding: $H_2O{\cdot}OH$, *Chem. Phys. Lett.*, **303**.96-100, 1999.

D. D. Wagman, W. H. Evans, V. B. Parker, R. H. Schumm, I. Harlow, S. M. Bailey, K. L. Churney, and R. L. Nuttall, The NBS tables of chemical thermodynamic properties: selected values for inorganic and C_1 and C_2 organic substances in SI units, *J. Phys.*

Chem. Ref. Data., **11**, Suppl. 2, 1982.

E. Woods III, S. F. Morris, C. N. Wivagg, and L. E. Healy, Probe molecule spectroscopy of NaCl aerosol particle surfaces, *J. Phys. Chem. A*, **109**, 10702-10709, 2005.

Y. M. Xie, and H. F. Schaefer, Hydrogen-bonding between the water molecule and the hydroxyl radical ($H_2O \cdot HO$): The global minimum, *J. Chem. Phys.*, **98**, 8829-8834, 1993.

A. Y. Zasypkin, V. M. Grigor'eva, V. N. Korchak, and Y. M. Gershenson, A Formula for summing of kinetic resistances for mobile and stationary media: I. Cylindrical reaction, *Kinetics and Catalysis*, **38**, 772-781, 1997

B. Zuberi, K. S. Johnson, G. K. Aleks, L. T. Molina, M. J. Molina, and A. Laskin, Hydrophilic properties of aged soot, *Geophys. Res. Lett.*, **32**, L01807, doi:10.1029/2004GL021496, 2005.

CRC Handbook of Chemistry and Physics (88^{th} Edition), CRC Press, Boca Raton, 2007.

Phase diagrams for ceramists, Volumes 1-8; ACerS-NIST Phase equilibrium diagrams, Volumes 9113, American Ceramic Society, Westerville, Ohio, 1964-2001.

Chapter 4

Release of Cl_2 from NaCl upon OH Uptake

4 1. Introduction

Atomic chlorine (Cl) is an extremely powerful oxidant with 1-2 orders of magnitude higher reactivity than OH [DeMore *et al.*, 1997]. For its higher reactivity, Cl is an important species in chemistry of the marine boundary layer and the coastal urban areas. Although the Cl mixing ratio of 1.3×10^5 atoms cm^{-3} in coastal area [Spicer *et al.*, 1998] is smaller than that of OH, oxidation of atmospheric trace species by Cl can occur at substantially faster rates. Besides its reaction with ozone in the stratosphere (Reaction 4.1) [Molina *et al.*, 1974], Cl can influence acidity (Reaction 4.2), oxidize various volatile organic compounds (Reaction 4.2), and perturb the ozone balance in the troposphere (Reactions 4.2 - 4.8) [Singh *et al.*, 1988; DeHaan *et al.*, 1999; Seinfeld *et al.*, 1998; Pechtl *et al.*, 2007]. Examples of Cl reactions important in the troposphere include the following:

$$Cl + O_3 \rightarrow ClO + O_2 \qquad (4.1)$$

$$Cl + R\text{-}H \rightarrow HCl + R\cdot \qquad (4.2)$$

The alkyl radical (R·) produced in Reaction 4.2 may further participate in HO_x and NO_x radical cycling, important in photochemical pollution formation:

$$R\cdot + O_2 + M \rightarrow RO_2 + M \qquad (4.3)$$

$$RO_2 + NO \rightarrow NO_2 + RO \qquad (4.4)$$

$$RO + O_2 \rightarrow R'CHO + HO_2 \qquad (4.5)$$

$$HO_2 + NO \rightarrow OH + NO_2 \qquad (4.6)$$

$$NO_2 + h\nu\ (\lambda < 420nm) \rightarrow NO + O(^3P) \qquad (4.7)$$

$$O(^3P) + O_2 + M \rightarrow O_3 + M \qquad (4.8)$$

Sources of atomic chlorine (Cl) in the troposphere include (i) the gas-phase reaction of OH with HCl [Singh *et al.*, 1988], (ii) the photodissociation of chlorine

monoxide (ClO), and (iii) the photodissociation of molecular chlorine (Cl_2):

$$Cl_2 + h\nu\ (\lambda < 470\text{nm}) \rightarrow 2Cl\cdot \qquad (4.9)$$

The mixing ratio of Cl_2 was measured in the marine boundary layer to be ~150 ppt [Spicer *et al.*, 1998]. This concentration exceeds predictions based on a mechanism for autocatalytic heterogeneous reactions of HOCl on sea salt aerosol and subsequent oxidation of Cl^- ions [Sander *et al.*, 1996; Vogt *et al.*, 1996], suggesting an additional, yet unrecognized Cl_2 source.

Another possible source for Cl radicals is the OH heterogeneous reaction with a deliquesced NaCl surface [Keene *et al.*, 1993, Oum *et al.*, 1998, Knipping *et al.*, 2000; 2002] (see Appendix 3-VII). This reaction can be also responsible for the chloride deficit (the low Cl/Na ratio) observed in sea-salt particles [Junge, 1956; Cicerone, 1981; Keene *et al.*, 1990; Mouri *et al.*, 1993; McInnes *et al.*, 1994] (see Section 1.5.2). Such mechanism may also explain release of Cl_2 from NaCl upon OH uptake. However, it is restricted to high relative humidity conditions, greater than the deliquescence RH of NaCl, characteristic of the lower troposphere.

The upper troposphere is rather under arid conditions, which would more likely enable such a $OH_{(g)} + NaCl_{(s)}$ heterogeneous mechanism. For example, the content of water vapor at altitudes ~5 km is limited to about 0.7 Torr of H_2O [Seinfeld and Pandis, 1998].

In addition, the vertical distribution of sea-salt aerosol shows an exponential decrease, which establishes a fairly constant profile above 900 m in the marine boundary layer [Gras, 1991; Jaenicke, 1993]. This indicates that approximately 5% of sea-salt aerosols still exist at higher altitudes in the troposphere. Furthermore, formation of Cl_2 in the upper troposphere would have important implications for Cl_2

dissociation in the presence of intense solar radiation at high altitudes.

In this chapter, a product study for the OH heterogeneous reaction with NaCl under dry to low relative humidity conditions is described. Since NaCl is the major component of sea salt, it is important to determine the net OH uptake on NaCl under various conditions relevant to the troposphere. This study provides experimental data essential to determining a mechanism for Cl_2 release from the OH reaction with sea salt at high altitude under arid conditions.

4. 2. Experimental

The experimental setup used was described previously in Chapters 2 and 3. Two differences should be noted: (i) an increased number of beads used to pack the reactor tubes (80 instead of 60), and (ii) no pre-pumping before the CI region. Both changes were made to increase the sensitivity to detection of gas-phase products, expected in relatively low concentrations. In particular, (ii) enabled all species in the flow tube to proceed to the CI region without any loss due to pumping, which was required under high relative humidity conditions (see Chapter 3) to minimize water interference (formation of water clusters) by preventing large amount of water molecules being introduced to the CI region.

To minimize possible secondary reactions by O_2 and HO_2, the H + NO_2 reaction was used for OH production. The CIMS sensitivity to OH was 4.2 [$\pm$0.3] $\times 10^7$ molecule cm^{-3} cps^{-1} under the dry condition, while it decreased by one order of magnitude under wet conditions (Section 2.2)

Instead of a halocarbon wax coating (termed 'the halocarbon wax reference'), bare glass beads without any coating were used in the reference tube (termed 'the glass

reference') to reduce the chlorine background observed from the OH + halocarbon wax reaction (see Section 4.3). Preparation of NaCl surfaces was done as described in Section 3.2.3.

X-ray photoelectron spectroscopy (XPS) was used to study the reaction products formed on a solid salt surface exposed to OH. Na(1s) spectra were analyzed offline by XPS with the Mg anode photon energy of 1253.6 eV and the incident angle of 10°. For NaCl deposition, a silicon wafer of 1×1 cm was dipped into a supersaturated NaCl solution and dried in an oven (~100℃).

Experimental results were simulated using ChemKin to elucidate the reaction mechanism of Cl_2 formation.

4. 3. Results

Mass spectra of the gas-phase products produced in a reactor flow tube packed with beads coated with NaCl (termed 'the reactor spectrum) were compared with reference spectra to determine which masses correspond to reaction products. Use of the parallel reactors enables identification and canceling out the background masses potentially arising from other OH heterogeneous reactions in the flow system. For example, although halocarbon wax (used for reactor wall deactivation) is essentially inert to OH reaction, the reaction probability is nonzero, reported at 6×10^{-4} [Bertram *et al.*, 2001]. We observed efficient Cl_2 production from halocarbon wax upon OH uptake as described later in this section.

Throughout the mass range of m/z = 5 amu (atomic mass units) to 170 amu, peaks at m/z 55 and 162 showed noticeable differences when the total flow was switched from the reaction tube to the reference tube, shown in Figure 4.1.

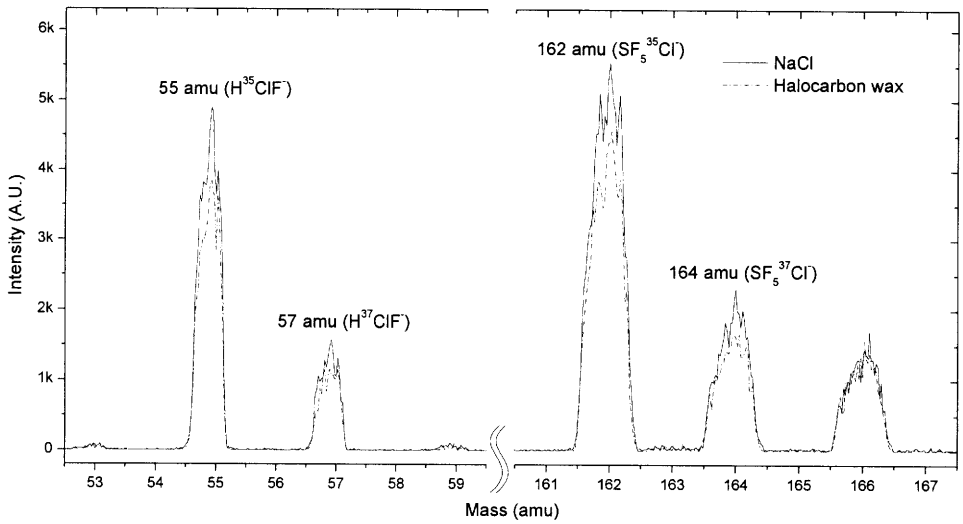

Figure 4.1. Mass spectra from the reactor and the halocarbon wax reference

These masses were assigned to $HClF^-$ (55 amu) and SF_5Cl^- (162 amu), which are likely the ion products of the electron transfer from SF_6^- to HCl [Huey *et al.*, 1995] according to the following reactions:

$$HCl + SF_6^- \rightarrow HClF^- (55\ amu) + SF_5 \qquad (4.10)$$

$$\rightarrow SF_5Cl^- (162\ amu) + HF \qquad (4.11)$$

$$\rightarrow SF_5^- (127\ amu) + HF + Cl \qquad (4.12)$$

with $k_{4.11}$ = 1.5 [± 30%]×10^{-9} cm^3 $molecule^{-1}$ s^{-1} and $k_{4.12}$ = 0.42 [± 30%]×10^{-9} cm^3 $molecule^{-1}$ s^{-1} [Streit, 1982]. The branching ratios for Reactions 4.10, 4.11, and 4.12 are 23%, 44%, and 33%, respectively [Streit, 1982]. The peaks at masses of 57, and 164 amu, corresponding to the Cl isotope (^{37}Cl), are also shown in Figure 4.2 with I_{57amu}/I_{55amu} = 0.31 and I_{164amu}/I_{162amu} = 0.39.

To remove the possible Cl contribution from the reference, bare glass beads

were used in place of the halocarbon wax coated beads. Figure 4.2 shows a decrease in the peak at 55 amu in the glass reference spectrum compared to that in the halocarbon wax reference spectrum.

The relative ratios of the intensities of the peak at 55 amu in the spectra was 1 : 0.83 : 0.63 (NaCl : Halocarbon wax : Glass). Therefore, 37% of the intensity of the peak in the NaCl reactor spectrum (Figure 4.1) was attributed to the OH heterogeneous reaction on NaCl.

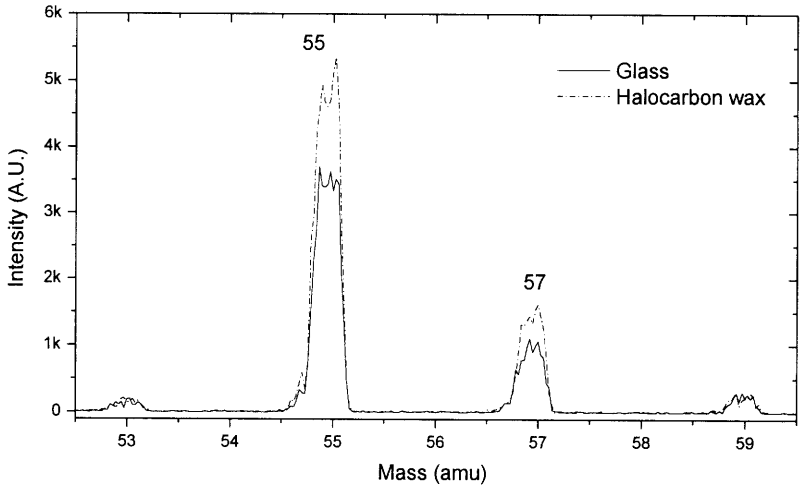

Figure 4.2. Comparison of the halocarbon waxed reference spectrum with the glass reference spectrum

The HCl signal (m/z = 55) was calibrated using known amounts of Cl_2 as follows:

$$Cl_2 + H \rightarrow HCl + Cl \qquad (4.13)$$

Since Reaction 4.13 is fast ($k_{4.13} = 2.0 \times 10^{-11}$ cm^3 molecule^{-1} s^{-1} [Berho *et al.*, 1999]) and irreversible ($k_{-4.13} = 4.18 \times 10^{-42}$ cm^3 molecule^{-1} s^{-1} [Baulch *et al.*, 1981]), in excess H,

Cl_2 transforms completely to HCl. HCl loss on NaCl surface was neglected since the reaction probability is relatively small (γ_{HCl}^{NaCl}=3 $\times 10^{-2}$, [Fenter et al., 1994]) and the reaction time for producing HCl through Reaction 4.13 (~ 10 ms) is longer than the residence time in the beads-packing (~ 4 ms). The CIMS sensitivity to HCl was found to be 3.7 $\times 10^{7}$ molecule cm^{-3} cps^{-1}.

A HCl (m/z = 55) signal was linearly dependent on the OH concentration both under dry and 6% RH conditions as shown in Figure 4.3. Assuming that formation of HCl is solely due the title reaction, the yield of HCl per OH was calculated to be 0.020 ± 0.002 under dry conditions and 0.022 ± 0.002 at 6% of RH. Accounting for the measured OH reaction probability of γ_{OH} = 0.045 ± 0.004 on NaCl (see Section3.3.6), the observed HCl was attributed to approximately half of OH uptake by NaCl.

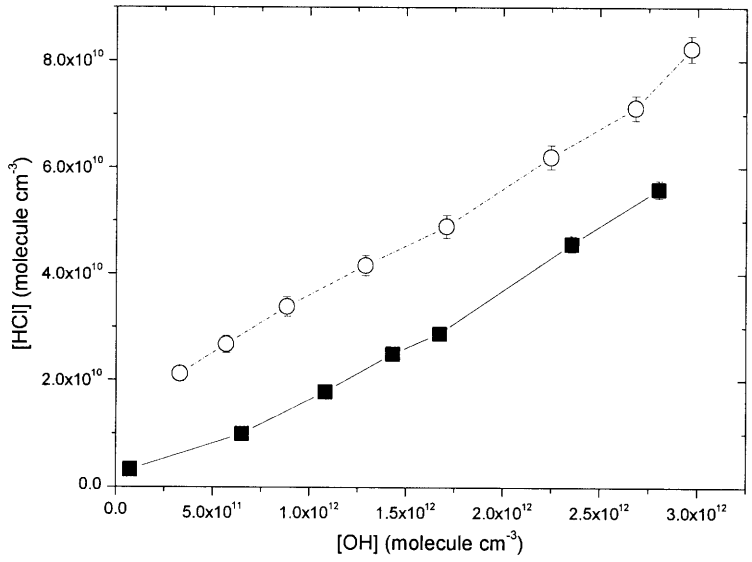

Figure 4.3. Dependence of [HCl] (m/z = 55) on [OH] under the dry conditions (■) and 6% RH (○).

As seen from Figure 4.4, the dependence of [HCl] on RH is non-monotonic. The initial small change in RH (0% → 2% RH) was unfavorable for the production of HCl, whereas the production of HCl increased with further increases in RH up to 9%.

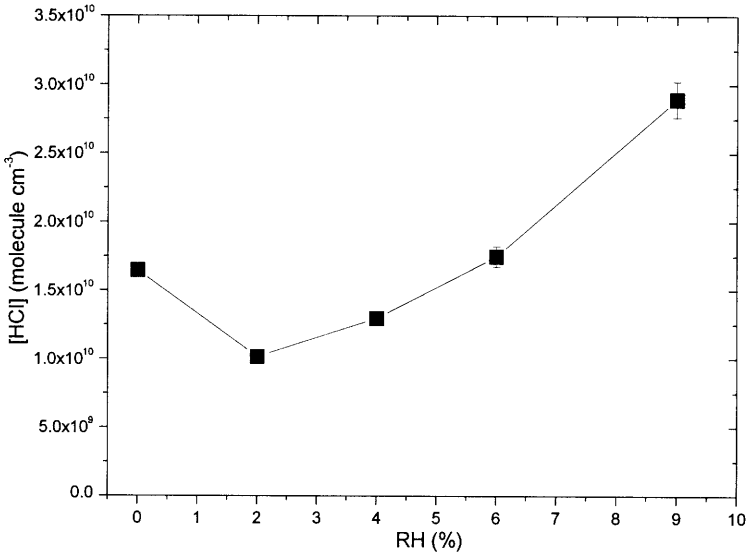

Figure 4.4. Dependence of [HCl] on RH

XPS spectra recorded for three NaCl samples were analyzed for changes in the Na(1s) signal, shown in Figure 4.5. In the figure, the samples were exposed to OH for 4 hours under dry and wet conditions: dry (thick solid line), 10% RH (thin solid line), and 80% RH (dashed line). For calibration, the blank spectra of NaCl (unexposed to OH), and NaOH are also shown. Compared to the unreacted NaCl, all three exposed samples show a shift of 0.4 eV in Na(1s) toward to that of NaOH. However, we were unable to see the shift dependence of Na(1s) on RH.

The observed Cl/Na ratios in the exposed samples obtained from XPS

measurements are listed in Table 4.1, showing that the OH exposure normally decreases the amount of surface chlorine. Moreover, the observed chlorine deficit was found to be even greater when the samples were exposed to OH under wet conditions. A significant chlorine deficit was observed when RH reached the values of higher than the deliquescence RH of NaCl (77%).

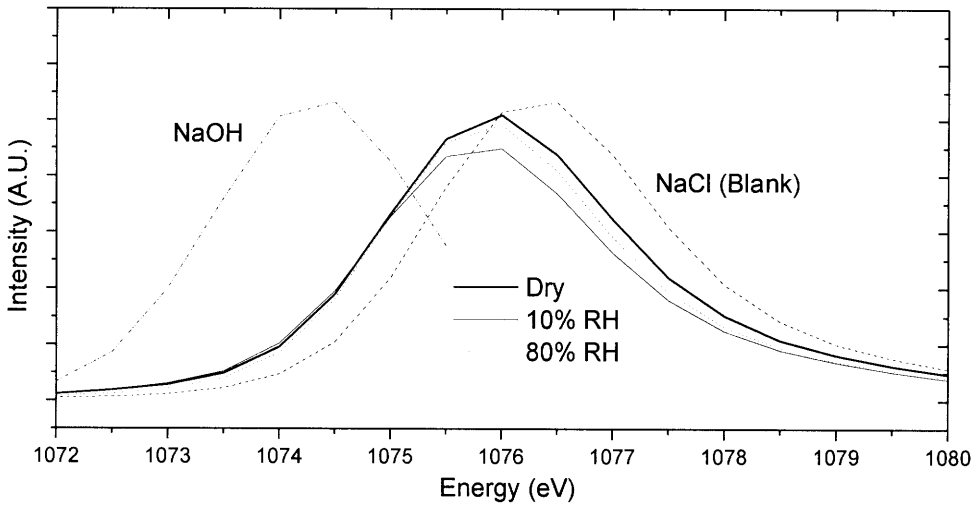

Figure 4.5. XPS spectra of Na(1s) for NaCl exposed to OH under different RH conditions: dry (thick solid line), 10% RH (thin solid line), and 80% RH (dotted line). Spectra for blank NaCl (unexposed to OH, dashed line) and NaOH (dash-dotted line) are shown for comparison.

Table 4.1. Cl/Na ratio for the unreacted and OH-exposed NaCl samples

RH	Blank	0%	10%	80%
Cl/Na	0.7470	0.7395	0.7366	0.6744

Although the possible peaks at m/z = 35 and 37 corresponding to atomic Cl

were observed at a trace level, the peak intensities were smaller than the same masses in the halocarbon wax reference spectrum, shown in Figure 4.6. This indicates that the species corresponding to the peaks were not only the products of the heterogeneous reaction, but also the products of gas phase reactions. One possible species to be assigned for 35 amu is $OH^-(H_2O)$ produced from the gas phase reaction of OH^- with H_2O likely introduced by a very small leak from ambient air (see Section 3.3.4.2.). The trace amount of H_2O is likely also responsible for the peak at 37 amu, assigned to $F^-(H_2O)$ from the reaction between SF_6^- and H_2O [Arnold *et al.*, 2001]. This is confirmed by the ratio of 37 to 35 amu (I_{37amu}/I_{35amu}). The intensity of the peak at 37 amu was 23% of the peak at 35 amu, which is smaller than the natural abundance of ^{37}Cl (32.6%).

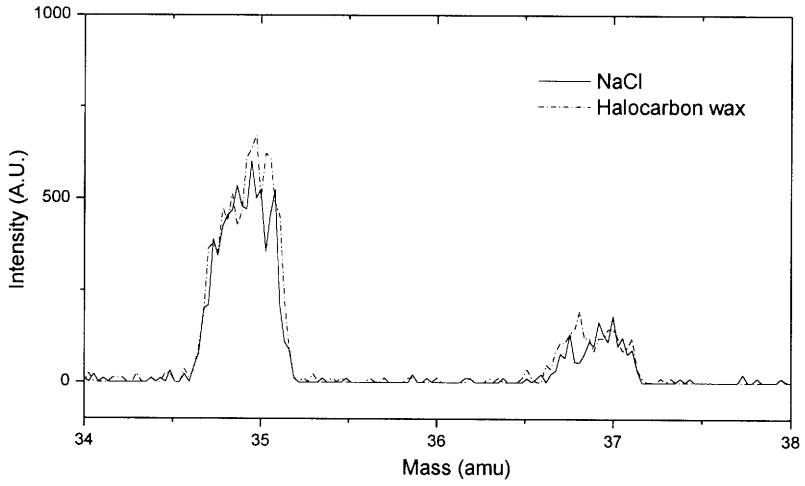

Figure 4.6. The observed peaks at m/z = 35 and 37.

The peaks at 52 and 70 amu corresponding to HOCl and Cl_2, respectively, were not observed within detection limit. HOCl can be detected as $HOClF^-$ (m/z = 71) by

the reaction with SF_6^- in the CI region. Although a peak at 71 amu was observed only under wet conditions, it is believed to correspond to $OH^-(H_2O)_3$. Therefore it was not possible to separate the two likely contributions to m/z = 71.

The spectrum for the reaction of OH on a sea salt surface was identical to that on NaCl within experimental uncertainty. Evidence of bromine (or iodine)-containing species (other components of sea salt) was not observed.

4. 4. Discussion

4. 4. 1. Reactions in the Flow System

Considering that many gas-phase species from the radical source and reactions coexisted in the flow tube system, the chemistry involved may be described by a complex set of reactions rather than a simple heterogeneous reaction between OH and the NaCl surface. The possible reactions include the following:

(R1) The heterogeneous reaction of OH with NaCl - The titled reaction

(R2) The heterogeneous reaction of unreacted gas-phase sources for OH generation on NaCl – The unreacted gas-phase sources including H_2, H, NO_2 ($H+NO_2$ scheme), O_2 ($H+O_2+M$ scheme), and O (from impurities described below).

(R3) The gas-phase reactions of OH with the species in (R2) – The secondary reaction of OH

(R4) All other gas-phase reactions involving the product of the title reaction

According to our kinetics simulation (ChemKin) with the reaction for OH

production (Reaction 2.2) and two secondary reactions of OH (Reactions 2.5 and 2.6), ~84% of H (4.2×10^{12} molecule cm^{-3}) was estimated to survive in order to reach the NaCl surface. Atomic O was produced from the dissociation of a ppm impurity of O_2 introduced with the He flow (as carrier flow for H_2) through the microwave discharge cavity. Atomic O reacts with vibrationally excited H_2 to produce H and OH [Han *et al.*, 2000; Balakrishnan, 2004].

$$H_2^* + O \rightarrow H + OH \qquad (4.14)$$

where H_2^* is vibrationally excited H_2 produced in the microwave discharge cavity.

Preliminary experiments showed that the heterogeneous uptake of H_2, NO_2, O_2, and O on NaCl were negligible compared to the OH uptake. However, the heterogeneous reaction of H was difficult to be distinguished since a small amount of OH was typically produced upon passing H_2 through a microwave cavity due to ppm impurities in the He carrier gas (Reaction 4.14). A background study was done to explore the contribution of H to the heterogeneous reaction on NaCl as shown in Figure 4.7. The background OH was produced from the reaction between H_2^* and O in absence of NO_2. The efficiencies of H production in the microwave discharge and the OH production by Reaction 4.14 were dependent on the flow rate of the He carrier gas. As the flow rate of He increased, the production of H was linearly enhanced while OH reached a maximum and then decreased. HCl followed OH, not H, indicating the negligible contribution of H in the heterogeneous reaction. Therefore, OH was the only species available to react with NaCl to a significant extent.

The secondary reaction of OH *(R3)* was reduced by controlling the initial concentrations of the reactants, H and NO_2 (or H and O_2 in the case of the NO_x-free OH production source). Within the lifetime of OH, t = 45 ms from production to detection,

only approximately 2.5% of OH (upper limit) was estimated to be consumed for the self-recombination (Reaction 2.5) under the usual condition of radical production. In fact, the loss of OH by secondary reactions was negligible unless the initial concentration of NO_2 did not exceed 1.5×10^{12} molecule cm^{-3} as seen in Figure 2.2 (see Chapter 2).

Although *R2* and *R3* may therefore be excluded, other interfering reactions *(R4)* must be identified in order to verify the reaction product(s).

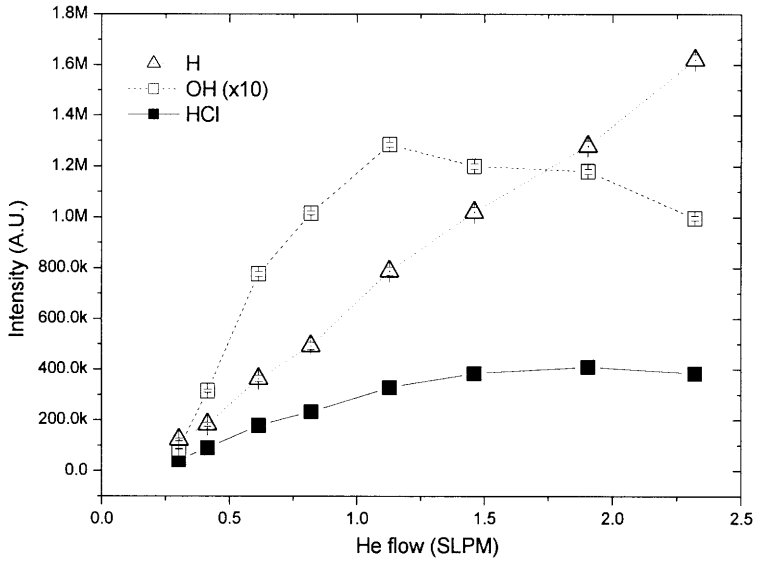

Figure 4.7. Dependence of H, OH and HCl on He flow

4.4.2. Verification of the Product of the Title Reaction

Although Cl_2 was not directly detected and only HCl was observed at m/z = 55 and 162, it is still under question whether HCl is the gas-phase product of the titled reaction, due to the possibility of interference of gas-phase reactions as *R4*. A potential

reaction and interfering source of chlorine-containing species is Reaction 4.13, which transforms Cl_2 into HCl in the presence of H at an extremely fast rate. Preliminary experiments for reproducibility of Reaction 4.13 in our system are described in Appendix 4-I. Since the reaction for OH production proceeded with excess H, most H ($\sim 4 \times 10^{12}$ molecule cm^{-3}) remained unreacted when the flow reached a NaCl surface. Therefore, there was a reasonable possibility that Reaction 4.13 took place if Cl_2 was released from the NaCl surface.

In contrast, Reaction 4.13 could be inhibited by introducing O_3, which removes H with an extremely fast rate ($k_{4.15} = 2.95 \times 10^{-11}$ cm^3 $molecule^{-1}$ s^{-1} [Yu *et al.*, 1997]:

$$H + O_3 \rightarrow OH + O_2 \qquad (4.15)$$

Kinetics modeling was performed to predict the gas phase chlorine-containing products from the titled reaction. The model was designed to investigate how added O_3 can inhibit the transformation of Cl_2 into HCl (Reaction 4.13). The reactions included in the model and the initial experimental concentrations of species are listed in Table 4.2 and Table 4.3, respectively. The initial concentrations of HCl and Cl_2 were determined based on two assumptions: A major product of the title reaction is likely HCl (*Assumption 1*) or Cl_2 (*Assumption 2*). Figure 4.8 shows the HCl concentration predicted based on *Assumption 1* (△) and *Assumption 2* (○), as well as the experimentally measured HCl concentration (■). The measured [HCl] agreed well with *Assumption 2*, providing support that Cl_2 is the gas-phase product of the titled reaction.

Table 4.2. The reactions included the kinetic model used in the present study.

No.	Reaction	k (cm^3 $molecule^{-1}$ s^{-1})	Reference
2.2	$H + NO_2 \rightarrow OH + NO$	1.3×10^{-10}	DeMore, 1997
2.5	$OH + OH + M \rightarrow H_2O_2 + M$	1.6×10^{-12}	DeMore, 1997
2.6	$OH + NO_2 + M \rightarrow HNO_3 + M$	3.8×10^{-12}	DeMore, 1997
4.16	$OH + Cl_2 \rightarrow HOCl + Cl$	6.3×10^{-14}	Bryukov, 2004
4.17	$OH + HCl \rightarrow H_2O + Cl$	8.0×10^{-13}	Atkinson, 2001
4.18	$OH + Cl \rightarrow HCl + O$	7.1×10^{-16}	Baulch, 1981
4.19	$OH + H_2 \rightarrow H_2O + H$	7.0×10^{-15}	Atkinson, 2004
4.20	$OH + HOCl \rightarrow H_2O + ClO$	5.0×10^{-13}	Atkinson, 2001
4.21	$OH + ClO \rightarrow HCl + O_2$	1.3×10^{-12}	Tyndall, 2002
4.22	$OH + O \rightarrow O_2 + H$	3.3×10^{-11}	Robertson, 2006
4.13	$Cl_2 + H \rightarrow HCl + Cl$	2.0×10^{-11}	Berho, 1999
4.23	$Cl_2 + Cl \rightarrow Cl_3$	1.5×10^{-16}	Hutton, 1965
4.24	$Cl_2 + O \rightarrow ClO + Cl$	4.3×10^{-14}	Baulch, 1981
4.25	$Cl + H_2 \rightarrow HCl + H$	1.8×10^{-14}	Atkinson, 2001
4.26	$Cl + HOCl \rightarrow HCl + ClO$	1.3×10^{-14}	Wang, 2003
4.16^{-1} [a]	$Cl + HOCl \rightarrow OH + Cl_2$	1.2×10^{-12}	Bryukov, 2004
4.27	$Cl + NO_2 + M \rightarrow ClONO + M$	3.7×10^{-12}	DeMore, 1997
4.25^{-1} [a]	$HCl + H \rightarrow H_2 + Cl$	7.5×10^{-14}	Allison, 1996
4.18^{-1} [a]	$HCl + O \rightarrow OH + Cl$	2.0×10^{-16}	Xie, 2003
4.28	$HOCl + H \rightarrow OH + HCl$	2.7×10^{-12}	Wang, 2003
4.29	$HOCl + O \rightarrow OH + ClO$	1.7×10^{-13}	Atkinson, 2001
4.30	$O + NO_2 + M \rightarrow NO_3 + M$	2.8×10^{-13}	DeMore, 1997
4.31	$O + ClO \rightarrow O_2 + Cl$	3.8×10^{-11}	Atkinson, 2001
4.32	$OH + O_3 \rightarrow HO_2 + O_2$	7.4×10^{-14}	Atkinson, 2004
4.15	$H + O_3 \rightarrow OH + O_2$	3.0×10^{-11}	Yu, 1997
4.33	$Cl_2 + O_3 \rightarrow ClO_2 + ClO$	3.0×10^{-28}	Bodenstein, 1929
4.34	$HCl + O_3 \rightarrow O_2 + HOCl$	4.7×10^{-24}	Leu, 1989
4.35	$Cl + O_3 \rightarrow O_2 + ClO$	1.2×10^{-11}	Atkinson, 2001
4.36	$O + O_3 \rightarrow O_2 + O_2$	8.0×10^{-15}	Atkinson, 2004

[a] Reverse reaction

Table 4.3. The initial species concentrations used in the two assumptions.

Species	Initial concentration (molecule cm^{-3})	
	Assumption 1 (HCl)	*Assumption 2* (Cl_2)
HCl	2.5×10^{10}	-
Cl_2	-	2.5×10^{10}
OH	1.2×10^{12}	
NO_2	2.0×10^{11}	
H	5.0×10^{12}	
O	5.0×10^{11}	
H_2	9.0×10^{13}	

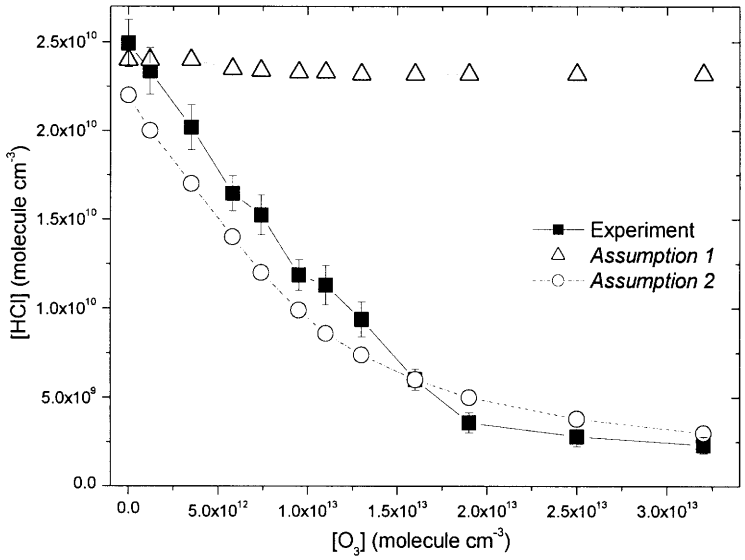

Figure 4.8. The [HCl] dependence on $[O_3]$

The chance of the transformation of atomic chlorine was negligible since the possible reaction (Reaction 4.25) is slow ($k_{4.25}$ = 1.77 $\times10^{-14}$ cm^3 $molecule^{-1}$ s^{-1} [Atkinson *et al.*, 2001]) and irreversible ($k^{-1}_{4.25}$ = 7.48 $\times10^{-14}$ cm^3 $molecule^{-1}$ s^{-1} [Allison *et al.*, 1996]). Only less than 1% of Cl could participate in this reaction even though

the high concentration of H_2 is taken into account.

$$Cl + H_2 \leftrightarrow HCl + H \qquad (4.25)$$

Upon OH exposure the shift of Na(1s) toward NaOH (Figure 4.5) implies that the title reaction causes substitution of Cl with OH or O in the lattice. Assuming that NaOH is the oxidized form of Na by OH uptake, the amount of oxidation by OH for 4 hours was estimated at 35% from the superposition of the XPS spectrum for NaOH and the unreacted NaCl basis set.

4.4.3. The Effect of RH and the Proposed Reaction Mechanism

The increase in the chlorine deficit (Table 4.1) and the yield of HCl upon OH uptake (Figure 4.4) under wet conditions indicates that Cl_2 release to the gas phase is enhanced by water adsorption. However, the observation described in Chapter 3 showed no significant water effect on OH uptake by NaCl in the range of 0 to 48% RH. This further indicates that OH loss on NaCl is independent of RH within experimental error. These contradictory phenomena imply that the uptake of OH on NaCl occurs through at least two mechanisms including the one responsible for the Cl_2 release.

Other mechanisms may not involve any chlorine-containing species, but produce H_2O or H_2O_2 through surface-catalyzed bimolecular reactions [Steinfeld *et al.*, 1998] even though H_2O_2 was not observed within detection limits (see Section 3.3.6.2). In case that H_2O or H_2O_2 production follows the Langmuir-Hinshelwood (L-H) mechanism, water adsorption would reduce the rate of product formation since the occupation of the active site by water decreases the probability for adsorbed OH to meet an adjacent OH ($k_{3.35}$ in Section 3.3.6.2). Moreover, water adsorption reduces the number of active sites available for OH uptake, resulting in a decrease in the number of

sites available for radical uptake [Remorov *et al.*, 2002], which also influences the release of Cl_2 as described later of this section.

In summary, the possible fates of adsorbed OH radicals on the active sites of NaCl are (i) desorbing to the gas-phase (no uptake), (ii) generating Cl_2, and (iii) generating other species. As RH increases, (ii) is enhanced (described further below), while (iii) is inhibited as described above so that the net uptake of OH does not change to a significant extent.

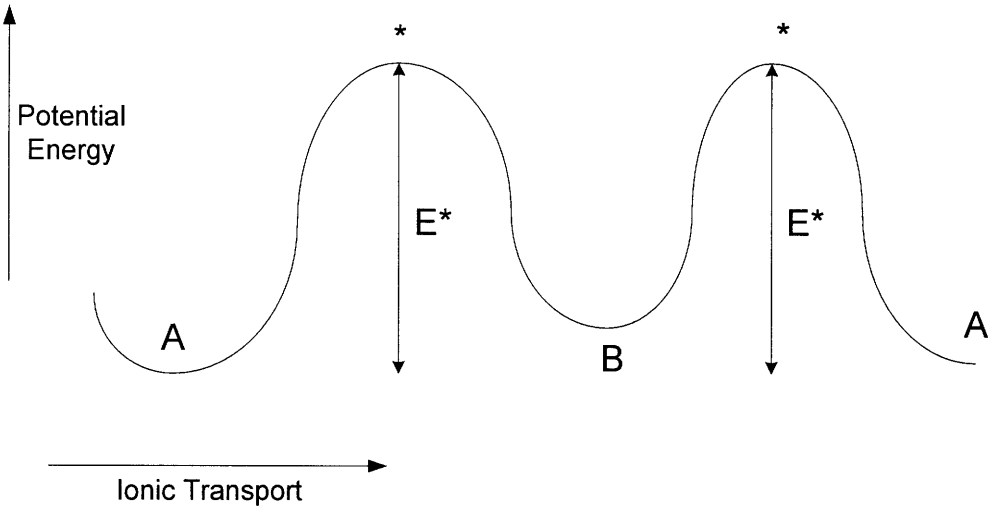

Figure 4.9. The Schematic of ionic transport in crystalline solids [West, 1984]

Returning to Cl_2 release (ii), a potential reaction mechanism is initiation by OH uptake on surface Cl^- active sites (formation of OH-Cl^-) followed by reaction with another Cl^- moved by ionic transport. The transport of ions is possible only when the vibrational energy of the bond is greater than the activation energy (E*) described in Figure 4.9 or via tunneling. Therefore, the probability of ionic transport between sites is proportional to $\exp(-E^*/kT)$ where E* is the activation energy, k is the Boltzmann

constant, and T is the temperature, following the Arrhenius equation [West, 1984]. Although E* of NaCl is not well defined, the lattice vibration of NaCl (164 cm^{-1} [West, 1984]) suggests that only a small population has energy greater than E* at room temperature. In this case, the step involving ionic transport heavily influences the net reaction rate.

Water adsorption likely lowers E* by perturbing ionic bonds, which results in an enhancement of ionic transport in the crystalline lattice. This is consistent with a previous observation by Hemminger [1999] showing that even very low vapor pressure of water (~2% RH) enhanced the surface ionic mobility. As a consequence, the Cl_2 release is expected to increase under wet conditions.

In contrast, the adsorption of water likely reduces the number of available sites for OH uptake as described in the early of this section. This effect competes with the positive effect of water described above with respect to the production of Cl_2. As seen in Figure 4.4, this screening effect of water caused the decrease in HCl when RH was increased from 0 to 2%, before the ionic mobility was enhanced. However, Cl_2 production recovered at RH = 6% and increased further in comparison to dry conditions due to the effective assistance of water for the enhancement of ionic mobility.

Since measurements were not made at RH > 9% due to the restriction of water to CIMS sensitivity for OH detection, it is not clear how the water affects the production of Cl_2 at high RH. Nevertheless, it is expected that the enhancement of the Cl_2 production converges to a certain maximum because the negative effect of water by screening available sites for OH adsorption is proportional to RH, whereas the extent of enhancement of ionic mobility becomes smaller as RH increases [Hemminger, 1999]. This is consistent with the observation by Oum *et al.* [1998], who observed formation of

Cl_2 only after the deliquescence RH of NaCl, indicating a sharp increase in the production rate of Cl_2 at this RH. In fact, a yield of HCl per OH was found to be 0.036 at RH = 9%, which is already close to the reaction probability of OH on NaCl (γ_{OH}^{NaCl} = 0.045 [± 0.004], see Chapter 3). Unless a catalytic mechanism is involved, the yield is not able to exceed this value.

4. 4. Summary

Mass spectra of the gas-phase species produced from the OH heterogeneous reaction with NaCl were obtained to characterize the reaction products and the kinetics mechanism. Although only peaks corresponding to HCl were observed, an applied kinetics model, and reactivity experiments with O_3 verified that Cl_2, a sole product of the heterogeneous reaction, transformed to HCl in the presence of H atoms. A Cl_2 yield per OH was determined to be 0.020 ± 0.002 and 0.022 ± 0.002 at 0 and 6% of RH, respectively. XPS characterization of the reacted NaCl surfaces showed a chlorine deficit by OH uptake, enhanced under wet conditions.

Enhancement in Cl_2 production was observed under wet conditions consistent with the measurement of the chlorine deficit in NaCl. Two reaction mechanisms were suggested to describe OH uptake by NaCl, including Cl_2 production.

Appendix 4-I. Transformation of Cl_2 into HCl in presence of H Atoms

Cl_2 reacts with H atoms to form HCl with the rate ($k_{4.13}$ = 2.0 $\times 10^{-11}$ cm^3 $molecule^{-1}$ s^{-1} [Berho *et al.*, 1999]), while the reverse reaction is extremely slow ($k^{-1}_{4.13}$ = 4.18 $\times 10^{-42}$ cm^3 $molecule^{-1}$ s^{-1} [Baulch *et al.*, 1981]).

$$Cl_2 + H \rightarrow HCl + Cl \qquad (4.13)$$

To verify the reproducibility of Reaction 4.13 in our system, a pure Cl_2 flow [99%, Matheson Tri Gas] was introduced with H_2 along with carrier gas flows of He and N_2 only. Masses corresponding to HCl (m/z = 55, 162) were not observed until H was produced upon ignition of the microwave discharge. The concentration of H was assumed to be proportional to the concentration of H_2 passing through the microwave discharge. Reaction 4.13 was reproduced in our system as shown in Figure 4.10 (a). In addition, the inhibition of Reaction 4.13 by Reaction 4.15 was also checked by introducing O_3. As more O_3 was introduced, the production of HCl from Cl_2 was reduced since more H was removed as seen in Figure 4.10 (b).

$$H + O_3 \rightarrow OH + O_2 \qquad (4.15)$$

with $k_{4.15}$ = 2.95 $\times 10^{-11}$ cm^3 $molecule^{-1}$ s^{-1} [Yu *et al.*, 1997].

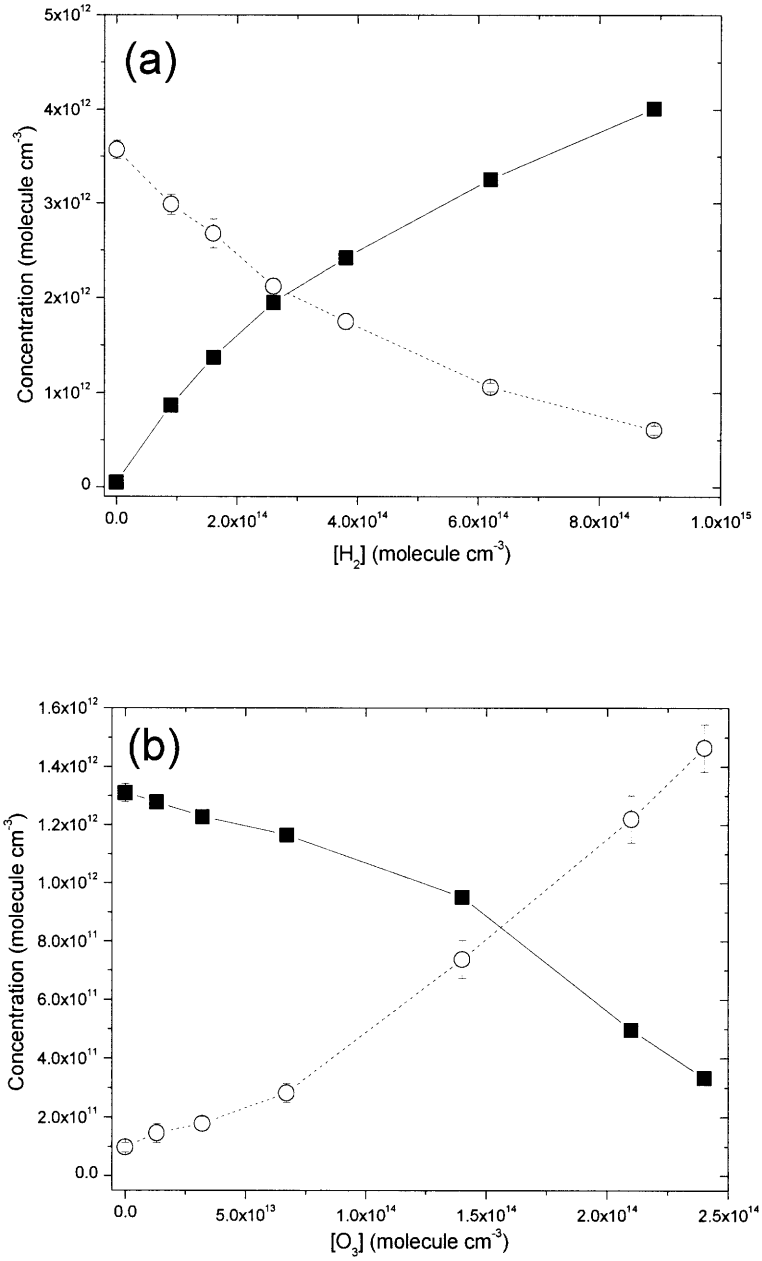

Figure 4.10. Anticorrelation between HCl (■) and Cl_2 (○) as H increases (a) and H decreases (b) in the presence of O_3

References for Chapter 4

T. C. Allison, G. C. Lynch, D. G. Truhlar, and M. S. Gordon, An improved potential energy surface for the H_2Cl system and its use for calculations of rate coefficients and kinetic isotope effects, *J. Phys. Chem.*, **100**, 13575-13587, 1996.

S. T. Arnold and A. A. Viggiano, Turbulent ion flow tube study of the cluster-mediated reactions of SF_6^- with H_2O, CH_3OH, and C_2H_5OH from 50 to 500 Torr, *J. Phys. Chem. A*, 105, 3527-3531, 2001.

R. Atkinson, D. L. Baulch, R. A. Cox, J. N. Crowley, R. F. Hampson, J. A. Kerr, M. J. Rossi, and J. Troe, Summary of evaluated kinetic and photochemical data for atomospheric chemistry, *IUPAC Subcommittee on Gas Kinetic Data Evaluation for Atmpospheric Chemistry Web Version*, 2001

R. Atkinson, D. L. Baulch, R. A. Cox, J. N. Crowley, R. F. Hampson, R. G. Hynes, M. E. Jenkin, M. J. Rossi, and J. Troe, Evaluated kinetic and photochemical data for atomospheric chemistry: Volume I – gas phase reaction of Ox, HOx, NOx and Sox species, *Atmos. Chem. Phys.*, **4**, 1461-1738, 2004.

N Balakrishnan, Quantum calculations of the $O(^3P) + H_2 \rightarrow OH + H$ reaction, *J. Phys. Chem.*, **121**, 6346-6352, 2004.

D. L. Baulch, J. Duxbury, S. J. Grant, and D. C. Montague, Evaluated kinetic data for high temperature reactions. Volume 4: Homogeneous gas phase reactions of halogen- and cyanide- containing species, *J. Phys. Chem. Ref. Data*, **10**, 1981.

F. Berho, M. –T. Rayez, and R. Lesclaux, UV absorption spectrum and self-reaction kinetics of the cyclohexadienyl radical, and stability of a series of cyclohexadienyl-type radicals, *J. Phys. Chem. A*, **103**, 5501-5509, 1999.

A. K. Bertram, A. V. Ivanov, M. Hunter, L. T. Molina, and M. J. Molina, The reaction probability of OH on organic surfaces of tropospheric interest, *J. Phys. Chem. A*, **105**, 9415-9421, 2001.

M. Bodenstein, E. Padelt, H-J. Schumacher, Die thermische reaction zwischen chlor und

ozon, *Z. Phys. Chem. Abt. B*, **5**, 209-232, 1929.

M. G. Bryukov, V. D. Knyazev, S. M. Lomnicki, C. A. McFerrin, and B. Dellinger, Temperature dependent kinetics of the gas-phase reactions of OH with Cl_2, CH_4, and C_3H_8, *J. Phys. Chem. A*, **108**, 10464-10472, 2004.

R. J. Cicerone, Halogens in the atmosphere, *Rev. Geophys. Space Phys.*, **19**, 123-139, 1981.

D. O. De Haan, T. Brauers, K. Oum, J. Stutz, T. Nordmeyer, and B. J. Finlayson-Pitts, Heterogeneous chemistry in the troposphere: experimental approaches and applications to the chemistry of sea salt particles, *Int. Rev. Phys. Chem.*, **18**, 343-385, 1999.

W. B. DeMore, S. P. Sander, D. M. Golden, R. F. Hampson, M. J. Kurylo, C. J. Howard, A. R. Ravishankara, C. E. Kolb, M. J. Molina, Chemical kinetics and photochemical data for use in stratospheric modeling, *JPL Publication*, 97-4, 1997.

F. F. Fenter, F. Caloz, and M. J. Rossi, Kinetics of nitric acid uptake by salt, *J. Phys. Chem.*, **98**, 9801-9810, 1994.

B. D. Finely and E. S. Saltzman, Measurement of Cl2 in coastal urban air, *Geophys. Res. Lett.*, **33**, L11809, doi:10.1029/2006GL025799, 2006.

J. L. Gras, Southern hemisphere tropospheric aerosol microphysics, *J. Geophys. Res.*, **96**, 5345-5356, 1991.

J. Han, X. Chen, and B. R. Weiner, Reaction dynamics of $O(^3P) + H_2$ (v=1), *Chem. Phys. Lett.*, 332, 243-250, 2000.

J. C. Hemminger, Heterogeneous chemistry in the troposphere: a modern surface chemistry approach to the study of fundamental processes, *Int. Rev. Phys. Chem.*, **18**, 387-417, 1999.

L. G. Huery, D. R. Hanson, and C. J. Howard, Reactions of SF_6^- and I^- with atmospheric trace gases, *J. Phys. Chem.*, **99**, 5001-5008, 1995.

E. Hutton, and M. Wright, Photoemissive and recombination reactions of atomic chlorine, *Trans. Faraday Soc.*, **61**, 78-89, 1965.

R. Jaenicke, Tropospheric aerosols, *Aerosol-Cloud-Climate Interactions*, Academic Press, San Diego, 1993.

C. E. Junge, Recent investigations in air chemistry, *Tellus*, **8**, 127-139, 1956.

W. C. Keene, A. A. P. Pszenny, D. J. Jacob, R. A. Duce, J. N. Galloway, J. J. Schultz-Tokos, H. Sievering, and J. F. Boatman, The geochemical cycling of reactive chlorine through the marine troposphere, *Global Biogeochem. Cycles*, **4**, 407-430, 1990.

E. M. Knipping, M. J. Lakin, K. L. Foster, P. Jungwirth, D. J. Tobias, R. B. Gerber, D. Dabdub, B. J. Finlayson-Pitts, Experiments and simulations of ion-enhanced interfacial chemistry on aqueous NaCl aerosols, *Science*, **288**, 301-306, 2000.

E. M. Knipping and D. Dabdub, Modeling Cl_2 formation from aqueous NaCl particles: Evidence for interfacial reactions and importance of Cl_2 decomposition in alkaline solution, *J. Geophys. Res.*, **107**, 4360, doi:10.1029/2001JD000867, 2002.

M-T. Leu, S. Hatakeyama, and K-J. Hsu, Rate constants for reactions between atmospheric reservoir species. 1. HCl, *J. Phys. Chem.*, **93**, 1989.

L. M. Mclnnes, D. S. Covert, P. K. Quinn, and M. S. Germani, Measurements of chloride depletion and sulfur enrichment in individual sea-salt particles collected from the remote marine boundary layer, *J. Geophys. Res.*, **99**, 8257-8268, 1994.

M. J. Molina and F. S. Rowland, Stratospheric sink for chlorofluoromethanes: chlorine atom-catalysed destruction of ozone, *Nature*, **249**, 810-812, 1974.

H. Mouri and K. Okada, Shattering and modification of sea-salt particles in the marine atmosphere, *Geophys. Res. Lett.*, **20**, 49-52, 1993.

K. W. Oum, M. J. Lakin, D. O. DeHaan, T. Brauers, and B. J. Finlayson-Pitts, Formation of molecular chlorine from the photolysis of ozone and aqueous sea-salt particles, *Science*, **279**, 74-77, 1998.

S. Pechtl and R. von Glasow, Reactive chlorine in the marine boundary layer in the outflow of polluted continental air : A model study, *Geophys. Res. Lett.*, **34**, L11813, 2007.

R. G. Remorov, Y. M. Gershenzon, L. T. Molina and M. J. Molina, Kinetics and mechanism of HO2 uptake by on solid NaCl, *J. Phys. Chem. A*, **106**, 4558-4565, 2002.

R. Robertson, and G. P. Smith, Temperature dependence of O + OH at 136 – 377 K using ozone photolysis, *J. Phys. Chem. A*, **110**, 6673-6679, 2006.

R. Sander, and P. J. Crutzen, Model study indicating halogen activation and ozone destruction in polluted air masses transported to the sea, *J. Geophys. Res.*, **101**, 9121-9138, 1996.

J. H. Seinfeld and S. N. Pandis, *Atmospheric Chemistry and Physics*. John Wiley & Sons, Inc., New York, 1998.

H. B. Sigh and J. F. Kasting, Chlorine-hydrocarbon photochemistry in the marine troposphere and lower stratosphere, J. Atmos. Chem., 7, 261-285, 1988.

C. W. Spicer, E. G. Chapman, B. J. Finlayson-Pitts, R. A. Plastridge, J. M. Hubbe, J. D. Fast, and C. M. Berkowitz, Unexpectedly high concentrations of molecular chlorine in coastal air, *Nature*, **394**, 353-356, 1998.

J. I. Steinfeld, J. S. Francisco, and W. L. Hase, *Chemical Kinetics and Dynamics (2nd Edition)*, Prentice Hall, Upper Saddle River, 1998.

G. E. Streit, Negative ion chemistry and the electron affinity of sulfur hexafluoride, *J. Chem. Phys.*, **77**, 826-833, 1982.

G. S. Tyndall, C. S. Kegley-Owen, J. J. Orlando, and A. Fried, Tunable diode laser study of the reaction OH + ClO → HCl + O_2, *J. Phys. Chem. A*, **106**, 1567-1575, 2002.

R. Vogt, P. J. Crutzen, and R. Sander, A mechanism for halogen release from sea-salt aerosol in the remote marine boundary layer, *Nature*, **383**, 327-330, 1996.

L. Wang, J. –Y. Liu, Z. –S. Li, X. –R. Huang, and C. –C. Sun, Theoretical study and rate constant calculations of the Cl + HOCl and H + HOCl reactions, *J. Phys. Chem. A*, **107**, 4921-4928, 2003.

A. R. West, *Solid state chemistry and its applications*, John Wiley & Sons Ltd, New York, 1984.

T. Xie, J. M. Bowman, K. A. Peterson, B. Ramachandran, Quantum calculations of the rate constant for the $O(^3P)$ plus HCl reaction on new ab initio $^3A''$ and $^3A'$ surfaces, *J. Chem. Phys.*, **119**, 9601-9608, 2003.

H. G. Yu and A. J. C. Varandas, Dynamics of H(D) + O_3 reactions on a double many-body expansion potential energy surface for ground state HO_3, *J. Chem. Soc. Faraday. Trans.*, **93**, 2651-2656, 1997.

Chapter 5

Conclusions

Controlling experimental conditions by targeting specific reactions enables simulation of the atmosphere under laboratory conditions, which provides fundamental knowledge about atmospheric chemistry. However, the deviation of these restricted conditions from reality carries limitations to explaining current phenomena in the atmosphere. This thesis focused on expanding the current state of knowledge for general application to the real atmosphere, particularly the troposphere.

Regarding the humidity, some part of the atmosphere is abundant in water vapor, whereas another part is arid. Information about the heterogeneous chemistry of gas-phase radicals on aerosols has been limited to specific reactions. One example is knowledge about the reaction probabilities of OH on the surfaces of tropospheric importance, which previous laboratory studies report only under dry conditions. In contrast, product studies have only been done under the extremely humid conditions. Therefore, heterogeneous chemistry of OH under complementary conditions was required to investigate the mechanism for application to the real troposphere.

Firstly, the effect of relative humidity on the OH uptake by organic and inorganic surfaces of tropospheric importance has been investigated. Due to diffusion limited conditions coming from introducing high water vapor, the flow tube setup was employed with three techniques: i) beads-packing, ii) parallel reactors with a reference, and iii) surface dilution. The virtual cylindrical reactor approximation successfully quantified the reaction probability of OH for the surfaces of interest. The effects were different depending on the characteristics of the aerosols. Hydrophobic organic aerosols were not influenced by the relative humidity for the uptake of OH radicals, whereas the presence of water vapor assisted uptake of OH on glutaric acid, a hydrophilic organic aerosol. Inorganic surfaces exhibited different behavior under wet

conditions. Only hygroscopic salts ($MgCl_2$, $CaCl_2$, and sea salt) showed noticeable changes in the uptake of OH while the others (NaCl, Na_2SO_4, and KCl) did not. This characteristic was determined by the cations, which are responsible for redistribution of surface ions. The most interesting observation was that sea salt reactivity with OH under wet conditions was dictated by $MgCl_2$ instead of NaCl, its major component. This was explained by the segregation effect of surface ions. The water effect on the OH uptake for mineral dust particles (SiO_2 and Al_2O_3) was positive resulting in the enhancement of the OH reactivity to a mineral dust surface under wet conditions.

Extending the application to humid conditions, these results can improve atmospheric models for better understanding about the atmosphere, in particular the troposphere. The categorization of organic aerosols with respect to their hydrophilicities will be useful for the models describing polluted urban areas. Furthermore, focus should be given to $MgCl_2$ reactivity in relation to the OH budget in the marine boundary layer or coastal urban area under wet conditions.

Secondly, production of Cl_2 from the heterogeneous reaction of OH on NaCl was studied under dry or low RH conditions to complement the current mechanism as reported in the literature, which covers only high RH conditions over the deliquescence RH.

Mass spectra of the gas phase reaction products and XPS characterization of Na(1s) provided information about the identification of the products, both gas-phase and solid state, the yield of the product, the effect of RH on product formation, and the reaction mechanism. Since oxidation of NaCl by OH produces Cl_2 even under arid conditions with a yield of approximately 2%, the budget of chlorine-containing species, particularly at the troposphere of high altitude, can be better estimated with these results.

It is expected that our study can significantly improve current atmospheric models for more realistic conditions, providing fundamental information regarding the heterogeneous chemistry of radicals, and suggesting interesting topics for future studies about the interaction between humidity and heterogeneous chemistry, and its mechanism. As a consequence, atmospheric science starting from simple cases for restricted applications will be able to continue progressing to advanced technologies for general application.

Chapter 6

Recommendations for Future Study

The following research topics are recommended for future studies regarding heterogeneous chemistry of radicals in the troposphere.

6.1. Drift Tube for Better Sensitivity

This thesis described how water interference on CIMS detection sensitivity was successfully reduced for studies performed under wet conditions. Nevertheless, the maximum relative humidity was limited to RH ~ 50% since sensitivity was still sacrificed with increasing relative humidity due to formation of water clusters. Therefore, a drift tube technique is recommended for better sensitivity.

A drift tube is designed for accelerating ions in a flow tube [Hansel *et al.*, 1995; Morrison *et al.*, 2001; de Gouw *et al.*, 2003]. A high voltage (~ 1 kV) can be applied over an array of electronically isolated metal rings connected with resistors to establish a homogeneous electric field. As a result, the velocity of ions in the drift tube (v_d) increases according to the following:

$$v_d = \mu \times E \qquad (6.1)$$

where μ is the ion mobility and E is the electric field. The accelerated ion velocity induces a dissociation of the water complex, such as $OH^-(H_2O)_n$ and $F^-(HF)_n$. The resulting enhancement of sensitivity for ion detection under high RH conditions both enables investigation of the RH effect on OH uptake under a wider range of RH values, and reduces the measurement uncertainty of the reaction probability of OH.

6.1. The RH Effect on HO_2 Uptake by Surfaces of Tropospheric Importance

With a high mixing ratio (40 ppt), HO_2 radical plays a key role in the oxidation chemistry of the troposphere including heterogeneous chemistry on aerosols.

Therefore, the investigation of RH effect on HO_2 uptake by the surfaces is important to improve tropospheric models. Recently, Remorov *et al.* [2002] reported that extremely low RH (~ 0.5 %) conditions reduced the reactivity of HO_2 on NaCl. For application to real tropospheric conditions, study under high RH (RH ≥ 50%) is required.

The technique employed in the present work can be used to increase the sensitivity to HO_2 detection and for quantification. The only difference would be use of a different reagent ion (F^-) for ionization of HO_2.

$$HO_2 + F^- \rightarrow O_2^- + HF \qquad (6.2)$$

Along with employment of a drift tube, the RH range can be extended to the deliquescence point of NaCl (RH ~78%). As a result, a study for the release of chlorine-contained species from NaCl upon HO_2 uptake can be performed to explore a potential new source of Cl in the troposphere.

References for Chapter 6

J. de Gouw, C. Warneke, T. Karl, G. Eerdekens, C. van der Veen, and R. Fall, Sensitivity and specificity of atmospheric trace gas detection by proton-transfer-reaction mass spectrometry, *Int. J. Mass. Spectrom.*, **223/224**, 365-382, 2003.

A. Hansel, A. Jordan, R. Holzinger, P. Prazeller, W. Vogel, and W. Lindinger, Proton transfer reaction mass spectroscopy: on-lin trace gas analysis at the ppb level, *Int. J. Mass Spectrom. Ion Processes*, **149/150**, 609-619, 1995.

G. C. Morrison and C. J. Howard, Selective detection of gas-phase aldehydes and ketones using protonated hydrazine, *Int. J. Mass Spectm.*, **210/211**, 503-509, 2001.

R. G. Remorov, Y. M. Gershenzon, L. T. Molina and M. J. Molina, Kinetics and mechanism of HO2 uptake by on solid NaCl, *J. Phys. Chem. A*, **106**, 4558-4565, 2002.

Biographical Note

Personal Information

Name : Jong-Ho Park
Date of Birth : Aug. 25th, 1973
Place of Birth : Seoul, South Korea
Citizenship : South Korea

Education

2002-08: Ph.D. in Physical Chemistry
Massachusetts Institute of Technology, Cambridge, MA
Research Advisor : Professor Mario J. Molina, 1995 Nobel Laureate
1999-01: M.S. in Physical Chemistry
Korea University, Seoul, Korea
Research Advisor : Professor Jong-Ho Choi
1993-99: B.S. in Chemistry
Korea University, Seoul, Korea

Professional Experience

2003-08: Research Assistant (the Laboratory of Atmospheric Chemistry, MIT)
2002-03: Teaching Assistant (Department of Chemistry, MIT)
2001-02: Assistant Research Scientist
(Nano-Environmental Science Lab., Korea University)
2001-02: Part-time Lecturer (Department of Chemistry, Korea University)
1994-06: Military Service (Army, Republic of Korea)

Awards and Hornors

2002-04: Kwanjeong International Scholarship
2000-01: Brain Korea 21 Fellowship
2001 : Korean Red Cross Award

Principal Research Interest

Atmospheric Chemistry, Heterogeneous Chemistry of Radicals in the Troposphere, Reaction Dynamics, Laser Spectroscopy, Reaction Kinetics, Mass Spectroscopy, Analytical Chemistry

Publications

1. Jong-Ho Park, Andrey V. Ivanov, and Mario J. Molina, The RH effect on OH uptake by surfaces of atmospheric importance, *J. Phys. Chem. A*, 2008, Submitted.
2. Jong-Ho Park, Andrey V. Ivanov, and Mario J. Molina, Release of Cl2 from NaCl upon OH uptake, *Geophys. Lett.*, 2008, Submitted.
3. Jong-Ho Park, Hohjai Lee, and Jong-Ho Choi, A theoretical study of the reaction of O(3P) with an allyl radical C3H5, *J. Chem. Phys.*, **119**, 8966-8978, 2003.
4. Jong-Ho Park, Hohjai Lee, Han-Cheol Kwon, Hee-Kyung Kim, Young-Sang Choi, and Jong-Ho Choi, Atom-radical reaction dynamics of $O(^3P) + C_3H_5 \rightarrow C_3H_4 + OH$: Nascent rovibrational state distributions of product OH, *J. Chem. Phys.*, **117**, 2017-2029, 2002.
5. Han-Cheol Kwon, Jong-Ho Park, Hohjai Lee, Hee-Kyung Kim, Young-Sang Choi, and Jong-Ho Choi, Crossed beam investigations of the reaction dynamics of $O(^3P)$ with allyl radical, C_3H_5, *J. Phys. Chem.*, **116**, 2675-2679, 2002.
6. Hee-Kyung Kim, Han-Cheol Kwon, Jong-Ho Park, Young-Sang Choi, and Jong-Ho Choi, Studies of radicals generated in supersonic flash pyrolysis by laser induced fluorescence spectroscopy, *Bull. Korean Chem. Soc.*, **20**, 1441-1446, 1999.